

The first hard X-ray spectral catalogue of Blazars observed by *NuSTAR*

Riccardo Middei,^{1,2*} Paolo Giommi,^{3,4,5,6} Matteo Perri,^{1,2} Sara Turriziani,⁷ Narek Sahakyan,^{8,6,9} Y. L. Chang¹⁰ C. Leto^{1,11} F. Verrecchia^{1,2}

¹ Space Science Data Center, SSDC, ASI, via del Politecnico snc, 00133 Roma, Italy

² INAF - Osservatorio Astronomico di Roma, via Frascati 33, I-00040 Monteporzio Catone, Italy

³ Institute for Advanced Study, Technische Universität München, Lichtenbergstrasse 2a, D-85748 Garching bei München, Germany

⁴ Center for Astro, Particle and Planetary Physics (CAP3), New York University Abu Dhabi, PO Box 129188 Abu Dhabi, United Arab Emirates;

⁵ Associated to Italian Space Agency, ASI, via del Politecnico snc, 00133 Roma, Italy

⁶ ICRA-Net, P.zza della Repubblica 10, 65122, Pescara, Italy

⁷ Physics Department, Gubkin Russian State University (National Research University), 65 Leninsky Prospekt, Moscow, 119991, Russian Federation

⁸ ICRA-Net-Armenia, Marshall Baghramian Avenue 24a, Yerevan 0019, Armenia

⁹ ICRA, Dipartimento di Fisica, Sapienza Università di Roma, P.le Aldo Moro 5, 00185 Rome, Italy

¹⁰ Tsung-Dao Lee Institute, Shanghai Jiao Tong University, 800 Dongchuan RD. Minhang District, Shanghai, China

¹¹ ASI - Italian Space Agency, Via del Politecnico snc, 00133, Rome, Italy

Accepted XXX. Received YYY; in original form ZZZ

ABSTRACT

Blazars are a peculiar class of active galactic nuclei (AGNs) that enlighten the sky at all wavelengths. The electromagnetic emission of these sources is jet-dominated resulting in a spectral energy distribution (SED) that has a typical double-humped shape. X-ray photons provide a wealth of information on the physics of each source as in the X-ray band we can observe the tail of SED first peak, the rise of the second one or the transition between the two. *NuSTAR*, thanks to its capability of focusing X-rays up to 79 keV provides broadband data particularly suitable to compute SEDs in a still poorly explored part of the spectrum. In the context of the Open Universe initiative we developed a dedicated pipeline, *NuSTAR_Spectra*, a shell-script that automatically downloads data from the archive, generates scientific products and carries out a complete spectral analysis. The script homogeneously extracts high level scientific products for both *NuSTAR*'s telescopes and the spectral characterisation is performed testing two phenomenological models. The corresponding X-ray properties are derived from the data best-fit and the SEDs are also computed. The systematic processing of all blazar observations of the *NuSTAR* public archive allowed us to release the first hard X-ray spectroscopic catalogue of blazars (*NuBlazar*). The catalogue, updated to September 30th, 2021, includes 253 observations of 126 distinct blazars, 30 of which have been multiply observed.

Key words: galaxies:active – quasars:general – X-rays:galaxies– Galaxies: BL Lacertae objects: – Methods: data analysis – Astronomical data bases:catalogues

1 INTRODUCTION

Active Galactic Nuclei (AGNs) are powerful, persistent extra-galactic sources powered by accretion onto a supermassive black hole (SMBH, 10^6 - 10^{10} M_⊙). Their broadband spectrum results from the interplay of thermal and non-thermal mechanisms that involve different structures from sub-parsec up to kilo parsecs scales (e.g. [Bianchi et al. 2012](#); [Netzer 2015](#); [Padovani et al. 2017](#)).

Blazars are a rare and highly peculiar class of AGN as they display a narrow relativistic jet that happens to be oriented towards the Earth. They radiate from radio wavelengths to the γ-ray domain (e.g. [Urry & Padovani 1995](#)), and, possibly, they also emit high-energy neutrinos ([IceCube Collaboration et al. 2018a](#); [Giommi et al. 2020b](#); [Giommi & Padovani 2021](#)). These sources are radio bright, show

prominent flux variability and sometimes large polarisation signals and they can be classified via physical and geometrical conditions as discussed by [Giommi et al. \(2012\)](#). The optical spectral properties of these sources are used to define two major classes, Flat-Spectrum Radio Quasars (FSRQs) and BL Lacertae objects (BL Lacs). Objects belonging to the first group, similarly to radio quiet AGNs, show broad emission lines, while a strongly variable and very often featureless continuum is typical of BL Lacs.

The spectral energy distribution (SED) of blazars has a characteristic double-peaked shape, see Fig. 1. The low energy part, normally assumed to be due to synchrotron emission, peaks at a frequency (ν_{peak}) that is located between far infrared and X-rays. This frequency is used to further classify blazars into low, intermediate, and high energy peaked, LBL ($\nu_{\text{peak}} < 10^{14}$ Hz), IBL (ν_{peak} is between 10^{14} and 10^{15} Hz), and HBL ($\nu_{\text{peak}} > 10^{15}$ Hz), respectively ([Padovani & Giommi 1995](#); [Abdo et al. 2010](#)). The

* E-mail: riccardo.middei@ssdc.asi.it

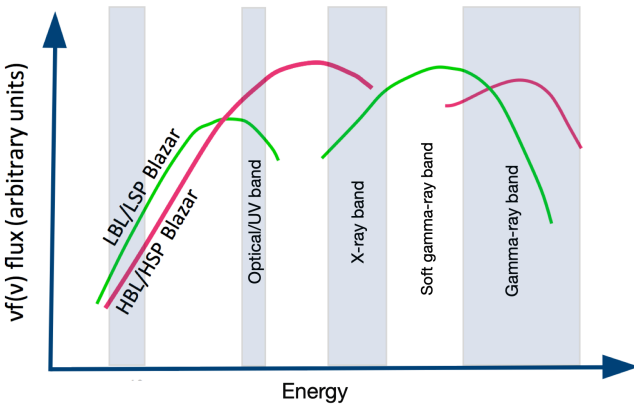


Figure 1. Blazar SEDs shown for different peak energies of the underlying two main emission bumps. LBLs sources have the maximum of their synchrotron power output in the infrared/optical band, while for HBL the peak occurs between the UV or X-ray domain. Moreover, the SED of an extreme class of blazars, the so-called ultra high energy BL Lacs (UHBLs) for which the maximum energy output of the synchrotron emission is well above the hard X-rays domain. It is worth noticing that for the same peak luminosity, the radio emission decreases by orders of magnitudes. Figure adapted from Giommi et al. (2002).

physical mechanism that generates the high energy part (commonly observed between the X-rays and the γ -rays) is still a debated matter. In the leptonic interpretation, two competing scenarios have been proposed, i.e., inverse Compton (IC) scattering of photons provided by the synchrotron emission (Synchrotron Self Compton, SSC; e.g. Maraschi et al. 1992; Mastichiadis & Kirk 2002) or produced outside the jet (e.g. Dermer & Schlickeiser 1993; Sikora et al. 1994; Błażejowski et al. 2000), with this often referred as External Compton (EC). The most likely external photon fields can be the photons reflected from the broad-line region or photons from a dusty torus. In the alternative hadronic scenario, the high energy peak is either due to proton synchrotron radiation (Aharonian 2000) or to emission processes of secondary particles produced in hadronic interactions in the jet (Mannheim 1993; Mücke et al. 2003). Blazars have a quite unique behaviour compared to other types of AGNs (see e.g. Maccacaro et al. 1984; Giommi et al. 1999; Rector et al. 2000b; Turriziani et al. 2019), as showed by the analysis of samples of X-ray selected blazars where no or even negative cosmological evolution were found (Rector et al. 2000a; Wolter & Celotti 2001), and the same trend was discussed in Ajello et al. (2014) for a sample of γ -ray selected sources.

In this paper we consider all blazars observed by the high energy satellite *NuSTAR*. Hard X-rays carry important information about blazars as shown by earlier *BeppoSAX*-based analyses (e.g. Tavecchio et al. 2000; Massaro et al. 2004a,c; Donato et al. 2005a), and by works based on INTEGRAL (e.g. Giannì et al. 2011) and Suzaku data (e.g. Stawarz 2014; Zhang et al. 2019, 2021), and numerous papers rely on *NuSTAR* data (Sbarato et al. 2013, 2016; Marcotulli et al. 2017; Bhatta et al. 2018; Ghisellini et al. 2019). However, an extensive study of the hard X-ray properties of blazars observed by *NuSTAR* has never been performed since most of the characterisations focuses on single sources or small samples. In an effort to facilitate sample studies we performed a systematic analysis of all the blazars included in the public *NuSTAR* archive, reporting their spectral properties in the first *NuSTAR* blazars catalogue (*NuBlazar*). Such a catalogue is based on the *NuSTAR_Spectra*

script, a software tool similar to *Swift_xrtproc* (Giommi et al. 2021), both developed in the context of the Open Universe (OU) initiative (Giommi et al. 2020a) in collaboration with Space Science Data Center (SSDC) of the Italian Space Agency (ASI).

2 BLAZARS IN THE *NuSTAR* PUBLIC ARCHIVE

NuSTAR (Harrison et al. 2013) is a NASA Small Explorer (SMEX) mission consisting of two co-aligned grazing incident hard-X-ray telescopes that collect light onto the two focal plane solid state detectors (FPMA/B). Thanks to its \sim 10 metres focal length mirror-detector design, *NuSTAR* is the first focusing high-energy X-ray mission, hence the first facility for which hard X-ray spectra are not background dominated. The *NuSTAR* broadband-pass is extremely suitable for addressing a number of different issues in AGNs physics, including the characterisation of the X-ray emission in blazars. In these sources, in fact, different components can be observed in the operating 3–79 keV energy range: the high frequency tail of the synchrotron peak in HBL blazars, the rising SSC component in LBL objects, or the transition between the low and high energy components. In the case of FSRQs dominated by EC emission (see e.g. Böttcher et al. 2013), *NuSTAR* data can be used to put constraints on the EC component, if the transition between SSC and EC components happens in the hard X-ray band (Sikora et al. 2013).

To compile the list of blazars included in the *NuSTAR* public archive, we cross-matched the Open Universe master list of blazars and blazar candidates (Giommi et al. 2019) with the list of all the *NuSTAR* observations carried out before the end of September 2021. The master list combines the *BZCAT* 5th edition (Massaro et al. 2015, 2016), the sample of blazars detected by Fermi LAT and reported in the 4LAC-DR2 catalogue (Ackermann et al. 2015b,a) and the 3HSP high energy peaked and extreme blazars list (Chang et al. 2019b,a). Our initial sample of *NuSTAR* observations of blazars consisted of 287 pointings including each of the sources in the master list within 7 arcmin from the center of the field of view. We then neglected all those observations with an exposure shorter than 2000 seconds in total for the two *NuSTAR* modules and those fields in which the background level was different between the *FPMA* and *FPMB* modules.

The remaining matches included sources such as NGC 1275, M87 and Centaurus A. These sources are located in the Perseus, Virgo and Centaurus clusters, respectively, thus their X-ray emission detect by *NuSTAR* is due to a nuclear and an extra-nuclear contribution emerging from the hot intracluster gas. The complex nature of these spectra is unsuitable for an automatic analysis, thus we did not consider observations belonging to any of these three sources. Finally, we excluded fields in which the source, if present, was characterised by a S/N too low to allow for a spectral characterisation.

These steps resulted in a final list of 253 exposures of 126 blazars. In Fig. 2 we show a sketch of the positions of the sources of the sample, whose details are given in Table A1.

3 DATA PROCESSING: THE *NuSTAR_Spectra* PIPELINE

To reduce and analyse in a homogeneous and automatic way the selected observations we developed the *NuSTAR_Spectra* pipeline, a shell-script based on the *NuSTAR* Data Analysis Software (NuSTARDAS¹), included in the *HEASoft* V6.29 package. The

¹ Developed at the ASI/SSDC

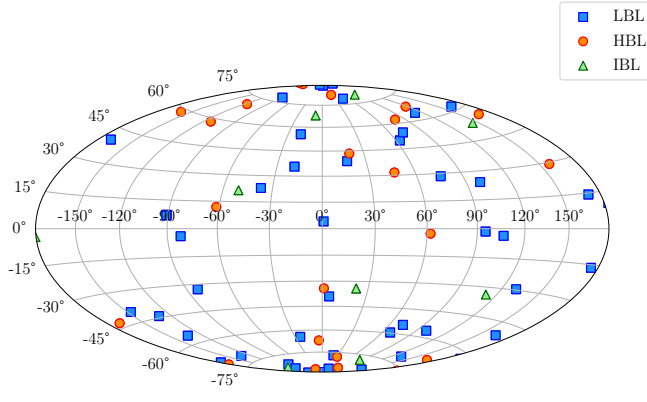


Figure 2. Hammer projection in galactic coordinates of all blazars observed with *NuSTAR* and studied in this work. For the sake of simplicity, we plotted uncertain type blazars in green as IBL sources.

calibration data files distributed with CALDB version 20211020 were adopted. Using the *NuSTAR_Spectra* pipeline it is possible to download data, generate high-level calibrated scientific products and perform spectral analyses via a simple command line.

As outcomes, *NuSTAR_Spectra* returns the FPMA/B source and background spectra, the corresponding ancillary and response files, the best-fit parameters for a power-law and a logarithmic parabola model, integrated fluxes in the 3-10 and 10-30 keV bands, and the best fit spectral data in $vF(v)$ units for SED plotting. Moreover, at the end of the procedure, various plots in gif format are created to facilitate visual inspection of the results of the analysis and of the products generated.

The following steps are executed within the *NuSTAR_Spectra* script:

- calibrated and filtered event files are downloaded from the SSDC repository² and saved into a folder named as the observation ID. The script does not perform an ex-novo data calibration (level 1 data) and screening (level 2 data) but relies on the level 2 event files generated at the *NuSTAR* SOC with default parameter settings and available for each observation ID directly from HEASARC (or SSDC mirror site) in the archive.
- the ftool *fselect* (Blackburn 1995) is used to read the event file and generate a new file in the 3-20 keV energy range. In this interval, the effective area of the modules *FPMA* and *B* is maximal and the background contribution is minimised. Using this file, the source count rate is derived.
- the *detect* task of the X-ray image package *Ximage* is launched to precisely locate the source in celestial coordinates. If no source is detected the script reports on this issue and stops.
- High-level science products for the detected source are extracted using the *nuproducts* routine. The source counts are extracted using a circular region, while the background is computed in an annulus centered on the source. The extraction radius/radii for the circle/annulus are automatically set to a value that is optimised depending on the source count rate. The higher/lower the count rate the larger/smaller will be the radius of the circular region which usually varies in the range of 30-70 arcsec. In a similar fashion, the annular region also scales maintaining a minimum separation of 50 arcsec between the

inner and outer radii. The ancillary and response matrices are computed at this stage and the spectra are grouped via the *grppha* standard command in order to have at least 1 count for bin.

• A spectral analysis is performed using the *Xspec* fitting package (Arnaud 1996) adopting Cash statistics (Cash 1979). The fit is performed from 3 keV up to the maximum energy where the signal is still present, typically between 20 and 79 keV. Spectra of module A and B are simultaneously fitted with a cross-calibration constant (found to be always within a few percent, Madsen et al. 2015a) and the Galactic column density is always taken into account with the *tbabs* model. Then, the fitting model can be described as: $tbabs \times const \times model$, where the latter term stands for power-law or logarithmic parabola. The logarithmic parabola is defined as

$$N(E) = (E/E_1)^{-\alpha - \beta \log(E/E_1)}, \quad (1)$$

where α accounts for the source photon index at the energy E_1 , β represents the curvature of the parabola and E_1 is a reference energy. When we process the data we obtain the best-fit values of normalisation and photon index for the power-law model, and the spectral index and the curvature for the logarithmic parabola. Finally, E_1 is set to 5 keV and kept fixed in agreement with Massaro et al. (2004a) and other *NuSTAR* studies (e.g. Baloković et al. 2016). Once the best parameters are estimated the script saves the observed flux in the 3-10 and 10-30 keV bands and the current best-fit in *Xspec* format. The choice for the flux ranges was driven by the effective area of the modules *FPMA* and *B* detector that is maximal between 3-20 keV.

• *NuSTAR_Spectra* uses the best-fit parameters to compute the X-ray SED from 3 keV up to the energy used to perform the spectral analysis. SEDs, are calculated separately for the two models. In particular, the power-law best-fitting the *FPMA/B* spectra is used to derive the SED of each observation. Though the *NuSTAR* band is only marginally affected by absorption, we de-absorbed the fluxes using the cross sections of Morrison & McCammon (1983) and setting the amount of absorbing material (N_H) equal to the Galactic value, the same value assumed for the fits.

• Finally, the pipeline saves gifs and other files of interest, i.e. those allowing for a different spectral analysis, and those containing the information on the flux and spectral parameters. In Fig. 3, we show an example of a spectral fit performed on 5BZB J0509+0541 (Obs. ID 090402637004) and the corresponding X-ray SED.

4 THE NUBLAZAR CATALOGUE

The catalogue resulting from our processing is called *NuBlazar* and presents the spectral and observational properties of 126 individual blazars, 30 of which have been multiply observed, for a total of 253 exposures. *NuBlazar* includes 80 LBLs, 32 HBLs and 14 blazars with intermediate SEDs (IBL). The redshifts of the LBLs cover the range 0.024 – 4.71, whereas IBLs and HBLs are relatively nearby with $z < 1$ and $z < 1.2$, respectively. We note, however, that redshift estimations are not available for 8 sources in the sample (see Table A1). Fig. 4, shows the redshift distribution of all sources in the catalog.

The spectral properties of each object have been derived using a power law and a logarithmic parabola to fit the spectra. In Fig. 5 the distributions of Cstat/d.o.f for these models are shown for the different blazars sub-classes. These distributions overlap for the cases of LBLs and IBLs, while significant differences are present for HBL sources. This implies that for LBLs and IBLs, the power law is a good representation of the data and adding curvature does not improve the fit. Instead, for HBLs, the logarithmic parabola model provides a

² [http://archive\(ssdc.asi.it/nustar/pubdata/](http://archive(ssdc.asi.it/nustar/pubdata/)

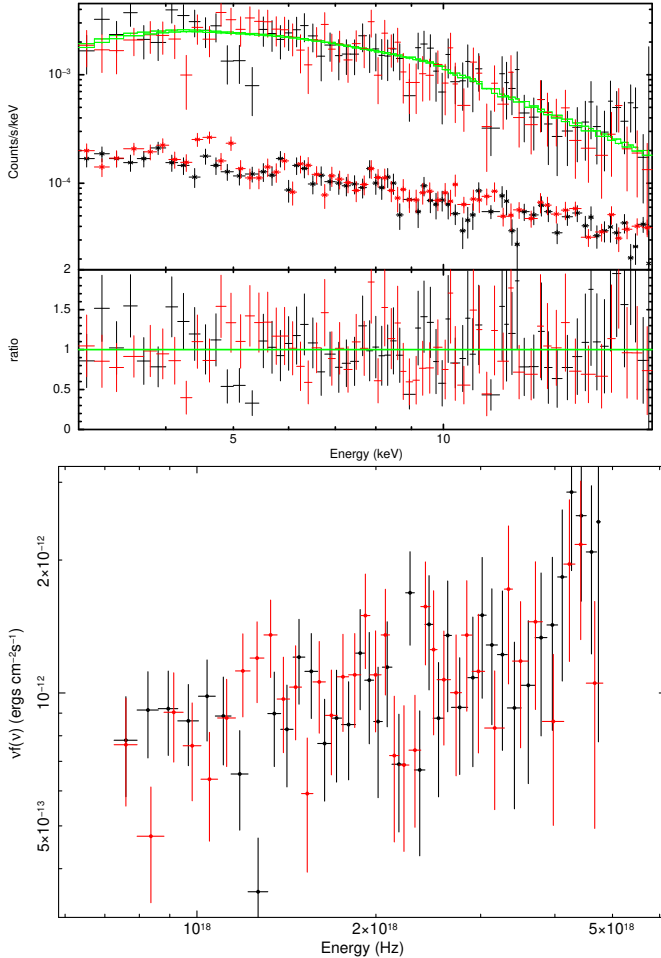


Figure 3. Top panel: The spectral fit to the FPMA (black) and FPMB (red) spectra of the source 5BZB J0509+0541 (Obs. ID 090402637004). Background spectra are also showed. The model (green) accounts for a power-law absorbed by the Galaxy. In this case, the maximum energy for the analysis correspond to 20 keV. Bottom panel: the corresponding spectral energy distribution is showed. Similar plots can be found for all the sources studied in the present paper at the web page <https://www.sscdc.asi.it/nustarblaz/>.

more appropriate description of the hard X-ray spectrum.

Table B1 reports the best fit values of the parameters for the power-law while Table B2 contains the information derived using the logarithmic parabola model. In Fig. 6 the photon index from the power law model is plotted as a function of the observed flux in the 3–10 keV band for different blazar spectral classes. Such a phenomenological parameter clearly separates HBL blazars, which are characterised by steeper Γ s, than LBL sources. In fact, for HBLs and average photon index of $<\Gamma>=2.56\pm0.30$ is found, while for LBLs we computed a spectral slope of $<\Gamma>=1.58\pm0.22$. Blazars with intermediate SEDs are mostly characterised by photon indices similar to those of LBLs, with a few exceptions.

In Fig. 7 the curvature parameter (β) only for HBL sources is shown, since, as said, a power law model is a good representation for LBLs and IBLs sources (see Fig. 5). The spectral curvature derived for these sources can be either positive or negative suggesting strong variations in the source spectral shape. Interestingly, the curvature is not always correlated with the source flux and it seems to depend on each specific source, see bottom panel in Fig. 7. This behaviour is

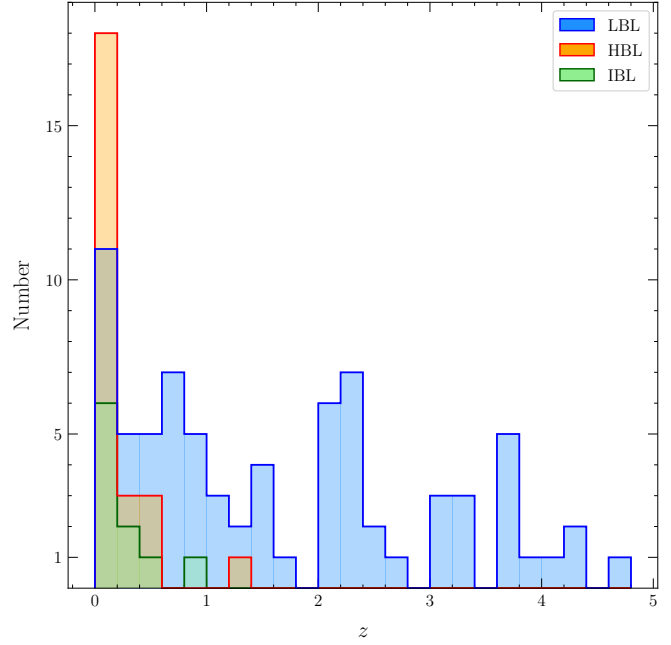


Figure 4. Redshift distributions for the different classes of blazars listed in the NuBlazar.

discussed in Section 5.

The power law slope as a function of the broadband (3–30 keV) flux is shown in Fig. 8 for a subsample of multiply observed blazars. For some source (e.g. Mkn 501, 1ES 0229+200) these two quantities are anti-correlated, while no trends are observed for other objects (e.g. PKS 2155-304). Interestingly, this trend holds or not independently of the SED class of the source as for the case of the two HBLs Mkn 501 and PKS 2155-304. In Fig. 9, we show the relation between the curvature parameter and the photon index for all the HBLs in the catalogue (shaded points). Moreover, we over plot the same parameters for the three blazars labelled, namely Mkn 421, Mkn 501 and PKS 2155-304. A weak and marginally significant anti-correlation is found between the spectral slope and the log parabola curvature ($P_{cc}=0.3$ and $P(<r>)=0.04$) for the whole sample of HBLs. However, we notice that that trend is driven by Mkn 421 data that are actually strongly anti-correlated. Once we do not consider data from this source, the trend is even less significant with a compatible correlation coefficient and a null probability of $P(<r>)=8\%$. We will further discuss these correlations for a selected sample of objects in the corresponding sub sections of Sect. 5.

4.1 Sources observed multiple times

Thirty objects in our list were observed by *NuSTAR* more than once (up to 26 times). Blazars are well known to show large amplitude flux changes at many frequencies and over a wide range of timescales. Our analysis confirms that the hard-X-ray energy band covered by *NuSTAR* is not an exception, as shown by Fig. 10 where the flux in the 3–30 keV band is plotted against time. A variety of estimators have been used to perform variability characterisations such as the power-spectral density (PSD e.g. Lawrence & Papadakis 1993; Uttley et al. 2002; Uttley & McHardy 2005), the fractional variability (e.g. Vaughan et al. 2003) and the structure function (SF) that has been used for ensemble studies (e.g. Vagnetti et al. 2011, 2016; Middei

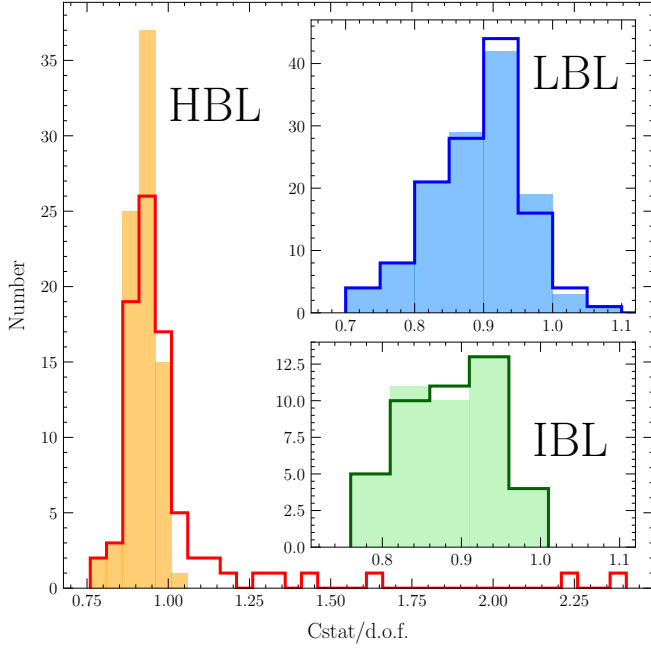


Figure 5. Distributions of the best fit statistics for the different sub-classes of blazars in our catalogue. Solid lines indicate the distributions corresponding to the power law model, while filled histograms refer to the log parabola model.

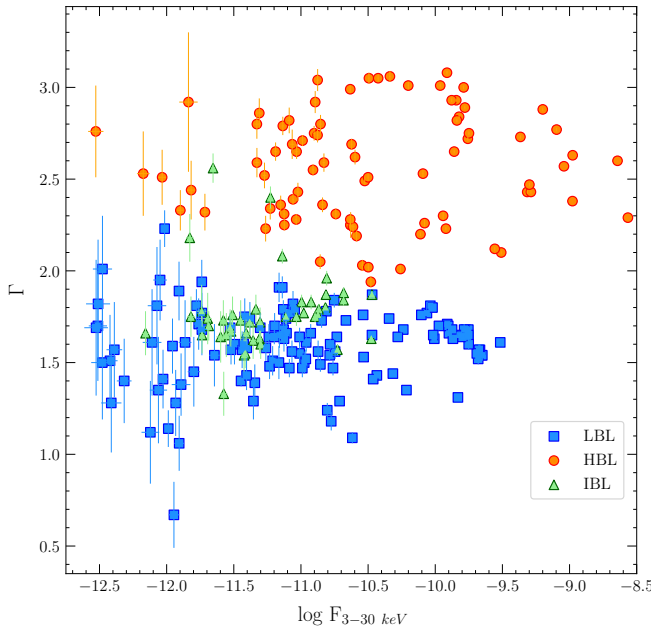


Figure 6. Photon index distributions for the different classes of blazars. HBLs have steeper spectra than LBL sources. The photon indices of IBLs are mostly flat, with occasional steeper values

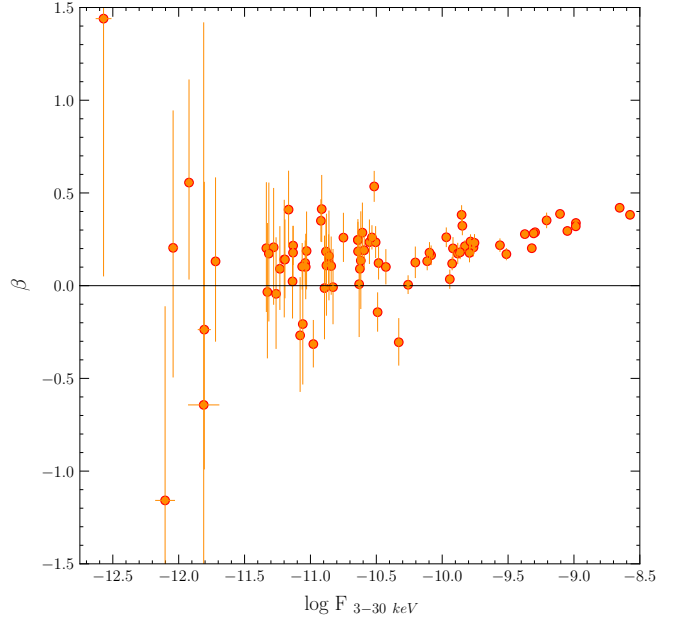


Figure 7. Top panel: curvature parameter is plotted against flux for HBL blazars. Bottom panel: Curvature parameter for the three sources labelled in the legend. The β parameter is positively correlated with the source flux in Mkn 421 and PKS 2155+304 while in Mkn 501 this trend is not observed.

et al. 2017; Paolillo et al. 2017) or single source analyses (e.g. Gallo et al. 2018). The so-called normalised excess variance (σ_{nxS}^2 , see e.g. Ponti et al. 2012) is another tool that allows for variability estimates even when light curves are sparsely sampled.

The σ_{nxS}^2 accounts for the mean quadratic variation corrected for the error, hence it provides a simple characterisation of the source intrinsic variability even for sources with only two flux measures at different epochs. This estimator is defined as $\sigma_{\text{nxS}}^2 = (S^2 - \sigma_{\text{err}}^2) / \langle f \rangle^2$, where $\langle f \rangle^2$ is the mean source flux computed over the available observations, S^2 is the light curve variance and the error term is the mean square photometric error associated to each flux. However,

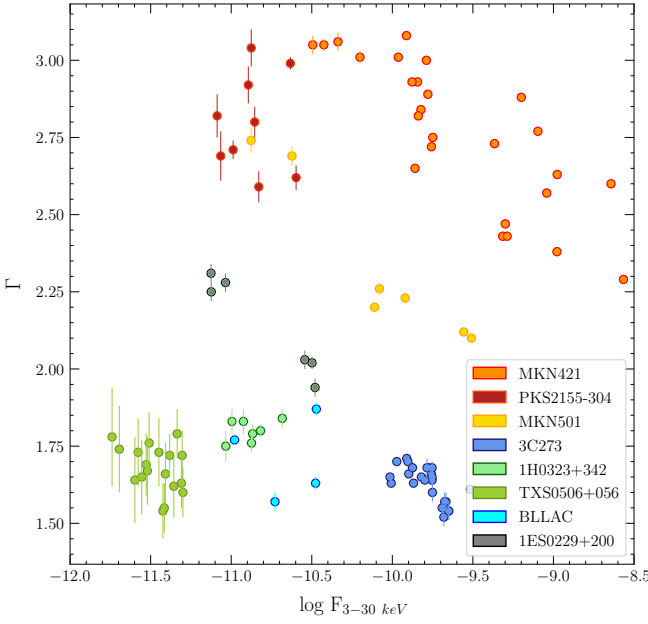


Figure 8. The photon index from the power law of the labelled sources is plotted as a function of the observed flux in the 3-30 keV band. For instance, both Mkn 421 and Mkn 501 show a typical harder when brighter behaviour.

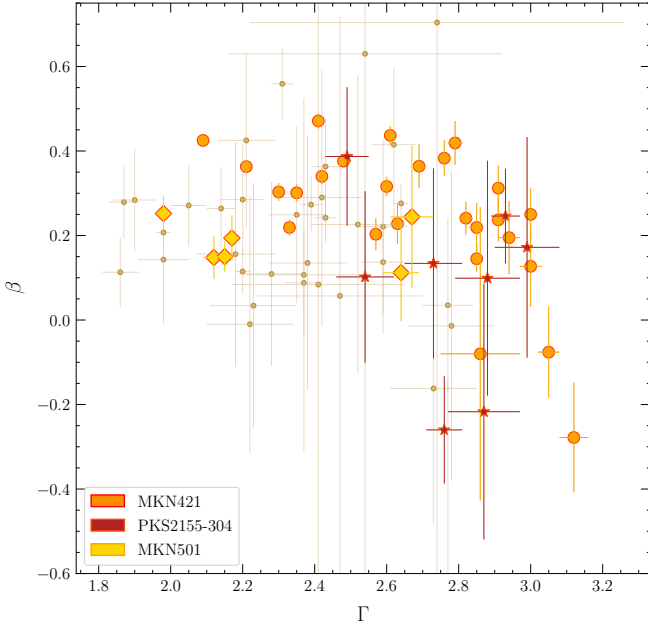


Figure 9. Spectral curvature as a function of the primary photon index for the HBL sources.

some caveats must be considered when using such an estimator. [Allevato et al. \(2013\)](#) pointed out that dealing with sparsely sampled light curves may underestimate the variability itself due to its red-noise nature. On the other hand, [Vagnetti et al. \(2016\)](#) urged caution on the use of this tool noting that cosmological time-dilation has to be accounted for and proposed a correction based on the ensemble properties of a statistically significant sample of radio quiet quasars.

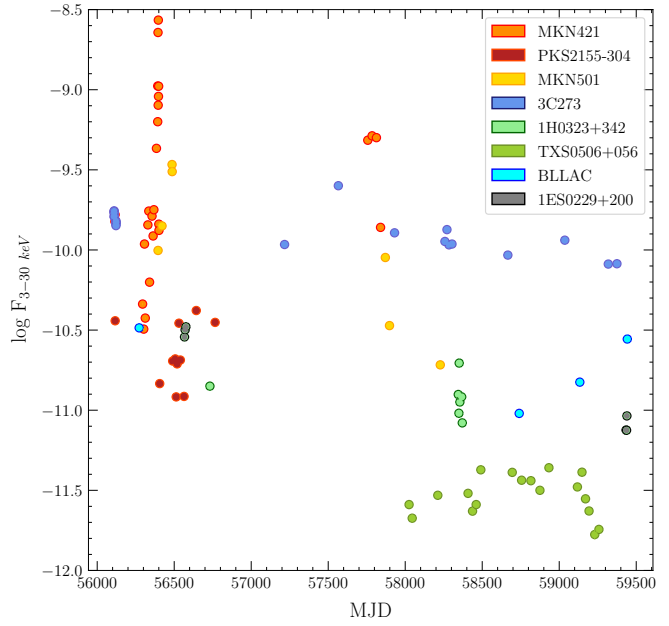


Figure 10. Light curves of a selection of blazars observed several times. Errors at 68% confidence level lie within the data points.

Table 1. Normalised excess variance in the 3-10 and 10-30 keV energy bands computed in the source reference frame. The length of the light curves are showed in years.

Source Name	σ_{nxS}^2 (3-10 keV)	σ_{nxS}^2 (10-30 keV)	z	Δt	Class	Obs
5BZBJ1104+3812	1.55±0.01	2.23±0.02	0.029	4.58	HBL	26
5BZQJ1229+0203	0.07±0.01	0.09±0.01	0.158	7.72	LBL	25
5BZBJ2158-3013	0.17±0.06	0.21±0.16	0.116	1.10	HBL	9
5BZBJ1653+3945	0.75±0.03	0.96±0.05	0.033	4.86	HBL	7
5BZUJ0324+3410	0.09±0.06	0.07±0.06	0.061	4.23	IBL	7
5BZGJ0232+2017	0.36±0.09	0.51±0.14	0.139	6.90	HBL	6
5BZBJ2202+4216	0.26±0.07	0.22±0.07	0.069	8.12	IBL	4
5BZQJ1256-0547	0.25±0.07	0.31±0.08	1.309	3.17	LBL	3
5BZBJ0507+6737	0.36±0.18	0.28±0.35	0.416	0.11	LBL	3

In other words, variability comparison of different sources must be performed over the same timescale. However, type 1 AGNs have a different driving emission mechanism, hence the correction by [Vagnetti et al. \(2016\)](#) may not be straightforwardly applied since we lack quantitative information on the ensemble variability properties of blazars. Bearing this in mind, we report in Table 1 the σ_{nxS}^2 . We notice that positive values for the σ_{nxS}^2 were derived only for 9 sources, meaning that flux changes for the not-listed sources are compatible with the noise. The normalised excess variance in the 3-10 and 10-30 keV energy bands weights the actual amount of variability for each source. Interestingly, the normalised excess variance derived for LBL objects is compatible between the two bands while HBL show larger variations in the 10-30 keV energy range. This suggestive trend can result off the presence of a single (for LBL) or two (for HBL) emission components acting in the full 3-30 keV energy range.

5 SPECTRAL ENERGY DISTRIBUTIONS AND COMMENTS ON SELECTED OBJECTS

The broad-band (radio to γ -ray) SED of all the sources in our sample have been assembled by combining the best fit spectral data derived in the previous sections with archival multi-frequency data, retrieved with the VOU-Blazars tool (Chang et al. 2019b) and the SSDC SED Builder tool³, as well as with the results of the Swift-XRT analysis of Giommi et al. (2021). The Swift-XRT SED data of the sources not included in Giommi et al. (2021) have been generated by us for this paper following the same procedure described in Giommi et al. (2021). In the following we plot and describe the SED of a small number of selected objects, where the archival data appears as orange points, the Swift-XRT data as light green points, and the *NuSTAR_Spectra* data as magenta circles. The SEDs of all the 126 objects in the sample are available on-line at

<https://openuniverse.asi.it/blazars/swift>.

5.1 Mkn 421

The HBL source Mkn 421 is one of the best studied BL Lacs shining in the local Universe ($z=0.03$, de Vaucouleurs et al. 1991). Due to its brightness and proximity this source has been the focus of a number of multiwavelength campaigns resulting in several papers dissecting its specific properties (e.g. Acciari et al. 2020; Paliya et al. 2015; Kapanadze et al. 2016; Baloković et al. 2016). Mkn 421 shows flux and spectral variations across the entire electromagnetic spectrum, the most prominent ones being in the X-ray and very high energy γ -ray bands. The *NuSTAR* observations demonstrate that Mkn 421 is highly variable also in the hard X-ray band, as it is clear from Fig. 10 and Fig. 11 and from the remarkable normalised excess variance listed in Table 1. The brightest X-ray flare was observed on MJD 56396.921 when the 3-10 keV flux was $(15.16 \pm 0.02) \times 10^{-10}$ erg cm $^{-2}$ s $^{-1}$ which exceeds the lowest flux measured by *NuSTAR* by ~ 65 times. In this period the source was in an active flaring state (Acciari et al. 2021) also in the Swift-XRT band (see Fig. 11 of Giommi et al. 2021). Together with the flux, the photon index also varies following a harder-when-brighter trend. The hardest index of 2.280 ± 0.003 was estimated during the brightest X-ray flare. The SED of Mkn 421 is shown in Fig. 11. It shows a clear trend of increase of the spectral curvature with flux. The curvature term β of *logpar* is well constrained in all the observations and switches from negative values to positive one (Fig. 7 lower panel). This parameter is strongly correlated with the source hard flux. We found indeed a $P_{\text{cc}}=0.75(0.73)$ with $P(<\text{r})\sim 2(4)\times 10^{-5}$. In principle, this curvature could be due to the cooling or escape of high-energy electrons, i.e., as the peak of the low energy component is at the X-ray band (10^{16} Hz), the radiative cooling time of the emitting electrons is of the order of one hour. Alternatively, the particle spectrum could be intrinsically curved. For example, Massaro et al. (2004b) showed that logarithmic parabola spectra are naturally formed for an energy-dependent statistical acceleration.

5.2 3C 273

3C 273 is a nearby ($z=0.158$) high-luminosity FSRQ (Strauss et al. 1992), with an extended radio jet showing superluminal motion (Seielstad et al. 1979; Pearson et al. 1981; Unwin et al. 1985). Being a highly variable bright source at almost all wavelengths 3C 273 has

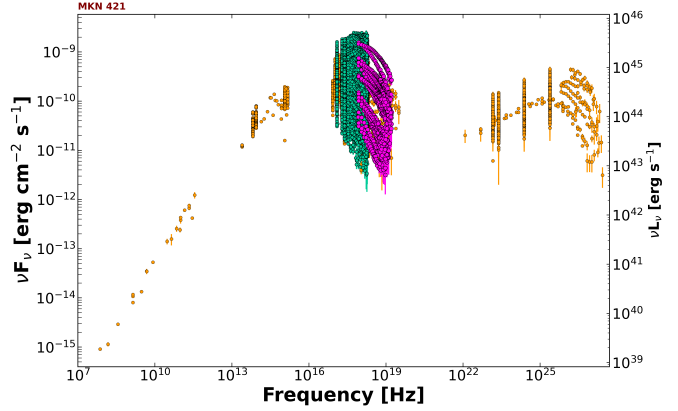


Figure 11. The SED of Mkn 421 build with *NuSTAR* (magenta) Swift-XRT (green) and multi-frequency archival data (orange). The *NuSTAR* data are from our analysis, the Swift-XRT points are from Giommi et al. (2021), and the archival data have been retrieved using the VOU_BlaZars and the SSDC SED Builder tools.

been monitored for many years with different instruments. *NuSTAR* observed this source 25 times between 2012 and 2021. The 2012 pointings were part of cross-calibration campaigns carried by the International Astronomical Consortium for High Energy Calibration (IACHEC) with Chandra, *NuSTAR*, *Swift*, Suzaku, and XMM-Newton observatories on 3C 273 and PKS 2155-304 (see Madsen et al. 2017). Combining the 2012 observations with data at other frequencies, Madsen et al. (2015b) showed that the *NuSTAR* spectrum cannot be fit simply by an absorbed power law, but the fit has residuals above ~ 20 keV, thus they investigated the coronal emission and put constraints on a weak Compton reflection component in the hard X-ray band. Fig. 10 shows the X-ray flux of 3C 273 in different snapshots, while the multiwavelength SED is shown in Fig. 12. The 3-10 keV flux does not show large variations with an average value of $\simeq 6.51 \times 10^{-11}$ erg cm $^{-2}$ s $^{-1}$; in the considered period, the highest and lowest flux differs only 3.1 times. In our analysis we did not find any correlation between the photon index (Γ) and the flux, although Γ changed significantly between different observations. During 2012, the photon index was mostly in the range $1.50 - 1.60$ while in later observations, it softened to values > 1.60 . The X-ray flux of 3C 273 versus the photon index is shown in Fig. 8. In this X-ray range, the emission is due to the rising part of the inverse Compton component, which is defined by the power-law index of the emitting electrons. Such a change can be easily explained by related changes in the emitting electron spectrum.

5.3 3C 279

3C 279 is a well-known FSRQ at $z = 0.536$ (Marziani et al. 1996). *NuSTAR* observed three times this source, twice in 2014 and one time in 2021. The corresponding SED is shown in Fig 13. The best fit value of Γ from our fits is ≤ 1.90 , consistent with an LBL-like object where the hard X-rays are from SSC emission of synchrotron emitting electrons. Although three observations are not sufficient to attempt to find statistically meaningful correlations between different parameters, we can report that the 3.0-10 keV flux significantly varied from $\sim 8 \times 10^{-12}$ erg cm $^{-2}$ s $^{-1}$ on MJD 56642.2 and 59317.1 to $\sim 1.85 \times 10^{-11}$ erg cm $^{-2}$ s $^{-1}$ on MJD 566578. Based on Fermi-LAT data, Hayashida et al. (2015) reported on intra-day variability and a

³ <https://tools.ssdc.asi.it/SED/>

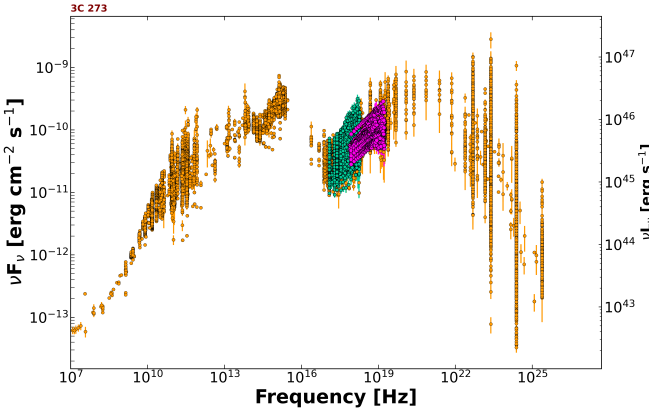


Figure 12. The SED of 3C 273. Data description and colour coding are the same as in Fig.11.

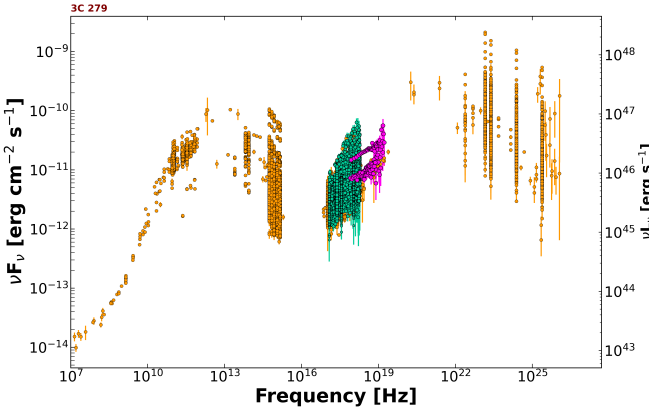


Figure 13. The SED of 3C 279. Data description and colour coding are the same as in Fig.11.

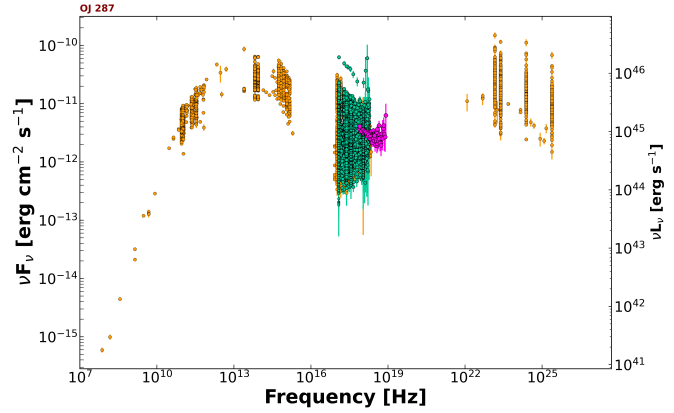


Figure 15. The SED of 5BZBJ 0854+2006 also known as OJ 287. Data description and colour coding are the same as in Fig.11.

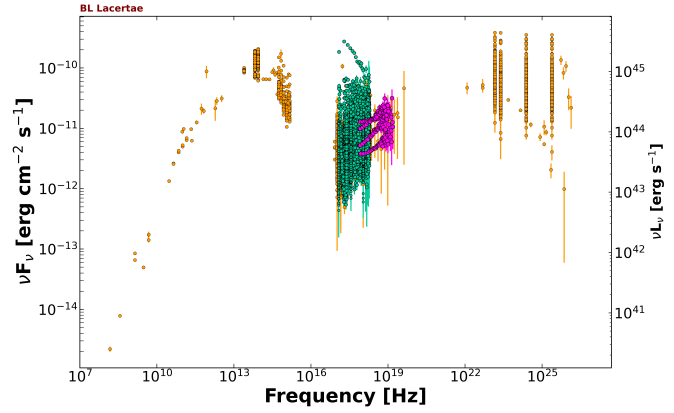


Figure 16. The SED of BL Lacertae. Data description and colour coding are the same as in Fig.11.

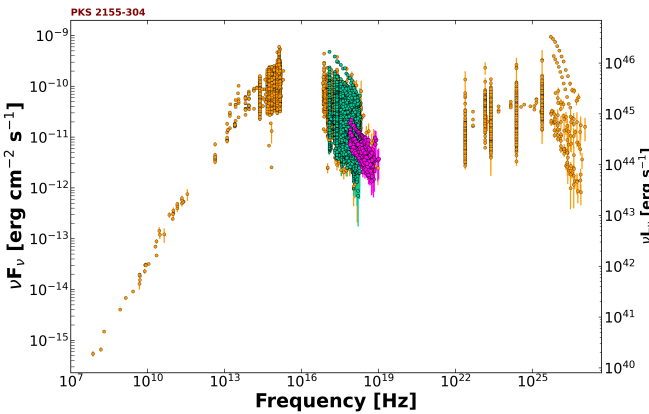


Figure 14. The SED PKS 2155-304. Data description and colour coding are the same as in Fig.11.

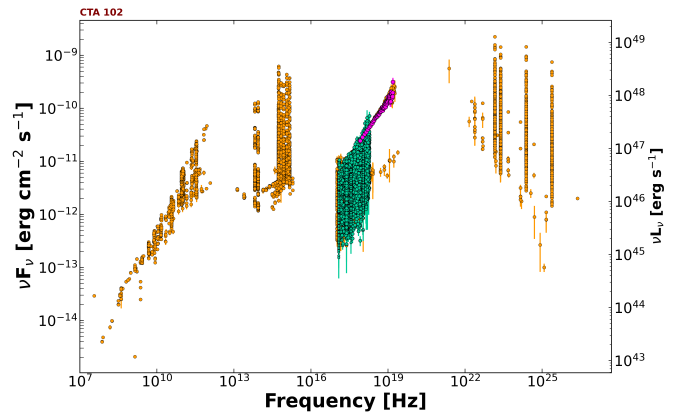


Figure 17. The SED of CTA 102. Data description and colour coding are the same as in Fig.11.

rapid γ -ray flare characterising the very high energy spectrum of this source. Yan et al. (2015), via SED modeling, attributed the X-ray emission to SSC, and the γ -ray emission to EC. This is particularly interesting as the origin of the hard X-ray emission in FSRQ-type blazars is still poorly understood (Sikora et al. 2013). In fact, FSRQs were not expected to be bright TeV sources, until TeV observatories reported the discovery of strong and highly variable emission in a number of them, including 3C 279 (MAGIC Collaboration et al. 2008). It has been then suggested that the TeV emission originates from a tail of high-energy electrons, whose synchrotron emission would appear in the hard X-ray band changing the spectral shape to softer slope, i.e. from $\Gamma \sim 1.5$ to $\Gamma \sim 2$ (see e.g. Donnarumma et al. 2013). Therefore, it is particularly important to study in detail the hard X-ray emission from such sources; on the other hand, it is clear that *NuSTAR* data alone cannot totally unveil the complexity of 3C 279. Future observations, especially obtaining X-ray polarimetry data (in't Zand et al. 2019), will help to better constrain the emission mechanism(s).

5.4 PKS 2155-304

PKS 2155-304 is a BL Lac at $z = 0.117$ (Falomo et al. 1993), detected well above the sensitivity limit at TeV energies (Chadwick et al. 1999). Giommi et al. (2002) reported results from three BeppoSAX observations, during which the spectral curvature remained in a narrow range (0.27–0.3) while the flux changed from 2.5 to 8.3×10^{-11} erg cm $^{-2}$ s $^{-1}$. Massaro et al. (2008) showed that in this source the X-ray emission is the high-energy end of the synchrotron emission, and that the SED peak location was falling outside the observational X-ray range. *NuSTAR* observed PKS 2155-304 nine times between 2012 and 2013. First results were reported by Madejski et al. (2016). The source flux was varying between $(5.57 \pm 0.16) \times 10^{-12}$ erg cm $^{-2}$ s $^{-1}$ and $(1.67 \pm 0.15) \times 10^{-11}$ erg cm $^{-2}$ s $^{-1}$ in the 3–10 keV band. As shown in Fig. 8, this HBL object has a Γ in the range 2.58–3.03 and does not show any evidence for a correlation between the photon index and the flux. On the other hand, the curvature parameter β switched between negative and positive values and is correlated with the source flux ($P_{cc}=0.92$ and $P(<r)=0.0004$), as in the case for Mkn 421, see Fig. 7. This may be due to a varying mix between the end of the synchrotron emission and the rise of the IC component. When the synchrotron component is bright and dominates the overall flux the spectrum is convex, whereas when the synchrotron emission is low the flux from the hard IC component is not negligible and the overall spectral curvature changes to a slightly concave shape.

5.5 OJ 287

OJ 287, also known as 5BZB J0854+2006, is a well-studied blazar at $z = 0.306$. It is considered the best candidate AGN for hosting a supermassive binary black hole (see e.g. Britzen et al. 2018). Recently, Meyer et al. (2019) described a low-state Fermi-LAT γ -ray spectrum associated with the kpc scale jet of OJ 287 that is consistent with the predictions of the IC/CMB model for their X-ray emission. However, Pal et al. (2020) reported a strong soft X-ray excess in the X-ray spectrum of OJ287 using XMM-Newton observations. Furthermore, Langejahn et al. (2020) showed that the *Swift*-BAT spectrum (20–100 keV) is well-described by a power-law with $\Gamma = 1.31$, using the 105-months *Swift*-BAT survey. *NuSTAR* observed OJ287 twice during two major flare events detected by Swift (in 2017 and 2020): although the 3.0–10.0 keV X-ray flux was similar ($\approx 3.5 \times 10^{-12}$ erg cm $^{-2}$ s $^{-1}$)

during these observations, the photon index varied. It was 2.03 ± 0.04 in 2017 and 2.42 ± 0.06 in 2020. These photon indices are significantly different than those estimated in the 0.1–50 keV band by BeppoSAX: in fact, these observations can be fitted to a power-law with $\Gamma = 1.95^{+0.30}_{-0.29}$ (24-Nov-1997) and $\Gamma = 1.64^{+0.22}_{-0.20}$ (20-Nov-2001, see Tab. 3 in Donato et al. 2005b). Therefore the observations by BeppoSAX and *NuSTAR* were probing probably two different source states. The observed multiwavelength SED during the flare activities of OJ 287 have been attributed to the emerging of a HBL-like broadband non-thermal emission component due to the tail of high-energy electrons generating synchrotron and dominating over IC in the hard X-ray band (see e.g. Komossa et al. 2020; Kushwaha et al. 2020). The combination of Swift-XRT and *NuSTAR* observations shown in Fig. 15 (green and magenta points respectively) show an X-ray spectrum that is dominated by a flat IC component during faint states and by the steep tail of the synchrotron component during high states. The two *NuSTAR* observations, which were performed when the source was in intermediate intensity state, clearly caught both components.

5.6 BL Lacertae

BL Lacertae, the prototype of the class of BL Lac objects, is a remarkable blazar not only for historical reasons and for its brightness, but also because it occasionally shows the presence of a broad H-alpha line (Corbett et al. 1996; Capetti et al. 2010), temporarily contradicting the definition of BL Lac objects as sources with featureless optical spectrum. The Swift-XRT data of this object also shows a widely changing behaviour (green points in Fig. 16), with a typically hard and variable X-ray spectrum, but also large soft X-ray flares (the largest one recorded in late 2020) during which the X-ray slope becomes much steeper, likely as the result of the synchrotron peak shifting to higher energies, turning this source from an IBL into a HBL blazar. The HBL component was interpreted as due to the emergence of synchrotron emission from freshly accelerated particles in a second emission zone (Sahakyan & Giommi 2021). *NuSTAR* observed BL Lac three times (Rani et al. 2017), in all cases detecting a hard X-ray spectrum, with a further flattening above 10 keV in at least two occasions (magenta points in Fig. 16). One of the *NuStar* observations was carried out five days after the large flare of 2020. The corresponding spectrum is the one with intermediate intensity and sharply hardening slope at high energies (see Fig. 16), probably indicating the on-set of a second, much harder component, detected also during the faintest state, independent of the softer (~ 1 –10 keV) X-ray emission and possibly related to the γ -ray emission. Detailed modeling of BL Lacertae SEDs between 2008 and 2021, including the periods of *NuSTAR* observations, is presented in Sahakyan & Giommi (2021).

5.7 CTA 102

CTA 102 is among the brightest FSRQs in the high energy γ -ray band despite its large distance, at $z = 1.037$. Fermi-LAT observations revealed that the flux of this blazar sometimes exceeds 10^{-5} photon cm $^{-2}$ s $^{-1}$ (Gasparyan et al. 2018). CTA 102 was observed by *NuSTAR* only once in 2016, during a major flare when it was also bright in γ -rays. As shown by the SED of Fig. 17, *NuSTAR* data probe the rise of the IC component at its maximum state ever observed in the hard X-rays. Our result ($\Gamma \sim 1.3$) is fully consistent with an earlier work (Gasparyan et al. 2018), which also showed that *Swift* monitoring detected a harder when brighter behaviour. The broadband SED of CTA 102, including the *NuSTAR* data (see

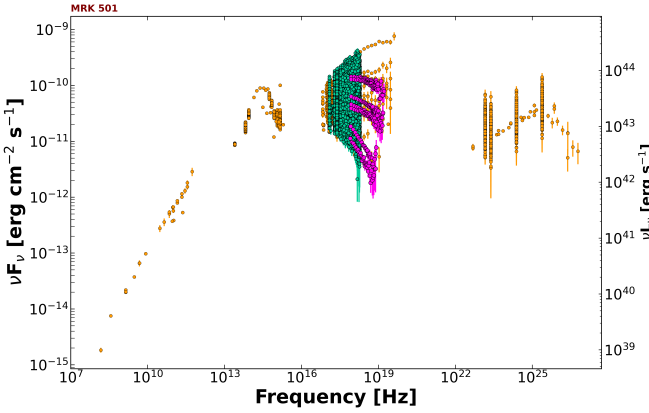


Figure 18. The SED of Mkn 501. Data description and colour coding are the same as in Fig. 11.

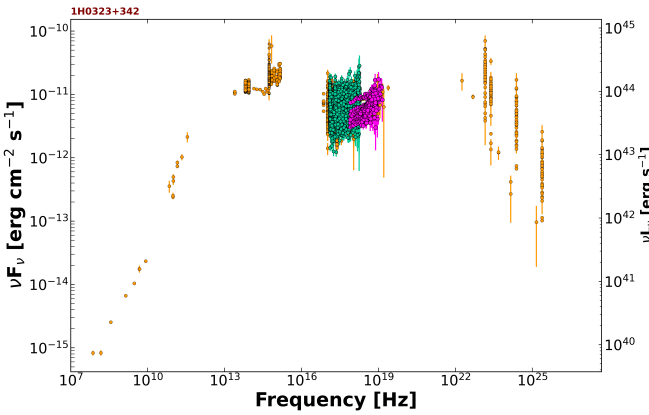


Figure 19. The SED of 1H 0323+342. Data description and colour coding are the same as in Fig. 11.

Fig. 17) was modeled assuming that the jet dissipation occurs close (within BLR) or far from (outside BLR) the central source. The SED of CTA 102 from X-ray to γ -ray bands was modeled considering the IC scattering of synchrotron, or BLR reflected, or torus photons (Sahakyan 2020).

5.8 Mkn 501

Mkn 501, a nearby ($z = 0.033$) HBL blazar (de Vaucouleurs et al. 1991) characterised by one the highest observed ν_{peak} values (Pian et al. 1998) and among the first BL Lac objects detected at TeV energies (Weekes et al. 1996; Whipple Collaboration: A. C. Breslin et al. 1999; Quinn et al. 1999). Its SED and variability properties have been widely studied based on many observations, including *NuSTAR* data and on multi-wavelength campaigns (e.g. Furniss et al. 2015; MAGIC Collaboration et al. 2020). *NuSTAR* observed this source 7 times between 2013 and 2018. Our analysis shows that as in the case of Mkn 421, Mkn 501 exhibits a typical harder when brighter behaviour. This behaviour is also evident in Fig. 8, which shows that the photon index is strongly anti-correlated with the 3-30 keV band flux ($P_{cc}=0.95, P(<r)=0.001$). The hardest index of 2.08 ± 0.01 was observed on MJD 56485.91 when the 3.0-10

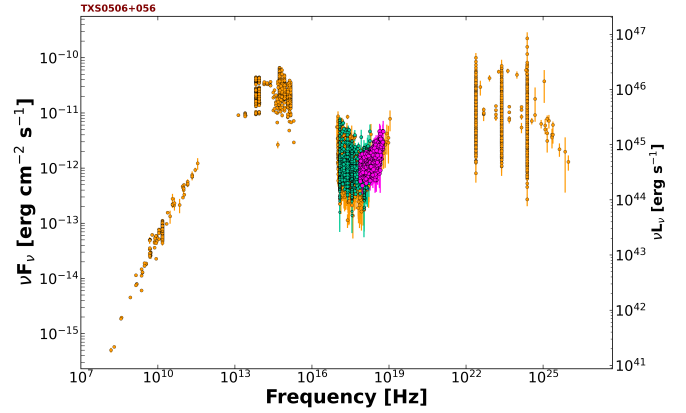


Figure 20. The SED of TXS0506+056. Data description and colour coding are the same as in Fig. 11.

keV flux was $(1.56 \pm 0.07) \times 10^{-10} \text{ erg cm}^{-2} \text{ s}^{-1}$. Interestingly, the curvature term β of *logpar* is well constrained in all the observations, and consistent with 0 in May 2017. However, β does not seem to be correlated with the flux, at variance with Mkn 421. From the SED of Fig. 18 we can infer that *NuSTAR* observations trace the high energy tail of the synchrotron emission.

5.9 1H 0323+342

1H 0323+342 is a nearby source ($z = 0.061$, Marcha et al. 1996), characterized by a flat radio spectrum and an IBL-like SED. It is listed among the blazars of uncertain type in the BZCAT catalog, however it has been classified by other authors as a γ -ray emitting narrow-line Seyfert 1 (γ NLS1), a rare class of AGNs with low black hole masses (see e.g. Paliya et al. 2014). In these sources, the jet emission contributes to the hard X-ray radiation, resulting in power-law dominated spectra. Kynoch et al. (2018) found that the broadband SED of 1H 0323+342 shows a high Compton dominance, as for FSRQs, but the luminosity is similar to a BL Lac. Furthermore, they reported the detection of a weak iron line feature with XMM-Newton. The multiwavelength SED of 1H 0323+342 and the X-ray (Swift-XRT) and γ -ray (Fermi-LAT) light curves are presented in Baghmanyan & Sahakyan (2018). *NuSTAR* observed this source 7 times (once in 2014 and the remaining 6 times in 2018). In these observations, the flux was found to be mostly at the level of $(4 - 6) \times 10^{-12} \text{ erg cm}^{-2} \text{ s}^{-1}$ and only on MJD 58350.62 it increased up to $(9.13 \pm 0.03) \times 10^{-12} \text{ erg cm}^{-2} \text{ s}^{-1}$. The photon index remained approximately constant ($\Gamma \sim 1.8$) in all observations. Recently, Mundo et al. (2020) presented X-ray spectral and timing analyses using all *NuSTAR* data together with simultaneous *XMM-Newton* coverage, showing that the X-ray emission in the 0.5-79 keV range (soft excess and iron line) can be described with a combination of a black body component and relativistic reflection model. They also found a hard excess at high energies, which can be explained as the contribution of non-thermal jet emission to the hard X-ray spectrum. Fig. 19 shows the SED of 1H 0323+342.

5.10 TXS 0506+056

TXS 0506+056 is a relatively bright BL Lac object with an IBL-like SED. This blazar became famous and widely studied after its asso-

ciation in September 2017 with the high-energy neutrino IceCube-170922A (IceCube Collaboration et al. 2018b,a; Padovani et al. 2018; Ansoldi et al. 2018). Before the occurrence of this event no redshift estimation was available for this object. Shortly afterward Paiano et al. (2018) obtained a high quality optical spectrum at the 10.4 m Gran Telescopio Canarias, which revealed very weak emission lines at the redshift of $z = 0.3365$. Padovani et al. (2019) showed that this source is in fact a masquerading BL Lac, that is a blazar that is intrinsically a FSRQ where the disk and broad-line emission is present but completely diluted by the strong non-thermal radiation from the jet. As part of the intense follow-up campaign aimed at studying in detail the likely electromagnetic counterpart to IceCube-170922A *NuSTAR* observed this blazar 18 times between 2017 and 2021. Our analysis does not show any correlation between different parameters, e.g. Γ versus flux. The photon index is hard with a mean of 1.67 and does not change substantially in different observations. The 3.0–10 keV X-ray flux is also relatively constant with only about a factor 2 difference between the highest and lowest states. The SED of this source is plotted in Fig. 20. The origin of multiwavelength emission from this source has been widely discussed in the literature where leptonic, hadronic and lepto-hadronic models have been considered (e.g., see Ansoldi et al. 2018; Keivani et al. 2018; Murase et al. 2018; Sahakyan 2018; Righi et al. 2019; Cerruti et al. 2019; Gao et al. 2019; Gasparyan et al. 2022).

6 FINAL COMMENTS

We have compiled *NuBlazar*, the first catalogue of hard X-ray spectra and spectral fit results through a standard processing of all the observations of the blazars included in the *NuSTAR* public archive as of September 2021. This database, which is analogous to the one presented by Giommi et al. (2021) for the sample of blazars frequently observed by Swift-XRT, includes 253 observations of 126 individual sources. The spectral data, along with other multi-frequency archival data sets, such as those that can be retrieved via e.g. the VOU_BlaZar tool and the SSDC SED builder, can be combined to build time-dependent SEDs and can be used for various purposes, including detailed physical model fitting. One such example is the recent work of Sahakyan & Giommi (2021), which fitted blazar models to 13 years of broad-band multi-frequency observations of BL Lacertae, the prototype of the class of blazars.

The sample of blazars observed by *NuSTAR* is heterogeneous as it is the result of a wide range of uncorrelated scientific projects carried out over the years as part of the guest observers and other *NuSTAR* observation programs. As such it does not accurately represent the underlying population of blazars; however it includes most of the well known objects, and it is sufficiently large to encompass blazars of all types.

The SEDs of the sources in the sample, some of which are shown from Fig. 11 to Fig. 20 confirm that *NuSTAR* probes the steep end of the very variable synchrotron emission in most HBL sources and of the hard Inverse Compton radiation in IBL and LBL blazars. In some cases, like OJ 287, both components have been detected (see Fig. 15). Within the statistical limits of the sample we note that the X-ray spectral slope in the *NuSTAR* energy range is a good predictor of the SED type of blazars independently of their flux. This is clear from Fig. 6 where HBLs and LBLs, are well separated, while IBLs are mostly located in the LBL area with only a few exceptions that occur when ν_{peak} moves to higher values.

Another well known characteristics of blazars' X-ray spectra is the presence of curvature, usually represented by a log parabola model

(Massaro et al. 2004a). In the *NuSTAR* energy band our results show that this feature is significantly detected (see Figs. 5) only in bright HBL sources where its amount depends on flux level (Fig. 7), likely reflecting the known correlation between ν_{peak} and source intensity (Giommi et al. 2021).

In closing, *NuSTAR* data had proven to be extremely suitable to investigate blazars properties (e.g. Γ , α and β), thus they are fundamental complement for currently operating X-ray mission such as IXPE (Weisskopf et al. 2016) that will provide the first spectro-polarimetric data.

7 ACKNOWLEDGEMENTS

The authors thank the referee for his/her useful comments to the paper. RM thanks Fausto Vagnetti for discussions and acknowledges financial support of INAF (Istituto Nazionale di Astrofisica), Osservatorio Astronomico di Roma, ASI (Agenzia Spaziale Italiana) under contract to INAF: ASI 2014-049-R.0 dedicated to SSDC. We acknowledge the use of data, analysis tools and services from the Open Universe platform, the ASI Space Science Data Center (SSDC), the Astrophysics Science Archive Research Center (HEASARC), the Astrophysics Data System (ADS), and the National Extra-galactic Database (NED). This work is based on observations obtained with: the *NuSTAR* mission, a project led by the California Institute of Technology, managed by the Jet Propulsion Laboratory and funded by NASA. NS acknowledges the support by the Science Committee of RA, in the frames of the research projects No 20TTCG-1C015 and 21T-1C260.

8 DATA AVAILABILITY

In agreement with our previous works based on the *Swift_deepsky* (Giommi et al. 2019) and the *Swift_xrtproc* software tools (Giommi et al. 2021), the *NuSTAR_Spectra* pipeline used in this work are made available as part of the OU and ASI Space Science Data Center's activities. All spectral fits products and SEDs of the sources observed by *NuSTAR*, generated as part of this work, are available either through the the SSDC web tools⁴ or within the OU platform in different forms, such as:

- a dedicated SSDC interactive web table at <https://www.ssdc.asi.it/nustarblaz/>
- through the VOU-BlaZars and other tools within the OU portal⁵
- through the BSDC VO query interface <http://vo.bsdc.icranet.org/>
- through the SSDC SED builder tool⁶.

REFERENCES

- Abdo A., et al., 2010, *ApJ*, 716, 30
 Acciari V. A., et al., 2020, *ApJS*, 248, 29
 Acciari V. A., et al., 2021, *MNRAS*, 504, 1427
 Ackermann M., et al., 2015a, VizieR Online Data Catalog, p. J/ApJ/810/14
 Ackermann M., et al., 2015b, *ApJ*, 810, 14
 Aharonian F. A., 2000, *New Astron.*, 5, 377

⁴ <https://www.ssdc.asi.it/>

⁵ <https://openuniverse.asi.it>

⁶ <https://tools.ssdc.asi.it/SED/>

- Ajello M., et al., 2014, *ApJ*, **780**, 73
- Allevato V., Paolillo M., Papadakis I., Pinto C., 2013, *ApJ*, **771**, 9
- Ansoldi S., et al., 2018, *ApJ*, **863**, L10
- Arnaud K. A., 1996, in Jacoby G. H., Barnes J., eds, Astronomical Society of the Pacific Conference Series Vol. 101, Astronomical Data Analysis Software and Systems V p. 17
- Baghmanyan V., Sahakyan N., 2018, *International Journal of Modern Physics D*, **27**, 1844001
- Baloković M., et al., 2016, *ApJ*, **819**, 156
- Bhatta G., Mohorian M., Bilinsky I., 2018, *A&A*, **619**, A93
- Bianchi S., Maiolino R., Risaliti G., 2012, *Advances in Astronomy*, **2012**, 782030
- Blackburn J. K., 1995, in Shaw R. A., Payne H. E., Hayes J. J. E., eds, Astronomical Society of the Pacific Conference Series Vol. 77, Astronomical Data Analysis Software and Systems IV p. 367
- Błażejowski M., Sikora M., Moderski R., Madejski G. M., 2000, *ApJ*, **545**, 107
- Böttcher M., Reimer A., Sweeney K., Prakash A., 2013, *ApJ*, **768**, 54
- Britzen S., et al., 2018, *MNRAS*, **478**, 3199
- Capetti A., Raiteri C. M., Buttiglione S., 2010, *A&A*, **516**, A59
- Cash W., 1979, *ApJ*, **228**, 939
- Cerruti M., Zech A., Boisson C., Emery G., Inoue S., Lenain J.-P., 2019, *MNRAS*, **483**, L12
- Chadwick P. M., et al., 1999, *ApJ*, **513**, 161
- Chang Y. L., Arsioli B., Giommi P., Padovani P., Brandt C., 2019a, VizieR Online Data Catalog, pp J/A+A/632/A77
- Chang Y. L., Arsioli B., Giommi P., Padovani P., Brandt C. H., 2019b, *A&A*, **632**, A77
- Corbett E. A., Robinson A., Axon D. J., Hough J. H., Jeffries R. D., Thurston M. R., Young S., 1996, *MNRAS*, **281**, 737
- Dermer C. D., Schlickeiser R., 1993, *ApJ*, **416**, 458
- Donato D., Sambruna R. M., Gliozzi M., 2005a, *A&A*, **433**, 1163
- Donato D., Sambruna R. M., Gliozzi M., 2005b, *A&A*, **433**, 1163
- Donnarumma I., Tramacere A., Turriziani S., Costamante L., Campana R., De Rosa A., Bozzo E., 2013, in European Physical Journal Web of Conferences. p. 04015 ([arXiv:1310.6965](https://arxiv.org/abs/1310.6965))
doi:10.1051/epjconf/20136104015
- Falomo R., Pesce J. E., Treves A., 1993, *ApJ*, **411**, L63
- Furniss A., Noda K., Boggs S., Chiang J., Christensen F., Craig W., Giommi P., et al. 2015, *ApJ*, **812**, 65
- Gallo L. C., Blue D. M., Grupe D., Komossa S., Wilkins D. R., 2018, *MNRAS*, **478**, 2557
- Gao S., Fedynitch A., Winter W., Pohl M., 2019, *Nature Astronomy*, **3**, 88
- Gasparyan S., Sahakyan N., Baghmanyan V., Zargaryan D., 2018, *ApJ*, **863**, 114
- Gasparyan S., Bégué D., Sahakyan N., 2022, *MNRAS*, **509**, 2102
- Ghisellini G., et al., 2019, *A&A*, **627**, A72
- Giannì S., de Rosa A., Bassani L., Bazzano A., Dean T., Ubertini P., 2011, *MNRAS*, **411**, 2137
- Giommi P., Padovani P., 2021, arXiv e-prints, p. [arXiv:2112.06232](https://arxiv.org/abs/2112.06232)
- Giommi P., Menna M. T., Padovani P., 1999, *MNRAS*, **310**, 465
- Giommi P., Capalbi M., Fiocchi M., Memola E., Perri M., Piranomonte S., Rebecchi S., Massaro E., 2002, in Giommi P., Massaro E., Palumbo G., eds, Blazar Astrophysics with BeppoSAX and Other Observatories. p. 63 ([arXiv:astro-ph/0209596](https://arxiv.org/abs/astro-ph/0209596))
- Giommi P., Padovani P., Polenta G., Turriziani S., D'Elia V., Piranomonte S., 2012, *MNRAS*, **420**, 2899
- Giommi P., et al., 2019, *A&A*, **631**, A116
- Giommi P., et al., 2020a, in S. F., ed., Space Capacity Building in the XXI Century. Studies in Space Policy. Springer, pp 377–386 ([arXiv:1805.08505](https://arxiv.org/abs/1805.08505))
doi:<https://doi.org/10.1007/978-3-030-21938-3>
- Giommi P., Glauch T., Padovani P., Resconi E., Turcati A., Chang Y. L., 2020b, *MNRAS*, **497**, 865
- Giommi P., et al., 2021, *MNRAS*, **507**, 5690
- Hi4PI Collaboration et al., 2016, *A&A*, **594**, A116
- Harrison F. A., et al., 2013, *ApJ*, **770**, 103
- Hayashida M., et al., 2015, *ApJ*, **807**, 79
- IceCube Collaboration et al., 2018a, *Science*, **361**, 147
- IceCube Collaboration et al., 2018b, *Science*, **361**, 147
- Kapanadze B., et al., 2016, *ApJ*, **831**, 102
- Keivani A., et al., 2018, *ApJ*, **864**, 84
- Komossa S., Grupe D., Parker M. L., Valtonen M. J., Gómez J. L., Gopakumar A., Dey L., 2020, *MNRAS*, **498**, L35
- Kushwaha P., Sarkar A., Gupta A. C., Tripathi A., Wiita P. J., 2020, *MNRAS*, **499**, 653
- Kynoch D., et al., 2018, *MNRAS*, **475**, 404
- Langejahn M., et al., 2020, *A&A*, **637**, A55
- Lawrence A., Papadakis I., 1993, *ApJ*, **414**, L85
- MAGIC Collaboration et al., 2008, *Science*, **320**, 1752
- MAGIC Collaboration et al., 2020, *A&A*, **637**, A86
- Maccacaro T., Gioia I. M., Maccagni D., Stocke J. T., 1984, *ApJ*, **284**, L23
- Madejski G. M., et al., 2016, *ApJ*, **831**, 142
- Madsen K. K., et al., 2015a, *ApJS*, **220**, 8
- Madsen K. K., et al., 2015b, *ApJ*, **812**, 14
- Madsen K. K., Beardmore A. P., Forster K., Guainazzi M., Marshall H. L., Miller E. D., Page K. L., Stuhlinger M., 2017, *AJ*, **153**, 2
- Mannheim K., 1993, *A&A*, **269**, 67
- Maraschi L., Ghisellini G., Celotti A., 1992, *ApJ*, **397**, L5
- Marcha M. J. M., Browne I. W. A., Impey C. D., Smith P. S., 1996, *MNRAS*, **281**, 425
- Marcotulli L., et al., 2017, *ApJ*, **839**, 96
- Marziani P., Sulentic J. W., Dultzin-Hacyan D., Calvani M., Moles M., 1996, *ApJS*, **104**, 37
- Massaro E., Perri M., Giommi P., Nesci R., 2004a, *A&A*, **413**, 489
- Massaro E., Perri M., Giommi P., Nesci R., 2004b, *A&A*, **413**, 489
- Massaro E., Perri M., Giommi P., Nesci R., Verrecchia F., 2004c, *A&A*, **422**, 103
- Massaro F., Tramacere A., Cavaliere A., Perri M., Giommi P., 2008, *A&A*, **478**, 395
- Massaro E., Maselli A., Leto C., Marchegiani P., Perri M., Giommi P., Piranomonte S., 2015, *Ap&SS*, **357**, 75
- Massaro E., Maselli A., Leto C., Marchegiani P., Perri M., Giommi P., Piranomonte S., 2016, VizieR Online Data Catalog, p. VII/274
- Mastichiadis A., Kirk J. G., 2002, *Publ. Astron. Soc. Australia*, **19**, 138
- Meyer E. T., Iyer A. R., Reddy K., Georganopoulos M., Breiding P., Keenan M., 2019, *ApJ*, **883**, L2
- Middei R., Vagnetti F., Bianchi S., La Franca F., Paolillo M., Ursini F., 2017, *A&A*, **599**, A82
- Morrison R., McCammon D., 1983, *ApJ*, **270**, 119
- Mücke A., Protheroe R. J., Engel R., Rachen J. P., Stanev T., 2003, *Astroparticle Physics*, **18**, 593
- Mundo S. A., et al., 2020, *MNRAS*, **496**, 2922
- Murase K., Oikonomou F., Petropoulou M., 2018, *ApJ*, **865**, 124
- Netzer H., 2015, *ARA&A*, **53**, 365
- Padovani P., Giommi P., 1995, *ApJ*, **444**, 567
- Padovani P., et al., 2017, *A&ARv*, **25**, 2
- Padovani P., Giommi P., Resconi E., Glauch T., Arsioli B., Sahakyan N., Huber M., 2018, *MNRAS*, **480**, 192
- Padovani P., Oikonomou F., Petropoulou M., Giommi P., Resconi E., 2019, *MNRAS*, **484**, L104
- Paiano S., Falomo R., Treves A., Scarpa R., 2018, *ApJ*, **854**, L32
- Pal M., Kushwaha P., Dewangan G. C., Pawar P. K., 2020, *ApJ*, **890**, 47
- Paliya V. S., Sahayanathan S., Parker M. L., Fabian A. C., Stalin C. S., Anjum A., Pandey S. B., 2014, *ApJ*, **789**, 143
- Paliya V. S., Böttcher M., Diltz C., Stalin C. S., Sahayanathan S., Ravikumar C. D., 2015, *ApJ*, **811**, 143
- Paolillo M., et al., 2017, *MNRAS*, **471**, 4398
- Pearson T. J., Unwin S. C., Cohen M. H., Linfield R. P., Readhead A. C. S., Seielstad G. A., Simon R. S., Walker R. C., 1981, *Nature*, **290**, 365
- Pian E., et al., 1998, *ApJ*, **492**, L17
- Ponti G., Papadakis I., Bianchi S., Guainazzi M., Matt G., Uttley P., Bonilla N. F., 2012, *A&A*, **542**, A83
- Quinn J., et al., 1999, *ApJ*, **518**, 693
- Rani P., Stalin C. S., Rakshit S., 2017, *MNRAS*, **466**, 3309
- Rector T. A., Stocke J. T., Perlman E. S., Morris S. L., Gioia I. M., 2000a, *AJ*, **120**, 1626

- Rector T. A., Stocke J. T., Perlman E. S., Morris S. L., Gioia I. M., 2000b, *AJ*, **120**, 1626
- Righi C., Tavecchio F., Pacciani L., 2019, *MNRAS*, **484**, 2067
- Sahakyan N., 2018, *ApJ*, **866**, 109
- Sahakyan N., 2020, *A&A*, **635**, A25
- Sahakyan N., Giommi P., 2021, arXiv e-prints, p. [arXiv:2108.12232](https://arxiv.org/abs/2108.12232)
- Sbarrato T., et al., 2013, *ApJ*, **777**, 147
- Sbarrato T., et al., 2016, *MNRAS*, **462**, 1542
- Seielstad G. A., Cohen M. H., Linfield R. P., Moffet A. T., Romney J. D., Schilizzi R. T., Shaffer D. B., 1979, *ApJ*, **229**, 53
- Sikora M., Begelman M. C., Rees M. J., 1994, *ApJ*, **421**, 153
- Sikora M., Janiak M., Nalewajko K., Madejski G. M., Moderski R., 2013, *ApJ*, **779**, 68
- Stawarz L., 2014, in Ishida M., Petre R., Mitsuda K., eds, Suzaku-MAXI 2014: Expanding the Frontiers of the X-ray Universe. p. 294
- Strauss M. A., Huchra J. P., Davis M., Yahil A., Fisher K. B., Tonry J., 1992, *ApJS*, **83**, 29
- Tavecchio F., et al., 2000, *ApJ*, **543**, 535
- Turriziani S., Fraga B., Giommi P., 2019, *MNRAS*, **489**, 3307
- Unwin S. C., Cohen M. H., Biretta J. A., Pearson T. J., Seielstad G. A., Walker R. C., Simon R. S., Linfield R. P., 1985, *ApJ*, **289**, 109
- Urry C. M., Padovani P., 1995, *PASP*, **107**, 803
- Uttley P., McHardy I. M., 2005, *MNRAS*, **363**, 586
- Uttley P., McHardy I. M., Papadakis I. E., 2002, *MNRAS*, **332**, 231
- Vagnetti F., Turriziani S., Trevese D., 2011, *A&A*, **536**, A84
- Vagnetti F., Middei R., Antonucci M., Paolillo M., Serafinelli R., 2016, *A&A*, **593**, A55
- Vaughan S., Edelson R., Warwick R. S., Uttley P., 2003, *MNRAS*, **345**, 1271
- Weekes T. C., et al., 1996, *A&AS*, **120**, 603
- Weisskopf M. C., et al., 2016, in den Herder J.-W. A., Takahashi T., Bautz M., eds, Society of Photo-Optical Instrumentation Engineers (SPIE) Conference Series Vol. 9905, Space Telescopes and Instrumentation 2016: Ultraviolet to Gamma Ray. p. 990517, doi:10.1117/12.2235240
- Whipple Collaboration: A. C. Breslin et al., 1999, arXiv e-prints, pp astro-ph/9906150
- Wolter A., Celotti A., 2001, *A&A*, **371**, 527
- Yan D., Zhang L., Zhang S.-N., 2015, *MNRAS*, **454**, 1310
- Zhang Z., Gupta A. C., Gaur H., Wiita P. J., An T., Gu M., Hu D., Xu H., 2019, *ApJ*, **884**, 125
- Zhang Z., Gupta A. C., Gaur H., Wiita P. J., An T., Lu Y., Fan S., Xu H., 2021, *ApJ*, **909**, 103
- de Vaucouleurs G., de Vaucouleurs A., Corwin Herold G. J., Buta R. J., Paturel G., Fouque P., 1991, Third Reference Catalogue of Bright Galaxies
- in't Zand J. J. M., et al., 2019, *Science China Physics, Mechanics, and Astronomy*, **62**, 29506

APPENDIX A: TABLES

Table A1: The 126 individual blazars resulting by the cross-matching procedure described in Sect. 2. The name of the source is taken from the corresponding catalog. The source's redshift is quoted in column 4 and column 5 accounts for their optical classification in accordance with the *BZCAT* 5th edition (Massaro et al. 2015, 2016). We used the following code: 1= BL Lac, 2=FSRQ, 3=Blazar Uncertain type, 4= BL Lac-galaxy dominated, 5= BL Lac candidate. The SED classification relies on a visual checks and previous papers. The Obs. columns accounts for the available observations for that specific source for which alternative name is given the 8th column. Finally, the “-“ sign is used when some information is missing.

Source	Ra	Dec	z	Class	SED class	Obs	Other name
5BZQJ0010+1058	2.62919080	10.9748622	0.089	2	LBL	1	III ZW2
5BZQJ0017+8135	4.28531170	81.5855933	3.387	2	LBL	3	S5 0014+81
5BZQJ0122+0310	20.5079583	3.1673333	4.000	2	LBL	1	3EG J0122+0310
5BZBJ0123-2310	20.9099580	-23.1829170	0.404	5	HBL	1	RXS J01236-2311
5BZQJ0126+2559	21.6783025	25.9836947	2.358	2	LBL	2	4C 25.05
5BZQJ0203+1134	30.9444042	11.5792806	3.639	2	LBL	1	PKS 0201+113
5BZGJ0214+5144	33.5747080	51.7477780	0.049	4	HBL	1	2MASX J02141794+5144520
5BZQJ0217+7349	34.3783883	73.8257281	2.367	2	LBL	1	HB89 0212+735
5BZQJ0225+1846	36.2694533	18.7802128	2.690	2	LBL	2	B0222+185
5BZQJ0229-3643	37.3685375	-36.7324503	2.115	2	LBL	1	PKS 0227-369
5BZGJ0232+2017	38.2025420	20.2881390	0.139	4	HBL	6	1ES 0229+200
5BZUJ0241-0815	40.2700000	-8.25577800	0.005	3	LBL	3	NGC 1052
5BZQJ0311-7651	47.9802104	-76.8641244	0.223	2	LBL	1	HB89 0312-770
5BZUJ0324+3410	51.1715054	34.1794044	0.061	3	IBL	7	1H 0323+342
3HSPJ032523.5-563545	51.3480420	-56.5957220	-	-	HBL	1	2MASX J03252346-5635443
5BZQJ0325+2224	51.4033929	22.4001014	2.066	2	LBL	1	TXS 0322+222
5BZBJ0349-1159	57.3465830	-11.9908330	0.188	1	HBL	1	1ES 0347-121
3HSPJ035257.5-683117	58.2394580	-68.5214170	0.087	1	HBL	1	PKS 0352-686
5BZQJ0359+5057	59.8739467	50.9639336	1.512	2	LBL	1	4C 50.11
5BZQJ0403-3605	60.9739579	-36.0838644	1.417	2	LBL	1	PKS 0402-362
5BZQJ0405-1308	61.3916804	-13.1371364	0.571	2	LBL	1	HB89 0403-132
5BZUJ0407-1211	61.9517954	-12.1935164	0.573	3	IBL	1	HB89 0405-123
5BZBJ0416+0105	64.2187083	1.0899722	0.287	1	HBL	1	1ES 0414+009
3C111	64.5886550	38.0266111	0.049	2	LBL	3	4FGL J0418.2+3807
5BZUJ0433+0521	68.2962313	5.3543389	0.033	3	LBL	2	3C 120
5BZQJ0449+1121	72.2819629	11.3579436	2.153	2	LBL	1	PKS 0446+11
5BZQJ0453-2807	73.3110279	-28.1270353	2.564	2	LBL	1	PKS 0451-28
5BZQJ0501-0159	75.3033742	-1.9872931	2.291	2	LBL	1	TXS 0458-020
5BZBJ0507+6737	76.9843750	67.6234444	0.416	1	HBL	3	1ES 0502+675
5BZBJ0509+0541	77.3581850	5.6931481	0.336	1	IBL	18	TXS 0506+056
PictorA	79.9571708	-45.7070000	0.035	-	LBL	1	3FGL J0519.2-4542
5BZUJ0522-3627	80.7416025	-36.4585689	0.056	3	LBL	1	PKS 0521-36
5BZQJ0525-2338	81.2771079	-23.6363350	3.100	2	LBL	1	PMN J0525-2338
5BZQJ0530+1331	82.7350696	13.5319861	2.070	2	LBL	1	PKS 0528+134
5BZBJ0543-5532	85.9883750	-55.5353610	0.273	1	HBL	1	1RXS J054357.3-553206
5BZQJ0555+3948	88.8783567	39.8136569	2.365	2	LBL	1	B3 0552+398
5BZQJ0623-6436	95.7821250	-64.6056670	0.129	2	IBL	1	2MASX J06230765-6436211
PKS0625-354	96.7781520	-35.4875690	0.055	-	IBL	1	3FGL J0627.0-3529
5BZBJ0630-2406	97.7480417	-24.1128056	1.239	1	HBL	1	2FGL J0630.9-2406
5BZQJ0635-7516	98.9437829	-75.2713372	0.653	2	LBL	1	PKS 0637-752
PMNJ0641M0320	100.4630538	-3.3190000	-	-	LBL	1	3FGL J0641.8-0319
5BZQJ0646+4451	101.6334413	44.8546083	3.396	2	LBL	1	1Jy 0642+44
5BZBJ0710+5908	107.6252920	59.1390000	0.125	1	HBL	3	RGB J0710+591
5BZBJ0721+7120	110.4727017	71.3434342	-	1	IBL	1	S5 0716+714
5BZQJ0733+0456	113.4893750	4.9373280	3.010	2	LBL	1	BZQ J0733+0456
5BZQJ0809+5341	122.4238862	53.6903033	2.133	2	LBL	1	SDSS J080941.74+534125.0
3HSPJ081003.3-752724	122.5136670	-75.4565560	-	-	IBL	1	2FGL J0811.1-7527

Table A1: continued.

Source	Ra	Dec	z	Class	SED class	Obs	Other name
5BZQJ0841+7053	130.3515217	70.8950481	2.218	2	LBL	2	HB89 0836+710
5BZUJ0847-2337	131.7566700	-23.6172200	0.059	3	HBL	1	PMN J0847-2337
5BZBJ0854+2006	133.7036454	20.1085114	0.306	1	IBL	2	OJ +287
5BZBJ0915+2933	138.9683400	29.5566783	-	1	HBL	2	TON 396
5BZQJ0948+0022	147.2388337	0.3737661	0.585	2	LBL	1	PMN J0948+0022
5BZBJ0955+3551	148.7828290	35.8502330	0.557	1	HBL	1	BZB J0955+3551
5BZQJ0956+2515	149.2078138	25.2544583	0.712	2	LBL	1	B2 0954+25
5BZQJ1028-0844	157.1616670	-8.7440560	4.276	2	LBL	1	NGC 1052
5BZQJ1044+8054	161.0960942	80.9109564	1.254	2	LBL	1	S5 1039+81
5BZUJ1058+0133	164.6233550	1.5663400	0.890	3	LBL	1	PKS B 1055+018
5BZBJ1103-2329	165.9067083	-23.4920000	0.186	1	HBL	1	1ES 1101-232
5BZBJ1104+3812	166.1138079	38.2088331	0.030	1	HBL	26	Mkn 421
5BZBJ1120+4212	170.2002770	42.2034620	0.001	1	HBL	1	RBS 0970
5BZQJ1130-1449	172.5293854	-14.8242742	1.184	2	LBL	1	PKS 1127-14
3C264	176.2708708	19.6063169	0.021	-	HBL	1	3FGL J1145.1+1935
5BZQJ1159+2914	179.8826413	29.2455075	0.729	2	LBL	2	FBQS J1159+2914
5BZQJ1220+0203	185.0495192	2.0617292	0.240	2	LBL	1	PKS J1220+0203
5BZBJ1221+3010	185.3414208	30.1769750	0.184	1	HBL	1	1ES 1218+304
5BZQJ1222+0413	185.5939567	4.2210489	0.966	2	LBL	1	PKS 1219+04
5BZQJ1229+0203	187.2779154	2.0523883	0.158	2	LBL	25	3C 273
5BZQJ1256-0547	194.0465271	-5.7893119	1.309	2	LBL	3	3C 279
5BZQJ1321+0023	200.4148579	0.3993439	1.618	2	LBL	1	NGC 5104
5BZQJ1332-0509	203.0186025	-5.1620292	2.150	2	LBL	1	PKS 1329-049
5BZQJ1337-1257	204.4157080	-12.9568580	0.539	2	LBL	1	HB89 1334-127
5BZQJ1354-0206	208.5287304	-2.1008858	3.716	2	LBL	1	PKS 1351-018
5BZQJ1357+1919	209.2684858	19.3187144	0.720	2	LBL	1	HB89 1354+195
5BZGJ1407+2827	211.7516250	28.4540830	0.077	4	LBL	1	OQ +208
5BZQJ1424+2256	216.1587248	22.9334972	3.620	2	LBL	1	QSO B1422+231
5BZBJ1428+4240	217.1360833	42.6723889	0.129	1	HBL	2	H 1426+428
5BZQJ1429+5406	217.3411670	54.1030780	3.013	2	LBL	1	BZQ J1429+5406
5BZQJ1430+4204	217.5989233	42.0768031	4.715	2	LBL	1	GB6 B1428+4217
3C303	220.7615829	52.0270189	0.141	-	LBL	1	3FGL J1442.6+5156
5BZQJ1443+2501	220.9870508	25.0290250	0.939	2	IBL	1	PKS 1441+25
5BZUJ1459+7140	224.7815996	71.6721853	0.910	3	LBL	2	3C 309.1
5BZQJ1505+0326	226.2769879	3.4418922	0.409	2	LBL	1	SDSS J150506.47+03
5BZQJ1510+5702	227.5121765	57.0453822	4.313	2	LBL	1	TXS 1508+572
5BZUJ1511+0518	227.9219437	5.3025719	0.084	3	LBL	1	PKS 1511+0518
5BZGJ1516+0015	229.1675830	0.2505280	0.052	4	LBL	1	CGCG021-063
3HSPJ151803.6-273131	229.5149580	-27.5253060	0.140	1	HBL	1	TXS 1515-273
5BZQJ1556-7914	239.2452904	-79.2345225	0.152	2	LBL	1	PKS 1549-79
5BZQJ1559+0304	239.8790525	3.0800714	3.895	2	LBL	1	PKS J1559+0304
5BZUJ1626-2951	246.5250867	-29.8574917	0.815	3	LBL	1	PKS 1622-29
5BZQJ1642+3948	250.7450413	39.8102758	0.593	2	LBL	1	3C 345
5BZQJ1644+2619	251.1838340	26.3178640	0.144	2	IBL	1	FBQS J1644+2619
5BZBJ1653+3945	253.4675696	39.7601692	0.033	1	HBL	7	Mkn 501
5BZQJ1656-3302	254.0702210	-33.0364110	2.400	2	LBL	1	2MASS J16561677-3302127
5BZGJ1719+4858	259.8102500	48.9804170	0.024	4	LBL	1	ARP 102B
5BZQJ1723+6547	260.8089088	65.7961606	1.442	2	LBL	6	1RXS J172313.5+654803
5BZBJ1800+7828	270.1902920	78.4677780	0.680	1	LBL	1	HB89 1803+784
5BZUJ1809-4552	272.4911325	-45.8780594	0.070	3	LBL	1	PKS 1806-458
5BZUJ1829+4844	277.3824204	48.7461556	0.695	3	LBL	1	3C 380
5BZQJ1833-2103	278.4162007	-21.0610479	2.507	2	LBL	2	PKS 1830-21
5BZQJ1849+6705	282.3169679	67.0949108	0.657	2	LBL	1	8C 1849+670
5BZQJ1924-2914	291.2127500	-29.2416890	0.353	2	LBL	2	HB89 1921-293
5BZQJ1927+7358	291.9520629	73.9671025	0.302	2	LBL	1	4C 73.18
5BZBJ1936-4719	294.2337920	-47.3306110	0.265	1	HBL	1	PMN J1936-4719
5BZQJ1939-1002	294.9885688	-10.0448667	3.787	2	LBL	1	PKS J1939-1002
5BZGJ1958-3011	299.5621250	-30.1865830	0.119	4	HBL	1	1RXS J195815.6-301119
5BZBJ1959+6508	299.9993837	65.1485144	0.047	1	HBL	2	1ES 1959+650

Table A1: continued.

Source	Ra	Dec	z	Class	SED class	Obs	Other name
5BZQJ2007-4434	301.9799346	-44.5789650	0.240	2	IBL	3	PKS 2004-447
5BZQJ2011-1546	302.8154621	-15.7778481	1.178	2	LBL	1	PKS 2008-159
5BZUJ2015+3710	303.8697075	37.1831983	-	3	LBL	2	QSO B2013+370
5BZQJ2022+6136	305.5278404	61.6163344	0.228	2	LBL	1	PKS 2021+614
5BZQJ2056-4714	314.0681658	-47.2465631	1.491	2	LBL	1	PKS 2052-47
3HSPJ205642.7+494006	314.1778750	49.6681940	-	-	HBL	1	IGR J20569+4940
5BZQJ2129-1538	322.3007325	-15.6447333	3.268	2	LBL	1	PKS 2126-15
5BZBJ2146-1344	326.6539580	-13.7335000	0.001	1	HBL	1	2FHL J2146.6-1345
5BZQJ2148+0657	327.0227442	6.9607233	0.999	2	LBL	1	PKS 2145+06
5BZQJ2151-3027	327.9813496	-30.4649158	2.345	2	LBL	2	PKS 2149-306
5BZBJ2158-3013	329.7169379	-30.2255883	0.116	1	HBL	9	PKS 2155-304
5BZBJ2202+4216	330.6803804	42.2777719	0.069	1	IBL	4	BL Lac
5BZQJ2211+1841	332.9745371	18.6971839	0.070	2	IBL	1	PG 2209+184
5BZQJ2232+1143	338.1517100	11.7308100	1.037	2	LBL	1	CTA 102
3HSPJ223248.8-202226	338.2033330	-20.3739440	-	-	HBL	1	1RXS J223249.5-202232
5BZQJ2251+2217	342.9729200	22.2936900	3.668	2	LBL	1	MG3 J225155+2217
5BZGJ2313+1444	348.4889170	14.7397780	0.164	4	HBL	1	RGB J2313+147
5BZUJ2333-2343	353.4801575	-23.7279603	0.048	3	IBL	1	PKS 2331-240
5BZBJ2347+5142	356.7701670	51.7049690	0.044	1	HBL	1	2MASX J23470479+5142179
5BZBJ2359-3037	359.7829580	-30.6279440	0.165	1	HBL	1	H 2356-309

APPENDIX B: SPECTRAL FITS

Table B1: Best-fit parameters derived for the 253 blazars observations presented in this paper and modelled using a power-law absorbed for the Galaxy. Columns 1 and 2 specify the name of the source and *NuSTAR* sequence. Columns 3 and 4 account for the observation date and the length of the exposure. The Galactic column density (taken from [H14PI \(Collaboration et al. 2016\)](#), and in units of 10^{22} cm^{-2}), the photon index, the normalisation (in units of photons $\text{keV}^{-1} \text{ cm}^{-2} \text{ s}^{-1}$) and the FPMA/B inter-calibration constant are reported in columns 5, 6, 7, 8, respectively. Column 9 accounts for the ratio between the Cstat/d.o.f.. The logarithm of the 3–10 keV (S) and 10–30 keV (H) fluxes estimated using a power-law are reported in columns 10 and 11, respectively. Finally, columns 12 and 13 refer to the maximum energy below which the spectral analysis was performed and the radius (in arcsec) of the extracting region used for the source.

Name	ObsID	Time(MJD)	Exposure(s)	N_{H}	Γ	Norm	Const	$C/\text{d.o.f.}$	$\log F_{\text{S}}^{\text{p}}$	$\log F_{\text{H}}^{\text{p}}$	E_{max} (keV)	Radius (arcsec)
5BZQJ0010+1058	60301014002	58098.64652	93441	0.059	1.76±0.01	4.501±0.114	0.98±0.01	0.94	-10.881±0.003	-10.799±0.003	79	70
5BZQJ0017+8135	60001098002	57012.69861	30947	0.128	1.74±0.05	1.166±0.132	0.93±0.05	0.96	-11.460±0.009	-11.370±0.013	25	40
5BZQJ0017+8135	60001098004	57045.10486	36376	0.128	1.68±0.05	0.965±0.098	0.99±0.05	0.91	-11.495±0.009	-11.374±0.012	35	40
5BZQJ0017+8135	90201019002	57490.02500	17292	0.128	1.66±0.07	0.965±0.144	0.98±0.07	0.89	-11.479±0.015	-11.348±0.020	25	40
5BZQJ0122+0310	60373002002	58131.87222	30717	0.030	1.38±0.17	0.088±0.033	0.97±0.15	0.85	-12.346±0.095	-12.081±0.056	20	30
5BZBJ0123-2310	60101060002	57273.18125	21719	0.012	2.45±0.07	4.541±0.616	0.91±0.06	0.91	-11.382±0.010	-11.645±0.021	25	40
5BZQJ0126+2559	60201047002	57768.05625	41657	0.067	1.58±0.07	0.395±0.056	1.00±0.06	0.92	-11.800±0.013	-11.627±0.016	25	40
5BZQJ0126+2559	60367001002	58121.66736	19830	0.067	1.60±0.11	0.341±0.082	1.09±0.11	0.79	-11.884±0.017	-11.723±0.036	20	40
5BZQJ0203+1134	60201010002	57700.71944	31588	0.059	1.71±0.14	0.239±0.070	1.03±0.13	0.73	-12.120±0.025	-12.012±0.044	20	30
5BZGJ0214+5144	60160094002	57417.38263	21364	0.146	2.05±0.04	4.264±0.337	0.94±0.04	0.99	-11.127±0.008	-11.191±0.011	35	60
5BZQJ0217+7349	60160099002	57442.45902	30254	0.266	1.54±0.03	1.495±0.099	0.98±0.03	0.96	-11.196±0.006	-11.000±0.011	35	60
5BZQJ0225+1846	60001101002	57015.43819	31973	0.094	1.53±0.02	2.612±0.115	0.96±0.02	1.00	-10.944±0.004	-10.747±0.005	65	70
5BZQJ0225+1846	60001101004	57040.16736	37398	0.094	1.64±0.02	2.197±0.117	0.99±0.03	0.95	-11.109±0.006	-10.970±0.009	45	60
5BZQJ0229-3643	60367002002	57975.49027	23205	0.024	1.35±0.29	0.050±0.032	0.74±0.20	0.84	-12.527±0.054	-12.243±0.070	20	30
5BZGJ0232+2017	10702609002	59434.24375	94265	0.078	2.25±0.03	3.518±0.185	1.02±0.03	0.91	-11.351±0.004	-11.514±0.008	65	50
5BZGJ0232+2017	10702609004	59437.20208	57535	0.078	2.31±0.03	4.007±0.273	1.01±0.03	0.92	-11.340±0.007	-11.534±0.009	45	50
5BZGJ0232+2017	10702609006	59439.21597	55520	0.078	2.28±0.03	4.578±0.281	1.04±0.03	0.92	-11.257±0.006	-11.434±0.008	45	50
5BZGJ0232+2017	60002047002	56567.00416	16233	0.078	2.03±0.03	8.333±0.520	0.99±0.03	0.89	-10.818±0.006	-10.872±0.010	45	70
5BZGJ0232+2017	60002047004	56570.97986	20258	0.078	2.02±0.02	9.027±0.448	1.01±0.02	0.96	-10.776±0.005	-10.824±0.007	65	70
5BZGJ0232+2017	60002047006	56575.96597	17993	0.078	1.94±0.03	7.894±0.417	0.98±0.03	0.97	-10.776±0.005	-10.785±0.008	45	70
5BZUJ0241-0815	60061027002	56337.41041	15564	0.029	1.18±0.05	0.618±0.065	1.02±0.05	1.05	-11.299±0.011	-10.929±0.013	25	60
5BZUJ0241-0815	60201056002	57770.00069	59604	0.029	1.29±0.02	0.965±0.040	0.97±0.02	1.28	-11.196±0.005	-10.885±0.005	79	60
5BZUJ0241-0815	90701624002	59412.24722	20265	0.029	1.24±0.04	0.681±0.064	1.03±0.05	1.04	-11.306±0.009	-10.968±0.012	35	50
5BZQJ0311-7651	60160145002	57466.71597	29755	0.078	1.79±0.05	1.249±0.141	0.99±0.05	0.98	-11.466±0.011	-11.401±0.015	25	40
5BZUJ0324+3410	60061360002	56731.73680	101447	0.117	1.80±0.02	2.619±0.090	1.02±0.02	0.90	-11.151±0.003	-11.089±0.005	79	60
5BZUJ0324+3410	60402003002	58344.63958	36233	0.117	1.79±0.03	2.278±0.142	0.99±0.03	0.90	-11.203±0.006	-11.136±0.008	45	60
5BZUJ0324+3410	60402003004	58348.59444	29592	0.117	1.83±0.04	1.876±0.161	1.00±0.04	0.85	-11.320±0.008	-11.274±0.011	35	50
5BZUJ0324+3410	60402003006	58350.61180	26273	0.117	1.84±0.03	3.879±0.220	1.01±0.03	0.86	-11.007±0.006	-10.962±0.008	45	70
5BZUJ0324+3410	60402003008	58354.63958	25443	0.117	1.83±0.04	2.182±0.185	1.02±0.04	0.93	-11.250±0.007	-11.202±0.013	35	50
5BZUJ0324+3410	60402003010	58366.58402	30256	0.117	1.76±0.03	2.090±0.150	1.01±0.03	0.95	-11.218±0.007	-11.136±0.011	35	60
5BZUJ0324+3410	60402003012	58370.60486	27653	0.117	1.75±0.05	1.417±0.136	0.96±0.04	0.89	-11.380±0.008	-11.294±0.014	35	50
3HSPI032523.5-563545	60160154002	58770.78541	23036	0.023	2.59±0.08	4.503±0.661	1.00±0.07	0.91	-11.492±0.013	-11.830±0.022	25	40
5BZQJ0325+2224	60101079002	57334.10833	22165	0.091	1.29±0.10	0.220±0.048	1.01±0.09	0.84	-11.839±0.017	-11.526±0.025	20	40
5BZB10349-1159	60101036002	57275.20208	33307	0.030	2.36±0.05	4.225±0.389	1.00±0.04	0.95	-11.355±0.007	-11.577±0.013	35	50
3HSPI035257.5-583117	60160169002	57492.32013	21196	0.070	2.31±0.03	9.640±0.619	1.00±0.03	1.00	-10.956±0.005	-11.148±0.010	35	70
5BZQJ0359+5057	60160177002	57370.98333	20494	0.692	1.56±0.04	1.759±0.137	1.00±0.04	0.88	-11.152±0.007	-10.962±0.010	35	60
5BZQJ0403-3605	60160179002	57518.84097	18803	0.007	1.51±0.08	0.529±0.090	0.94±0.07	0.90	-11.625±0.016	-11.422±0.019	25	40

Table B1: continued.

Name	ObsID	Time(MJD)	Exposure(s)	N _H	Γ	Norm	Const	C/d.o.f.	$\log F_{\text{S}}^{\text{pl}}$	$\log F_{\text{H}}^{\text{pl}}$	E _{max} (keV)	Radius (arcsec)
5BZQJ0405-1308	60160181002	58838.56319	21186	0.041	1.63±0.07	0.857±0.121	1.03±0.07	0.87	-11.506±0.014	-11.361±0.019	25	40
5BZUJ0407-1211	60463011002	58936.53541	33601	0.035	1.75±0.03	1.948±0.133	1.02±0.03	0.90	-11.240±0.006	-11.156±0.008	35	60
5BZB0416+0105	60101035002	57351.70902	34260	0.077	2.79±0.05	10.254±0.906	0.91±0.04	0.98	-11.271±0.008	-11.706±0.013	35	50
3C111	60202061002	58113.69100	22881	0.285	1.77±0.01	13.929±0.431	0.98±0.02	0.96	-10.405±0.003	-10.325±0.005	79	70
3C111	60202061004	58116.10900	52979	0.285	1.76±0.01	12.491±0.264	0.98±0.01	0.98	-10.448±0.002	-10.365±0.003	79	70
3C111	60202061006	58487.38900	55429	0.285	1.68±0.01	7.429±0.178	0.97±0.01	0.95	-10.607±0.002	-10.480±0.003	79	70
5BZUJ0433+0521	60001042002	56329.53194	21582	0.103	1.81±0.01	16.299±0.454	0.99±0.01	0.94	-10.366±0.003	-10.311±0.004	79	70
5BZUJ0433+0521	60001042003	56329.99375	127672	0.103	1.80±0.01	16.300±0.184	0.99±0.01	1.02	-10.354±0.001	-10.291±0.001	79	70
5BZQJ0449+1121	60101078002	57358.09097	20517	0.123	1.61±0.29	0.086±0.054	1.00±0.26	0.76	-12.494±0.052	-12.339±0.082	20	30
5BZQJ0453-2807	60101080002	57359.03194	19517	0.023	1.39±0.10	0.286±0.062	1.01±0.09	0.80	-11.797±0.021	-11.532±0.026	20	40
5BZQJ0501-0159	60367003001	58234.29583	20623	0.064	1.64±0.07	0.677±0.108	1.02±0.07	0.86	-11.616±0.017	-11.475±0.019	25	40
5BZB0507+6737	60202026002	57694.41388	24647	0.093	2.75±0.04	16.342±1.223	0.95±0.03	0.96	-11.043±0.006	-11.459±0.013	35	60
5BZB0507+6737	60202026004	57721.20208	20697	0.093	2.80±0.08	6.698±1.025	1.03±0.07	0.85	-11.463±0.014	-11.902±0.022	25	40
5BZB0507+6737	60202026006	57749.12916	25273	0.093	2.52±0.07	4.444±0.601	0.98±0.06	0.87	-11.448±0.010	-11.748±0.020	25	40
5BZB0509+0541	60502053002	58694.89305	22353	0.116	1.63±0.08	0.565±0.094	1.08±0.08	0.95	-11.689±0.015	-11.543±0.022	25	40
5BZB0509+0541	60502053004	58755.82361	31748	0.116	1.72±0.07	0.587±0.090	1.06±0.07	0.85	-11.738±0.014	-11.634±0.021	25	40
5BZB0509+0541	60502053006	58816.08750	20266	0.116	1.62±0.10	0.489±0.102	0.95±0.09	0.82	-11.741±0.017	-11.587±0.026	20	40
5BZB0509+0541	60502053008	58874.80277	19397	0.116	1.73±0.11	0.519±0.118	1.04±0.10	0.80	-11.801±0.018	-11.704±0.030	20	40
5BZB0509+0541	60502053010	58933.10833	21483	0.116	1.72±0.08	0.704±0.120	0.97±0.08	0.93	-11.660±0.015	-11.557±0.023	25	40
5BZB0509+0541	60602004002	59118.11180	23714	0.116	1.66±0.10	0.483±0.098	1.03±0.09	0.96	-11.780±0.019	-11.649±0.032	20	40
5BZB0509+0541	60602004004	59147.90000	27498	0.116	1.60±0.08	0.539±0.087	0.94±0.07	0.93	-11.688±0.012	-11.528±0.019	25	40
5BZB0509+0541	60602004006	59170.71944	25070	0.116	1.76±0.10	0.481±0.103	1.04±0.10	0.93	-11.854±0.019	-11.771±0.032	20	40
5BZB0509+0541	60602004008	59193.60138	27013	0.116	1.73±0.11	0.385±0.084	1.18±0.11	0.84	-11.930±0.021	-11.833±0.029	20	40
5BZB0509+0541	60602004010	59230.57013	25126	0.116	1.78±0.16	0.301±0.097	1.07±0.15	0.94	-12.077±0.030	-12.007±0.041	20	30
5BZB0509+0541	60602004012	59257.80972	25592	0.116	1.74±0.14	0.298±0.090	1.02±0.13	0.86	-12.045±0.022	-11.951±0.036	20	30
5BZB0509+0541	90301618002	58025.09444	27608	0.116	1.69±0.10	0.395±0.085	0.99±0.09	0.83	-11.890±0.019	-11.775±0.026	20	40
5BZB0509+0541	90301618004	58045.43472	21285	0.116	1.64±0.14	0.297±0.089	1.02±0.13	0.81	-11.975±0.023	-11.834±0.040	20	30
5BZB0509+0541	90401610002	58211.55277	25946	0.116	1.54±0.09	0.344±0.069	0.96±0.08	0.88	-11.832±0.017	-11.639±0.027	20	40
5BZB0509+0541	90402637002	58407.86527	31882	0.116	1.55±0.08	0.362±0.061	1.00±0.08	0.80	-11.820±0.013	-11.633±0.019	25	40
5BZB0509+0541	90402637004	58437.05972	27204	0.116	1.65±0.12	0.333±0.084	0.99±0.11	0.83	-11.931±0.023	-11.793±0.032	20	30
5BZB0509+0541	90402637006	58460.75416	25769	0.116	1.67±0.11	0.379±0.083	1.01±0.10	0.87	-11.890±0.018	-11.762±0.028	20	40
5BZB0509+0541	90402637008	58490.88263	26311	0.116	1.79±0.08	0.766±0.124	0.95±0.07	0.92	-11.673±0.014	-11.603±0.021	25	40
PictorA	60101047002	57359.23600	117036	0.036	1.78±0.02	0.174±0.035	1.01±0.09	0.89	-11.148±0.003	-11.078±0.004	25	30
5BZUJ0522-3627	60160232002	59338.01111	23319	0.032	1.87±0.02	6.897±0.309	1.01±0.02	0.92	-10.783±0.004	-10.759±0.006	65	70
5BZQJ0525-2338	60160234002	57869.29930	20879	0.021	1.48±0.07	0.460±0.075	1.02±0.08	0.93	-11.659±0.015	-11.538±0.021	25	40
5BZQJ0530+1331	60160238002	58509.06319	20054	0.236	1.54±0.17	0.209±0.074	0.91±0.14	0.83	-12.053±0.029	-11.859±0.048	20	30
5BZB0543-5532	60101058002	57374.75069	37537	0.055	2.65±0.05	6.971±0.658	1.02±0.04	0.84	-11.344±0.008	-11.711±0.014	35	40
5BZQJ0555-3948	90401003002	58126.98333	28563	0.270	1.58±0.07	0.557±0.081	0.97±0.06	0.99	-11.658±0.011	-11.484±0.015	25	40
5BZQJ0623-6436	60160263002	58010.86180	41687	0.040	1.75±0.04	1.185±0.109	1.01±0.04	0.86	-11.457±0.009	-11.373±0.012	35	40
PKS0625-354	60301007002	58047.65000	51837	0.063	2.56±0.08	1.962±0.290	1.02±0.07	0.99	-11.825±0.014	-12.143±0.020	25	40
5BZBJ0630-2406	60001140002	56947.74375	66469	0.081	2.76±0.25	0.396±0.191	1.19±0.24	0.95	-12.667±0.049	-13.089±0.078	20	30
5BZQJ0635-7516	60160272002	57362.11875	15173	0.072	1.50±0.09	0.568±0.109	0.99±0.08	0.84	-11.584±0.017	-11.372±0.025	20	40
PMNJ0641-0320	80001003002	56776.41736	21353	0.586	1.09±0.03	0.716±0.052	0.99±0.03	0.93	-11.178±0.006	-10.757±0.008	35	60
5BZQJ0646-4451	60201011002	57720.53888	32065	0.108	1.89±0.16	0.260±0.087	0.99±0.14	0.82	-12.218±0.028	-12.200±0.035	20	30
5BZB0710+5908	60101037002	57266.24375	3931	0.043	2.25±0.07	10.952±1.482	1.02±0.06	0.89	-10.857±0.012	-11.020±0.023	25	70
5BZB0710+5908	60101037004	57266.50763	26440	0.043	2.25±0.02	11.074±0.554	0.99±0.02	0.91	-10.858±0.005	-11.024±0.007	65	70
5BZB0710+5908	60101037006	57267.24375	4641	0.043	2.24±0.06	11.270±1.376	0.98±0.06	0.92	-10.841±0.010	-11.001±0.020	25	70

Table B1: continued.

Name	ObsID	Time(MJD)	Exposure(s)	N _H	Γ	Norm	Const	C/d.o.f.	$\log F_{\text{H}}^{\text{pl}}$	$\log F_{\text{S}}^{\text{pl}}$	E _{max} (keV)	Radius (arcsec)
5BZBJ0721+7120	90002003002	57046.11527	18564	0.029	1.96±0.04	3.815±0.313	1.03±0.04	1.00	-11.101±0.008	-11.118±0.013	35	60
5BZQJ0733+0456	60501037002	58779.45208	60473	0.069	1.28±0.27	0.019±0.011	1.09±0.26	0.80	-12.900±0.066	-12.583±0.080	20	30
5BZQJ0809+5341	80001004002	56785.43819	28004	0.038	1.12±0.28	0.024±0.015	1.28±0.32	0.78	-12.666±0.056	-12.267±0.070	20	30
3HSP108.1003.3-752724	60001142002	56901.19861	112366	0.078	1.66±0.12	0.085±0.021	1.10±0.12	0.94	-12.530±0.022	-12.397±0.031	25	30
5BZQJ0841+7053	60002045002	56641.65347	29678	0.028	1.65±0.02	4.034±0.180	0.99±0.02	0.88	-10.846±0.005	-10.709±0.006	65	70
5BZQJ0841+7053	60002045004	56675.20208	36324	0.028	1.64±0.01	6.190±0.190	0.99±0.02	0.99	-10.655±0.003	-10.516±0.004	79	70
5BZUJ0847-2337	60101059002	57375.63263	32066	0.082	2.34±0.06	3.349±0.371	1.01±0.05	0.89	-11.438±0.008	-11.646±0.018	35	40
5BZB10854+2006	90201054002	57852.44861	52838	0.024	2.08±0.04	2.376±0.188	1.00±0.04	0.88	-11.401±0.009	-11.482±0.011	35	40
5BZB10854+2006	906011616002	58973.85833	29268	0.024	2.40±0.06	3.840±0.450	1.04±0.06	0.78	-11.424±0.010	-11.665±0.016	25	40
5BZB10915+2933	90101021002	57433.24722	49991	0.018	2.51±0.15	0.755±0.210	1.04±0.13	0.76	-12.211±0.024	-12.508±0.040	20	30
5BZB10915+2933	90201047002	57794.52500	31066	0.018	2.53±0.23	0.560±0.244	1.12±0.20	0.88	-12.349±0.032	-12.654±0.077	20	30
5BZQJ0948+0022	60201052002	57696.17083	192997	0.047	1.40±0.03	0.232±0.016	1.02±0.03	0.86	-11.896±0.006	-11.636±0.009	45	40
5BZB10955+3551	90501658002	58859.04583	25389	0.011	2.23±0.07	2.464±0.342	0.94±0.06	0.92	-11.493±0.012	-11.649±0.018	25	40
5BZQJ0956+2515	60301019002	58105.99027	63387	0.034	1.81±0.09	0.291±0.056	1.03±0.09	0.86	-12.109±0.015	-12.052±0.025	25	30
5BZQJ1028-0844	60373001002	58089.20902	30593	0.046	1.68±0.14	0.238±0.068	1.08±0.13	0.86	-12.102±0.031	-11.983±0.041	20	30
5BZQJ1044+8054	90201018002	57490.28194	14653	0.021	1.50±0.06	0.875±0.116	1.03±0.06	0.92	-11.395±0.012	-11.183±0.014	25	50
5BZUJ1058+0133	604666004002	58230.63263	19514	0.029	1.69±0.08	0.661±0.117	1.01±0.08	1.00	-11.665±0.016	-11.551±0.025	25	40
5BZB1103-2329	60101033002	57399.87569	52097	0.051	2.49±0.02	23.048±0.725	0.95±0.01	1.00	-10.707±0.002	-10.991±0.005	79	70
5BZB1104+3812	10002015001	56115.08055	42014	0.013	2.84±0.01	232.487±3.570	1.00±0.01	1.04	-9.951±0.001	-10.414±0.002	79	70
5BZB1104+3812	10002016001	56116.07361	24870	0.013	2.89±0.01	280.488±5.131	1.03±0.01	1.04	-9.902±0.002	-10.389±0.003	79	70
5BZB1104+3812	60002023002	56294.77847	9146	0.013	3.06±0.03	107.210±6.427	0.97±0.03	0.98	-10.440±0.006	-11.015±0.011	45	70
5BZB1104+3812	60002023004	56302.05277	22639	0.013	3.05±0.03	72.592±3.316	0.98±0.02	0.89	-10.598±0.003	-11.165±0.008	79	70
5BZB1104+3812	60002023006	56307.03888	24183	0.013	3.01±0.01	231.632±5.389	0.99±0.01	0.97	-10.071±0.002	-10.620±0.004	79	70
5BZB1104+3812	60002023008	56312.09791	24947	0.013	3.05±0.02	85.315±3.422	0.97±0.02	1.01	-10.529±0.004	-11.097±0.007	79	70
5BZB1104+3812	60002023010	56329.01111	19317	0.013	2.93±0.01	262.005±5.988	0.97±0.01	1.09	-9.961±0.002	-10.469±0.004	79	70
5BZB1104+3812	60002023012	56335.01111	14797	0.013	2.72±0.01	215.671±5.086	0.97±0.01	0.95	-9.902±0.002	-10.305±0.005	79	70
5BZB1104+3812	60002023014	56339.98333	17374	0.013	3.01±0.02	133.849±4.928	0.99±0.02	0.97	-10.309±0.003	-10.858±0.006	79	70
5BZB1104+3812	60002023016	56355.96250	16859	0.013	3.00±0.01	337.485±7.835	0.98±0.01	1.01	-9.898±0.002	-10.441±0.004	79	70
5BZB1104+3812	60002023018	56362.95902	17461	0.013	3.08±0.01	294.912±7.815	0.97±0.01	0.97	-10.013±0.002	-10.598±0.005	79	70
5BZB1104+3812	60002023020	56368.07673	16559	0.013	2.75±0.01	98.729±5.224	0.98±0.01	0.98	-9.890±0.002	-10.306±0.003	79	70
5BZB1104+3812	60002023022	56384.71944	24786	0.013	2.73±0.01	535.753±6.121	0.99±0.01	1.16	-9.510±0.001	-9.915±0.002	79	70
5BZB1104+3812	60002023024	56392.89305	57688	0.013	2.88±0.01	1050.830±20.640	0.95±0.01	1.07	-9.323±0.001	-9.806±0.003	79	70
5BZB1104+3812	60002023025	56393.04236	57645	0.013	2.63±0.01	1076.350±5.130	0.98±0.01	2.25	-9.136±0.001	-9.490±0.001	79	70
5BZB1104+3812	60002023027	56394.85833	7667	0.013	2.60±0.01	2197.470±19.960	0.97±0.01	1.66	-8.806±0.001	-9.147±0.001	79	70
5BZB1104+3812	60002023029	56395.90000	16533	0.013	2.77±0.01	1088.820±11.350	0.98±0.01	1.35	-9.234±0.001	-9.663±0.002	79	70
5BZB1104+3812	60002023031	56396.90347	15701	0.013	2.29±0.01	1405.080±8.210	0.98±0.01	2.41	-8.783±0.001	-8.970±0.001	79	70
5BZB1104+3812	60002023033	56397.91736	17306	0.013	2.57±0.01	823.302±7.892	0.97±0.01	1.27	-9.210±0.001	-9.535±0.002	79	70
5BZB1104+3812	60002023035	56398.93125	20317	0.013	2.38±0.01	646.106±5.328	0.97±0.01	1.46	-9.180±0.001	-9.408±0.001	79	70
5BZB1104+3812	60002023037	56400.01111	17782	0.013	2.82±0.01	215.778±5.158	0.97±0.01	1.03	-9.970±0.002	-10.423±0.004	79	70
5BZB1104+3812	60002023039	56401.02152	15939	0.013	2.93±0.01	242.810±6.423	0.97±0.01	0.98	-9.995±0.002	-10.504±0.004	79	70
5BZB1104+3812	60202048002	57756.99375	23692	0.013	2.43±0.01	334.716±3.753	0.95±0.01	1.06	-9.506±0.001	-9.764±0.002	79	70
5BZB1104+3812	60202048004	57784.99027	21586	0.013	2.43±0.01	351.616±3.959	0.97±0.01	1.13	-9.480±0.001	-9.734±0.002	79	70
5BZB1104+3812	60202048006	57812.92430	23908	0.013	2.47±0.01	377.420±4.104	0.96±0.01	1.18	-9.483±0.001	-9.761±0.002	79	70
5BZB1104+3812	60202048008	57839.91041	31158	0.013	2.65±0.01	148.727±2.747	0.97±0.01	0.93	-10.014±0.002	-10.382±0.003	79	70
5BZB1104+3812	60101062002	57330.23333	22465	0.018	2.86±0.08	7.886±1.161	0.97±0.06	0.86	-11.436±0.015	-11.910±0.026	25	40
5BZQJ1130-1449	9070160802	59274.45555	23063	0.035	1.47±0.04	1.326±0.103	0.98±0.04	0.90	-11.190±0.010	-10.964±0.009	35	60
3C264	60501016002	58678.80277	55098	0.019	2.33±0.11	0.700±0.158	1.00±0.10	0.94	-12.109±0.016	-12.313±0.036	25	30

Table B1: continued.

Name	ObsID	Time(MJD)	Exposure(s)	N _H	Γ	Norm	Const	C/d.o.f.	$\log F_{\text{S}}^{\text{pl}}$	$\log F_{\text{H}}^{\text{pl}}$	E _{max} (keV)	Radius (arcsec)
5BZQJ1159+2914	60463037002	58626.66388	16921	0.016	1.61±0.23	0.151±0.075	0.95±0.20	0.77	-12.247±0.038	-12.094±0.054	20	30
5BZQJ1159+2914	60463037004	59390.53194	17418	0.016	1.55±0.07	0.920±0.129	1.04±0.07	0.92	-11.413±0.013	-11.228±0.018	25	40
5BZQJ1220+0203	60301001002	57910.86875	50415	0.018	1.77±0.04	1.316±0.105	1.03±0.04	0.89	-11.427±0.007	-11.353±0.011	35	40
5BZB11221+3010	60101034002	57349.04583	49457	0.019	2.55±0.03	10.836±0.564	0.99±0.02	0.91	-11.081±0.005	-11.398±0.009	65	60
5BZQJ1222+0413	60301018002	57931.60486	32153	0.016	1.43±0.08	0.276±0.046	1.00±0.07	0.92	-11.845±0.013	-11.601±0.018	25	40
5BZQJ1229+0203	00015011001	56109.87569	2882	0.017	1.54±0.02	20.364±1.101	1.00±0.03	0.94	-10.060±0.005	-9.870±0.006	45	70
5BZQJ1229+0203	00015012001	56109.94166	2894	0.017	1.54±0.03	20.377±1.281	0.99±0.03	0.93	-10.057±0.006	-9.865±0.009	35	70
5BZQJ1229+0203	00015013001	56110.01111	2575	0.017	1.57±0.03	21.193±1.344	0.96±0.03	0.96	-10.065±0.006	-9.889±0.007	35	70
5BZQJ1229+0203	00015014001	56110.08055	2669	0.017	1.57±0.03	20.790±1.370	0.90±0.03	0.93	-10.073±0.006	-9.897±0.010	35	70
5BZQJ1229+0203	00015015001	56110.14652	2848	0.017	1.52±0.03	18.099±1.220	0.89±0.03	0.97	-10.094±0.006	-9.892±0.009	35	70
5BZQJ1229+0203	00015017001	56110.28194	3005	0.017	1.55±0.03	19.440±1.366	0.91±0.03	0.88	-10.092±0.007	-9.910±0.010	35	70
5BZQJ1229+0203	10002020001	56122.00416	244059	0.017	1.68±0.01	21.519±0.134	1.00±0.01	1.07	-10.140±0.001	-10.018±0.001	79	70
5BZQJ1229+0203	10002020003	57216.58402	49370	0.017	1.71±0.03	17.075±0.282	0.98±0.01	0.92	-10.267±0.002	-10.163±0.002	79	70
5BZQJ1229+0203	10012001002	56121.07361	5160	0.017	1.64±0.02	20.773±0.878	0.99±0.02	0.93	-10.129±0.004	-9.990±0.005	65	70
5BZQJ1229+0203	10012002001	56121.19513	6191	0.017	1.65±0.02	21.051±0.878	1.00±0.02	1.02	-10.130±0.004	-9.996±0.005	65	70
5BZQJ1229+0203	10012003001	56121.33055	6219	0.017	1.66±0.02	21.664±0.873	1.01±0.02	0.95	-10.128±0.004	-9.999±0.005	79	70
5BZQJ1229+0203	10012004001	56121.46597	6226	0.017	1.68±0.02	22.622±0.999	0.85±0.02	0.92	-10.119±0.004	-9.998±0.007	65	70
5BZQJ1229+0203	10012005001	56121.60138	6147	0.017	1.65±0.02	21.116±0.937	1.02±0.02	0.92	-10.127±0.005	-9.992±0.005	65	70
5BZQJ1229+0203	10012006001	56121.73680	5211	0.017	1.60±0.03	18.731±1.151	0.99±0.03	0.95	-10.140±0.006	-9.979±0.007	35	70
5BZQJ1229+0203	10012007001	56121.86875	4534	0.017	1.68±0.03	21.354±1.367	1.04±0.03	0.91	-10.149±0.008	-10.031±0.008	35	70
5BZQJ1229+0203	10202020002	57565.79930	35403	0.017	1.61±0.01	33.594±0.406	0.99±0.01	0.99	-9.900±0.001	-9.747±0.001	79	70
5BZQJ1229+0203	10302020002	57930.73680	35333	0.017	1.65±0.01	18.115±0.312	0.98±0.01	0.95	-10.194±0.002	-10.058±0.002	79	70
5BZQJ1229+0203	10402020002	58271.08402	16063	0.017	1.64±0.01	18.733±0.478	0.98±0.01	0.92	-10.174±0.003	-10.035±0.003	79	70
5BZQJ1229+0203	10402020004	58284.18819	21117	0.017	1.66±0.01	15.540±0.381	0.99±0.01	0.94	-10.269±0.003	-10.139±0.003	79	70
5BZQJ1229+0203	10402020006	58303.72291	40180	0.017	1.70±0.01	16.745±0.297	0.99±0.01	0.93	-10.264±0.002	-10.152±0.002	79	70
5BZQJ1229+0203	10502620002	58666.52708	49119	0.017	1.70±0.01	14.346±0.250	0.99±0.01	0.91	-10.333±0.002	-10.2221±0.002	79	70
5BZQJ1229+0203	10602606002	59036.20555	43684	0.017	1.68±0.01	17.236±0.292	1.02±0.01	0.92	-10.240±0.002	-10.120±0.002	79	70
5BZQJ1229+0203	10702608002	59374.77500	35767	0.017	1.63±0.01	11.237±0.247	0.99±0.01	0.91	-10.387±0.002	-10.241±0.003	79	70
5BZQJ1229+0203	60601004002	59318.61527	18507	0.017	1.65±0.01	11.563±0.371	0.98±0.02	0.91	-10.389±0.003	-10.253±0.004	79	70
5BZQJ1229+0203	80301602002	58287.75069	60655	0.017	1.63±0.01	15.487±0.217	0.98±0.01	0.93	-10.248±0.001	-10.103±0.002	79	70
5BZQJ1256-0547	60002020002	56642.24375	39512	0.022	1.73±0.02	3.179±0.142	1.03±0.02	0.91	-11.015±0.004	-10.922±0.006	65	70
5BZQJ1256-0547	60002020004	56657.99027	42733	0.022	1.74±0.01	6.701±0.195	0.97±0.01	0.87	-10.693±0.002	-10.601±0.004	79	70
5BZQJ1256-0547	60061005001	59317.12916	18321	0.022	1.84±0.04	3.343±0.264	1.15±0.04	0.93	-11.073±0.006	-11.034±0.009	35	60
5BZQJ1321+0023	60370003002	58130.42777	20643	0.018	1.81±0.32	0.148±0.102	0.86±0.24	0.87	-12.402±0.055	-12.346±0.081	20	30
5BZQJ1332-0509	60160541002	57902.34097	21281	0.020	1.45±0.19	0.119±0.149	1.06±0.18	0.96	-12.230±0.033	-11.998±0.053	20	30
5BZQJ1337-1257	60160547002	59072.57708	14040	0.054	1.82±0.07	1.551±0.219	1.05±0.07	0.93	-11.388±0.011	-11.334±0.022	25	50
5BZQJ1354-0206	60201012002	57878.92083	53037	0.030	1.41±0.16	0.063±0.022	1.01±0.15	0.76	-12.472±0.031	-12.2220±0.042	20	30
5BZQJ1357+1919	60463043002	59003.93125	21595	0.030	1.65±0.07	0.838±0.123	0.96±0.06	0.88	-11.533±0.012	-11.400±0.018	25	40
5BZGJ1407+2827	60201043002	57557.00763	50899	0.014	1.06±0.15	0.034±0.012	1.07±0.15	0.70	-12.471±0.032	-12.045±0.038	20	30
5BZQJ1424+2256	60301020002	58117.87916	100962	0.035	2.23±0.10	0.437±0.083	1.03±0.09	0.92	-12.245±0.017	-12.401±0.029	25	30
5BZB1428+4240	60601024002	59042.71597	53782	0.010	2.28±0.02	11.653±0.409	0.99±0.02	0.89	-10.853±0.003	-11.033±0.006	79	70
5BZQJ1428+4240	90701613002	59311.24027	27743	0.010	2.01±0.02	15.322±0.501	0.99±0.02	0.93	-10.538±0.003	-10.583±0.005	79	70
5BZQJ1429+5406	60501036002	58680.89305	45024	0.010	1.59±0.15	0.116±0.036	1.24±0.16	0.83	-12.346±0.026	-12.184±0.033	20	30
5BZQJ1430+4204	60463048002	59094.04583	21728	0.017	1.74±0.09	0.625±0.121	0.98±0.08	0.99	-11.918±0.015	-11.743±0.024	25	30
3C303	60463048002	59137.11180	38177	0.031	2.18±0.13	0.606±0.160	0.96±0.11	0.90	-12.068±0.021	-12.199±0.038	20	30
5BZQJ1443+2501	90101004002	57137.11180	23555	0.029	1.57±0.10	0.364±0.076	1.01±0.09	0.88	-11.834±0.018	-11.661±0.027	20	40

Table B1: continued.

Name	ObsID	Time(MJD)	Exposure(s)	N _H	Γ	Norm	Const	C/d.o.f.	$\log F_{\text{H}}^{\text{pl}}$	$\log F_{\text{S}}^{\text{pl}}$	E _{max} (keV)	Radius (arcsec)
5BZUJ1459+7140	60376006002	58073.37569	60888	0.029	1.60±0.06	0.398±0.047	1.03±0.06	0.93	-11.815±0.009	-11.654±0.015	25	40
5BZQJ1505+0326	60201044002	57796.28888	115134	0.035	1.14±0.10	0.034±0.008	0.94±0.10	0.80	-12.524±0.019	-12.137±0.025	25	30
5BZQJ1510+5702	60201013002	57873.15000	36763	0.015	1.28±0.18	0.057±0.023	0.96±0.16	0.87	-12.420±0.032	-12.104±0.045	20	30
5BZUJ1511+0518	60401024002	58491.58055	69625	0.034	1.40±0.23	0.031±0.016	1.02±0.21	0.85	-12.767±0.040	-12.506±0.063	20	30
5BZGJ1516+0015	60463050002	58924.21944	35117	0.042	1.69±0.08	0.390±0.069	1.06±0.08	0.92	-11.891±0.014	-11.774±0.025	25	40
3HSP151803.6-273131	90501608002	58544.59791	33728	0.075	2.65±0.04	9.957±0.785	0.96±0.04	0.94	-11.188±0.007	-11.554±0.012	35	50
5BZQJ1556-7914	60160627002	57581.44166	17293	0.090	1.73±0.04	2.075±0.188	1.00±0.04	0.95	-11.198±0.009	-11.102±0.012	35	60
5BZQJ1559+0304	60373003002	58160.64305	53208	0.056	1.70±0.30	0.042±0.027	1.12±0.29	0.79	-12.871±0.058	-12.762±0.078	20	30
5BZQJ1626-2951	60160638002	57653.02847	20652	0.136	1.66±0.05	1.450±0.150	0.95±0.04	0.88	-11.300±0.088	-11.167±0.014	25	50
5BZQJ1642+3948	60160647002	58088.08055	24333	0.009	1.56±0.06	0.838±0.104	0.96±0.05	0.90	-11.466±0.011	-11.288±0.019	25	40
5BZQJ1644+2619	60301017002	58136.21250	52318	0.050	1.75±0.11	0.234±0.054	1.07±0.11	0.93	-12.164±0.025	-12.080±0.032	20	30
5BZB11653+3945	60002024002	563395.10486	18269	0.017	2.26±0.02	40.112±1.223	1.03±0.02	0.94	-10.304±0.003	-10.474±0.004	79	70
5BZB11653+3945	60002024004	56420.83402	26143	0.017	2.23±0.02	53.988±1.156	0.99±0.01	0.99	-10.151±0.002	-10.306±0.004	79	70
5BZB11653+3945	60002024006	56485.89652	10848	0.017	2.10±0.01	103.931±2.156	0.99±0.01	0.95	-9.7680±0.002	-9.856±0.003	79	70
5BZB11653+3945	60002024008	56486.84444	10338	0.017	2.12±0.01	97.267±2.191	0.97±0.01	1.01	-9.8120±0.002	-9.909±0.003	79	70
5BZB11653+3945	60202049002	57870.93472	23127	0.017	2.20±0.01	32.385±0.944	0.96±0.01	1.02	-10.348±0.003	-10.485±0.004	79	70
5BZQJ1723+3945	60202049004	57897.92430	23774	0.017	2.69±0.03	27.341±1.423	0.99±0.02	0.95	-10.773±0.004	-11.157±0.008	65	70
5BZB11653+3945	60466006002	58227.62916	23040	0.017	2.74±0.04	17.044±1.254	0.99±0.03	0.93	-11.018±0.005	-11.432±0.012	35	60
5BZQJ1656-3302	60160657002	57292.58333	21127	0.235	1.61±0.05	1.185±0.127	1.00±0.05	0.97	-11.350±0.011	-11.189±0.017	25	50
5BZGJ1719+44858	60160662002	57350.19513	22348	0.020	1.70±0.07	0.867±0.123	1.11±0.07	0.94	-11.555±0.013	-11.446±0.020	25	40
5BZB11653+3945	60511001002	58756.58402	74126	0.034	1.57±0.26	0.040±0.022	1.04±0.24	0.74	-12.788±0.052	-12.611±0.063	20	30
5BZQJ1723+6547	60511002002	58758.94166	77397	0.034	1.51±0.25	0.033±0.018	1.01±0.23	0.79	-12.836±0.049	-12.633±0.061	20	30
5BZQJ1723+6547	60511003002	58760.28541	68363	0.034	2.01±0.29	0.093±0.056	0.91±0.23	0.82	-12.757±0.060	-12.802±0.084	20	30
5BZQJ1723+6547	60511005002	58852.55625	84338	0.034	1.82±0.35	0.055±0.041	1.01±0.30	0.78	-12.838±0.064	-12.787±0.112	20	30
5BZQJ1723+6547	60511008001	58910.32708	70234	0.034	1.69±0.37	0.040±0.032	0.86±0.26	0.84	-12.887±0.057	-12.773±0.112	20	30
5BZQJ1723+6547	60511009001	58911.60138	68280	0.034	1.50±0.31	0.028±0.019	1.11±0.31	0.89	-12.896±0.064	-12.688±0.095	20	30
5BZB11800+7828	60464146002	59350.73680	19580	0.032	1.47±0.05	0.797±0.095	0.99±0.05	0.96	-11.417±0.011	-11.193±0.017	25	50
5BZUJ1809-4552	60464148002	58231.58750	24610	0.096	1.75±0.10	0.587±0.126	1.01±0.10	0.91	-11.764±0.020	-11.679±0.029	20	40
5BZUJ1829+4844	60160690002	58928.79236	19482	0.063	1.64±0.05	1.157±0.134	1.05±0.06	0.92	-11.386±0.009	-11.247±0.014	25	50
5BZQJ1833-2103	60160692002	57492.76805	21784	0.187	1.43±0.02	2.560±0.128	0.96±0.02	0.91	-10.878±0.005	-10.629±0.006	45	70
5BZQJ1833-2103	8046628002	58550.84791	41050	0.187	1.41±0.02	2.329±0.086	0.95±0.02	0.90	-10.909±0.003	-10.654±0.005	79	70
5BZQJ1849+6705	00463066002	59002.59791	25728	0.049	1.95±0.22	0.219±0.101	0.95±0.19	0.73	-12.342±0.041	-12.358±0.060	20	30
5BZQJ1924-2914	00464163002	59314.87569	16341	0.069	1.91±0.08	1.513±0.235	1.05±0.07	0.95	-11.468±0.012	-11.460±0.023	25	40
5BZQJ1924-2914	60464163004	59317.62916	21639	0.069	1.91±0.06	1.609±0.209	1.03±0.06	0.89	-11.443±0.011	-11.437±0.017	25	40
5BZQJ1927+7358	60160712002	57760.54930	33198	0.066	1.79±0.04	1.492±0.130	0.99±0.04	0.86	-11.383±0.008	-11.315±0.013	35	50
5BZB11936-4719	60101057002	57469.73680	20833	0.052	2.43±0.02	6.500±0.645	0.98±0.05	0.92	-11.215±0.009	-11.469±0.016	35	50
5BZQJ1939-1002	60373004002	58200.58055	39106	0.097	1.94±0.12	0.430±0.103	1.00±0.10	0.80	-12.036±0.019	-12.043±0.033	20	30
5BZGJ1958-3011	60101056002	57340.80625	52763	0.075	2.39±0.03	5.500±0.348	1.03±0.03	0.90	-11.259±0.006	-11.492±0.009	45	50
5BZB11959+6508	60002055002	56917.10833	19589	0.101	2.30±0.02	59.595±1.782	0.98±0.01	0.96	-10.159±0.003	-10.346±0.004	79	70
5BZB11959+6508	60002055004	56922.08750	20311	0.101	2.53±0.02	67.907±2.015	0.96±0.01	0.98	-10.267±0.003	-10.570±0.006	79	70
5BZQJ2007-4434	60201045002	57684.52500	60474	0.030	1.70±0.08	0.277±0.049	1.00±0.08	0.88	-12.047±0.012	-11.935±0.023	25	30
5BZQJ2007-4434	80201024002	57517.68125	49070	0.030	1.65±0.10	0.221±0.047	1.07±0.10	0.78	-12.110±0.018	-11.975±0.021	25	30
5BZQJ2007-4434	90501649002	58788.54930	29872	0.030	1.33±0.12	0.144±0.037	1.16±0.13	0.76	-12.048±0.019	-11.753±0.032	20	30
5BZQJ2011-1546	60160729002	57689.09097	20879	0.058	1.52±0.05	0.950±0.103	1.03±0.05	0.85	-11.377±0.009	-11.176±0.012	25	50
5BZUJ2015-3710	30460021002	58129.10833	59299	1.080	1.64±0.04	0.748±0.070	1.02±0.04	0.83	-11.587±0.007	-11.427±0.013	35	40
5BZUJ2015-3710	60160732002	57537.61875	12636	1.080	1.56±0.06	1.311±0.169	0.99±0.06	0.89	-11.284±0.010	-11.085±0.015	25	50
5BZQJ2022+6136	60401023002	58306.83055	64139	0.136	0.67±0.18	0.011±0.005	1.00±0.15	0.85	-12.660±0.038	-12.039±0.040	20	30

Table B1: continued.

Name	ObsID	Time(MJD)	Exposure(s)	N_{H}	Γ	Norm	Const	C/d.o.f.	$\log F_{\text{S}}^{\text{pl}}$	$\log F_{\text{H}}^{\text{pl}}$	E_{max} (keV)	Radius (arcsec)
5BZQJ2056-4714	60160748002	58955.50416	32753	0.028	1.47±0.05	0.629±0.071	1.01±0.05	0.89	-11.515±0.010	-11.289±0.015	25	40
3HSPI205642.7+494006	30161001002	57339.79583	32667	1.010	2.51±0.02	26.464±1.008	0.98±0.02	0.93	-10.685±0.003	-10.960±0.005	79	70
5BZQJ2129-1538	60401029002	58386.09791	33166	0.045	1.60±0.03	1.739±0.107	0.99±0.03	0.85	-11.172±0.005	-11.010±0.008	45	60
5BZBJ2146-1344	60401026002	58256.16041	42137	0.037	2.32±0.10	1.051±0.207	1.14±0.10	0.92	-11.928±0.016	-12.127±0.028	25	30
5BZQJ2148-0657	60160768002	58074.20902	21278	0.044	1.49±0.04	1.132±0.102	0.98±0.04	0.83	-11.277±0.008	-11.062±0.011	35	50
5BZQJ2151-3027	60001099002	56643.20902	38429	0.016	1.35±0.01	3.513±0.096	1.06±0.01	0.92	-10.679±0.003	-10.397±0.003	79	70
5BZQJ2151-3027	60001099004	56765.62916	44015	0.016	1.44±0.01	3.455±0.100	0.99±0.01	0.89	-10.753±0.003	-10.513±0.003	79	70
5BZBJ2158-3013	10002010001	56116.60833	33807	0.013	2.99±0.02	47.936±2.138	0.98±0.02	0.92	-10.743±0.004	-11.283±0.007	79	70
5BZBJ2158-3013	60002022002	56405.82361	44949	0.013	2.71±0.03	12.305±0.762	0.99±0.03	0.95	-11.135±0.005	-11.531±0.010	45	60
5BZBJ2158-3013	60002022004	56489.95208	13822	0.013	2.59±0.05	13.997±1.295	1.02±0.04	0.96	-10.994±0.008	-11.329±0.013	35	60
5BZBJ2158-3013	60002022006	56506.91041	10923	0.013	3.04±0.07	29.572±3.171	1.00±0.05	0.91	-10.981±0.010	-11.543±0.016	25	60
5BZBJ2158-3013	60002022008	56512.91736	13438	0.013	2.82±0.07	12.259±1.617	0.99±0.06	0.87	-11.218±0.011	-11.673±0.020	25	50
5BZBJ2158-3013	60002022010	56518.91041	10493	0.013	2.92±0.06	23.060±2.624	0.98±0.05	0.87	-11.012±0.009	-11.517±0.019	25	60
5BZBJ2158-3013	60002022012	56530.82708	11341	0.013	2.62±0.04	25.295±1.822	1.01±0.03	0.94	-10.758±0.007	-11.107±0.011	35	70
5BZBJ2158-3013	60002022014	56539.91388	12259	0.013	2.80±0.05	20.072±2.007	0.95±0.04	0.98	-10.988±0.008	-11.431±0.018	25	60
5BZBJ2158-3013	60002022016	56563.95555	11499	0.013	2.69±0.08	9.853±1.427	0.87±0.06	0.94	-11.215±0.011	-11.600±0.025	25	50
5BZBJ2202+4216	60001001002	56272.60833	21856	0.175	1.87±0.02	6.826±0.328	0.95±0.02	0.90	-10.787±0.004	-10.759±0.006	65	70
5BZBJ2202+4216	60501024002	58740.23333	210850	0.175	1.77±0.01	1.678±0.053	0.99±0.02	0.95	-11.321±0.004	-11.243±0.004	79	50
5BZBJ2202+4216	90601630002	59133.58750	30430	0.175	1.57±0.03	1.865±0.114	1.01±0.03	0.99	-11.126±0.006	-10.950±0.008	45	60
5BZBJ2202+4216	90701628002	59442.08750	20005	0.175	1.63±0.02	3.845±0.208	0.99±0.03	0.89	-10.857±0.005	-10.710±0.008	45	70
5BZQJ2211+1841	60301015002	58080.65347	101573	0.041	1.87±0.02	3.126±0.106	0.98±0.02	0.94	-11.127±0.003	-11.103±0.005	79	60
5BZQJ2232+1143	90202044002	57752.53800	28549	0.049	1.31±0.01	6.969±0.159	1.02±0.01	0.89	-10.311±0.002	-10.006±0.003	65	70
3HSPI223348.8-202226	90502616001	58576.08750	5098	0.033	2.92±0.38	2.620±1.929	1.03±0.30	0.87	-11.956±0.060	-12.460±0.096	20	30
5BZQJ2251+2217	60160805002	58975.23600	48905	0.046	1.77±0.11	0.289±0.066	1.02±0.10	0.84	-12.080±0.022	-12.002±0.030	20	30
5BZGJ2313+1444	60101061002	57172.07361	21655	0.050	2.44±0.16	1.057±0.337	1.14±0.16	0.76	-12.009±0.025	-12.266±0.040	20	30
5BZUJ2333-2343	60160832002	57233.00416	21085	0.017	1.88±0.03	4.304±0.276	0.99±0.03	0.99	-10.993±0.005	-10.973±0.010	35	70
5BZB12347-5142	60160836002	59052.80972	20744	0.141	2.36±0.04	8.642±0.657	1.00±0.04	0.91	-11.045±0.007	-11.263±0.013	35	60
5BZB12359-3037	60160840002	57526.68819	21829	0.012	2.19±0.03	10.693±0.563	1.00±0.03	0.91	-10.825±0.005	-10.959±0.009	45	70

Table B2: Best-fit parameters derived for the 253 blazars observations modelled using a logarithmic parabola absorbed for the Galaxy. Columns 1 and 2 specify the object name and *NuSTAR* observation ID. Columns from 3 and 4 account for the observation date and the length of the exposure. The Galactic column density (taken from [H14PI Collaboration et al. 2016](#), and in units of 10^{22} cm^{-2}), α , β , the normalisation and the FPMAB inter-calibration constants are reported in columns 5, 6, 7, 8, and 9, respectively. Then, column 10 accounts for the ratio between the Cstat/d.o.f.. The logarithm of the 3–10 keV (S) and 10–30 keV (H) fluxes (in units of $1/\text{erg cm}^{-2} \text{ s}^{-1}$) estimated using the logarithmic-parabola are reported in columns 11 and 12, respectively. Finally, columns 13 and 14 refer to the maximum energy below which the spectral analysis was performed and the radius (in arcsec) of the extracting region used for the source.

Name	ObsID	Time(MJD)	Exposure(s)	N_H	α	β	Norm	Const	C/d.o.f.	$\log F_\text{S}$	$\log F_\text{H}$	E_max (keV)	Radius (arcsec)
SBZQJ0010+058	60301014002	58098464652	93441	0.059	1.78±0.02	-0.047±0.037	2.66±0.03	0.98±0.01	0.94	-10.88±0.002	-10.796±0.004	79	70
SBZQJ0017+8135	600101098002	57012.69861	30947	0.128	1.73±0.11	0.039±0.327	0.70±0.03	0.93±0.05	0.96	-11.460±0.009	-11.374±0.020	25	40
SBZQJ0017+8135	600101098004	57045.10486	36376	0.128	1.65±0.09	0.070±0.173	0.64±0.03	0.99±0.05	0.91	-11.495±0.009	-11.379±0.016	35	40
SBZQJ0017+8135	90201019002	57490.02500	17292	0.128	1.52±0.14	0.338±0.364	0.67±0.04	0.98±0.07	0.89	-11.478±0.013	-11.378±0.024	25	40
SBZQJ0122+4310	60373002002	58131.87222	30717	0.030	1.49±0.34	-0.289±0.309	0.10±0.01	0.97±0.15	0.85	-12.304±0.027	-11.998±0.069	20	30
SBZB0123+2310	60101060002	57273.18125	21719	0.012	2.41±0.11	0.141±0.357	0.89±0.04	0.91±0.06	0.91	-11.382±0.010	-11.662±0.028	25	40
SBZQJ0126+2559	60201047002	57768.05625	41657	0.067	1.49±0.14	0.191±0.383	0.31±0.02	1.00±0.06	0.92	-11.800±0.011	-11.644±0.029	25	40
SBZQJ0126+2559	60367010002	58121.66736	19830	0.067	1.68±0.22	-0.209±0.532	0.26±0.02	1.09±0.11	0.79	-11.885±0.022	-11.698±0.044	20	40
SBZQJ0203+1134	60201010002	57700.71944	31588	0.059	1.56±0.27	0.426±0.706	0.15±0.02	1.03±0.13	0.73	-12.118±0.027	-12.065±0.060	20	30
SBZGJ0214+5144	60160094002	57417.38263	21364	0.146	2.00±0.07	0.125±0.921	1.57±0.05	0.94±0.04	0.98	-11.127±0.007	-11.201±0.015	35	60
SBZQJ0217+7349	60160099002	57442.45902	30254	0.266	1.47±0.06	0.138±0.149	1.26±0.03	0.98±0.03	0.96	-11.196±0.006	-11.008±0.010	35	60
SBZQJ0225+1846	60011011002	57015.43819	31973	0.094	1.45±0.04	0.131±0.063	2.23±0.04	0.96±0.02	1.00	-10.945±0.004	-10.750±0.005	65	70
SBZQJ0225+1846	60011011004	57040.16736	37398	0.094	1.50±0.05	0.292±0.088	1.55±0.03	0.99±0.03	0.93	-11.109±0.004	-10.984±0.006	45	60
SBZQJ0229-3643	60367002002	57975.49027	23205	0.024	1.45±0.58	0.275±0.359	0.06±0.01	0.75±0.20	0.85	-12.529±0.043	-12.210±0.144	20	30
SBZGJ0232+2017	10702609002	59434.24375	94265	0.078	2.17±0.05	0.216±0.107	0.95±0.02	1.01±0.03	0.91	-11.351±0.005	-11.533±0.011	65	50
SBZGJ0232+2017	10702609004	59437.20208	57535	0.078	2.25±0.06	0.178±0.140	0.98±0.02	1.01±0.03	0.92	-11.340±0.006	-11.552±0.013	45	50
SBZGJ0232+2017	10702609006	59439.21597	55520	0.078	2.23±0.05	0.122±0.140	1.18±0.03	1.04±0.03	0.91	-11.257±0.005	-11.445±0.011	45	50
SBZGJ0232+2017	60002047002	56567.00416	16233	0.078	1.94±0.06	0.235±0.112	3.19±0.07	0.99±0.03	0.89	-10.818±0.006	-10.892±0.011	45	70
SBZGJ0232+2017	60002047004	56567.97986	20258	0.078	1.92±0.04	0.234±0.083	3.51±0.07	1.01±0.02	0.95	-10.776±0.005	-10.839±0.008	65	70
SBZGJ0232+2017	60002047006	56567.95597	17993	0.078	1.89±0.05	0.122±0.080	3.47±0.07	0.98±0.03	0.97	-10.776±0.005	-10.792±0.008	45	70
SBZUJ0241-0815	600160127002	56337.41041	15564	0.029	1.70±0.11	0.983±0.213	0.91±0.04	1.02±0.05	0.99	-11.295±0.009	-11.002±0.017	25	60
SBZUJ0241-0815	60201056002	57770.00069	59604	0.029	0.78±0.04	0.808±0.067	1.13±0.02	0.97±0.02	1.06	-11.202±0.004	-10.894±0.005	79	60
SBZUJ0241-0815	9071624002	59412.24722	20265	0.029	0.85±0.10	0.710±0.164	0.90±0.04	1.03±0.05	0.99	-11.306±0.008	-11.001±0.012	35	50
SBZUJ0241-0815	601610145002	57446.71597	29755	0.078	1.78±0.10	0.034±0.226	0.70±0.03	0.99±0.05	0.99	-11.465±0.010	-11.404±0.018	25	40
SBZUJ0324+3410	600161360002	56731.73680	101447	0.117	1.85±0.03	0.095±0.223	1.44±0.02	1.02±0.02	0.90	-11.151±0.003	-11.295±0.005	79	60
SBZUJ0324+3410	60402003002	58344.63958	36233	0.117	1.83±0.06	0.073±0.100	1.28±0.03	0.99±0.03	0.90	-11.203±0.007	-11.132±0.009	45	60
SBZUJ0324+3410	60402003004	58348.59444	29592	0.117	1.85±0.08	0.045±0.152	0.98±0.03	1.00±0.04	0.85	-11.320±0.008	-11.271±0.012	35	50
SBZUJ0324+3410	60402003012	58337.60486	26273	0.117	1.84±0.10	0.044±0.149	2.02±0.04	1.01±0.03	0.86	-11.107±0.005	-10.962±0.008	45	70
SBZUJ0324+3410	60160154002	58770.78541	23036	0.023	2.54±0.12	0.202±0.356	0.70±0.04	0.99±0.07	0.91	-11.491±0.011	-11.854±0.031	25	40
SBZUJ0324+3410	60101079002	57334.10833	22165	0.091	1.23±0.21	0.161±0.343	0.27±0.02	1.01±0.09	0.84	-11.838±0.016	-11.544±0.044	20	40
SBZB0349-1159	60101036002	57275.20208	33307	0.030	2.23±0.08	0.410±0.210	0.96±0.03	1.00±0.04	0.94	-11.354±0.008	-11.620±0.016	35	50
3HSIP032523.5-563545	60160154002	58770.78541	21196	0.070	2.22±0.06	0.259±0.134	2.38±0.06	1.00±0.03	0.99	-10.956±0.005	-11.172±0.011	35	70

Table B2: continued.

Name	ObsID	Time(MJD)	Exposure(s)	N_H	α	β	Norm	Const	C/d.o.f.	$\log F_S^{\text{logpar}}$	$\log F_H^{\text{logpar}}$	$E_{\text{max}} (\text{keV})$	Radius (arcsec)
5BZQJ0359+5057	60160177002	57370.98333	20494	0.692	1.53±0.07	0.070 ^{+0.133} _{-0.131}	1.43±0.04	1.00±0.04	0.88	-11.152±0.007	-10.966±0.010	35	60
5BZQJ0403-3605	60160179002	57518.84097	18803	0.007	1.46±0.16	0.128 ^{+0.331} _{-0.331}	0.46±0.03	0.94±0.07	0.90	-11.625±0.015	-11.434±0.027	25	40
5BZQJ0405-1308	60160181002	58838.56319	21186	0.041	1.58±0.13	0.124 ^{+0.328} _{-0.328}	0.62±0.03	1.03±0.07	0.87	-11.505±0.013	-11.372±0.029	25	40
5BZUJ0407-1211	60463011002	58936.53541	33601	0.035	1.74±0.06	0.034 ^{+0.176} _{-0.176}	1.16±0.03	1.02±0.03	0.90	-11.240±0.006	-11.158±0.011	35	60
5BZBJ0416+0105	60101035002	57351.170902	34260	0.077	2.78±0.07	0.023 ^{+0.207} _{-0.207}	1.16±0.04	0.91±0.04	0.98	-11.271±0.006	-11.709±0.023	35	50
3C111	60202061002	58113.69100	22881	0.285	1.74±0.03	0.065 ^{+0.045} _{-0.045}	8.06±0.10	0.98±0.02	0.96	-10.405±0.003	-10.327±0.005	79	70
3C111	60202061004	58116.10900	52979	0.285	1.70±0.02	0.125 ^{+0.031} _{-0.031}	7.29±0.06	0.98±0.01	0.97	-10.449±0.002	-10.370±0.003	79	70
3C111	60202061006	58487.38900	55429	0.285	1.61±0.02	0.122 ^{+0.033} _{-0.033}	5.00±0.05	0.97±0.01	0.93	-10.607±0.002	-10.483±0.003	79	70
5BZUJ0433+0521	600101042002	56329.53194	21582	0.103	1.84±0.02	0.042 ^{+0.034} _{-0.034}	8.80±0.10	0.99±0.01	0.94	-10.366±0.003	-10.310±0.003	79	70
5BZUJ0449+1121	60101078002	57358.09097	20517	0.123	1.41±0.59	0.603 ^{+0.916} _{-0.916}	0.06±0.01	1.00±0.26	0.76	-12.490±0.057	-12.411±0.142	20	30
5BZQJ0453-2807	60101080002	57359.03194	19517	0.023	1.47±0.21	0.224 ^{+0.478} _{-0.478}	0.31±0.02	1.01±0.09	0.80	-11.798±0.016	-11.505±0.039	20	40
5BZBJ0501-0159	60367003001	58234.29583	20623	0.064	1.54±0.15	0.251 ^{+0.360} _{-0.360}	0.48±0.03	1.02±0.07	0.86	-11.615±0.013	-11.497±0.029	25	40
5BZBJ0507+6737	60202026002	57694.41388	24647	0.093	2.64±0.06	0.413 ^{+0.184} _{-0.184}	1.99±0.05	0.95±0.03	0.95	-11.043±0.007	-11.506±0.014	35	60
5BZBJ0507+6737	60202026004	57721.20208	20697	0.093	2.81±0.12	0.034 ^{+0.172} _{-0.172}	0.74±0.04	1.03±0.07	0.85	-11.463±0.014	-11.897±0.037	25	40
5BZBJ0507+6737	60202026006	57749.12916	25273	0.093	2.46±0.11	0.207 ^{+0.358} _{-0.358}	0.77±0.04	0.98±0.06	0.87	-11.448±0.010	-11.772±0.029	25	40
5BZBJ0509+0541	60502053002	58694.89305	22353	0.116	1.39±0.16	0.587 ^{+0.310} _{-0.310}	0.41±0.03	1.08±0.08	0.94	-11.687±0.016	-11.595±0.032	25	40
5BZBJ0509+0541	60502053004	58755.82361	31748	0.116	1.78±0.14	0.155 ^{+0.346} _{-0.346}	0.37±0.02	1.06±0.07	0.85	-11.738±0.013	-11.619±0.027	25	40
5BZBJ0509+0541	60502053006	58816.08775	20266	0.116	1.84±0.19	0.611 ^{+0.248} _{-0.248}	0.36±0.03	0.95±0.09	0.81	-11.744±0.015	-11.512±0.040	20	40
5BZBJ0509+0541	60502053008	58874.80277	19397	0.116	1.79±0.21	0.171 ^{+0.513} _{-0.513}	0.32±0.03	1.04±0.10	0.80	-11.801±0.019	-11.682±0.055	20	40
5BZBJ0509+0541	60502053010	58933.10833	21483	0.116	1.85±0.15	0.318 ^{+0.493} _{-0.493}	0.24±0.03	0.97±0.08	0.93	-11.661±0.016	-11.527±0.030	25	40
5BZBJ0509+0541	606020204002	59118.11180	23714	0.116	1.58±0.19	0.243 ^{+0.224} _{-0.224}	0.35±0.02	1.03±0.09	0.96	-11.779±0.017	-11.677±0.044	20	40
5BZBJ0509+0541	606020204004	59147.90000	27498	0.116	1.57±0.15	0.091 ^{+0.326} _{-0.326}	0.41±0.02	0.94±0.07	0.93	-11.688±0.013	-11.537±0.027	25	40
5BZBJ0509+0541	606020204006	59170.71944	25070	0.116	1.65±0.20	0.325 ^{+0.307} _{-0.307}	0.29±0.02	1.04±0.10	0.93	-11.852±0.017	-11.810±0.057	20	40
5BZBJ0509+0541	606020204008	59193.60138	27013	0.116	1.78±0.20	0.139 ^{+0.493} _{-0.493}	0.24±0.02	1.18±0.11	0.85	-11.930±0.018	-11.815±0.045	20	40
5BZBJ0509+0541	606020204010	59230.57013	25126	0.116	2.06±0.27	-0.844 ^{+0.699} _{-0.699}	0.17±0.02	1.08±0.15	0.94	-12.081±0.022	-11.894±0.069	20	40
5BZBJ0509+0541	606020204012	59257.80972	25592	0.116	1.84±0.27	-0.310 ^{+0.676} _{-0.676}	0.18±0.02	1.02±0.13	0.86	-12.047±0.029	-11.912±0.071	20	40
5BZBJ0509+0541	90301618002	58025.09444	27608	0.116	1.86±0.19	-0.491 ^{+0.475} _{-0.475}	0.26±0.02	0.99±0.09	0.82	-11.893±0.015	-11.712±0.053	20	40
5BZBJ0509+0541	90301618004	58045.43472	21285	0.116	1.53±0.28	0.323 ^{+0.706} _{-0.706}	0.21±0.02	1.02±0.13	0.81	-11.974±0.027	-11.873±0.069	20	40
5BZBJ0509+0541	90401610002	58211.55277	25946	0.116	1.49±0.19	0.134 ^{+0.679} _{-0.679}	0.29±0.02	1.08±0.15	0.94	-12.081±0.022	-11.655±0.032	20	40
5BZBJ0509+0541	90402637002	58407.86527	31882	0.116	1.45±0.16	0.226 ^{+0.438} _{-0.438}	0.30±0.02	1.00±0.08	0.79	-11.819±0.015	-11.654±0.032	25	40
5BZBJ0509+0541	90402637004	58437.05972	27204	0.116	1.79±0.23	-0.401 ^{+0.332} _{-0.332}	0.23±0.02	0.99±0.11	0.82	-11.933±0.020	-11.743±0.053	20	40
5BZBJ0509+0541	90402637006	58460.75416	25769	0.116	1.46±0.21	0.589 ^{+0.524} _{-0.524}	0.26±0.02	1.01±0.10	0.86	-11.887±0.020	-11.831±0.048	20	40
5BZBJ0509+0541	90402637008	58490.388263	26311	0.116	1.74±0.15	0.128 ^{+0.538} _{-0.538}	0.43±0.03	0.95±0.07	0.93	-11.672±0.015	-11.616±0.030	25	40
PictorA	60101047002	57359.23600	117036	0.036	1.73±0.03	0.098 ^{+0.329} _{-0.329}	0.09±0.01	1.01±0.09	0.89	-11.344±0.009	-11.727±0.021	35	40
5BZUJ0522-3627	60160232002	59338.01111	23319	0.032	1.84±0.04	0.076 ^{+0.051} _{-0.051}	3.38±0.06	1.01±0.02	0.92	-10.783±0.004	-10.763±0.007	65	70
5BZQJ0525-2338	60160234002	57869.29930	20879	0.021	1.39±0.16	0.191 ^{+0.989} _{-0.989}	0.43±0.03	1.02±0.08	0.93	-11.658±0.016	-11.454±0.026	25	40
5BZQJ0530+331	60160238002	58509.06319	20054	0.236	1.43±0.33	0.308 ^{+0.822} _{-0.822}	0.18±0.02	0.91±0.14	0.83	-12.051±0.030	-11.896±0.075	20	30
5BZBJ0543-5532	60101058002	57374.75069	37537	0.055	2.61±0.08	0.141 ^{+0.781} _{-0.781}	0.98±0.03	1.02±0.04	0.84	-11.148±0.004	-11.082±0.004	25	30
5BZQJ0555+3948	90401003002	58126.38333	28563	0.270	1.68±0.14	-0.239 ^{+0.209} _{-0.209}	0.44±0.02	0.97±0.06	0.99	-11.659±0.012	-11.462±0.028	25	40
5BZQJ0623-6436	60160263002	58010.86180	41687	0.040	1.82±0.08	-0.150 ^{+0.74} _{-0.74}	0.70±0.02	1.01±0.04	0.86	-11.458±0.010	-11.362±0.015	35	40
PKS0625-354	60301007002	58047.65000	51837	0.063	2.58±0.12	-0.85 ^{+0.554} _{-0.554}	0.32±0.02	1.02±0.07	1.00	-11.826±0.014	-12.132±0.038	25	40
5BZBJ0630-2406	60011140002	56947.74375	66469	0.081	2.48±0.39	1.440 ^{+1.640} _{-1.640}	0.05±0.01	1.18±0.24	0.95	-12.664±0.035	-13.282±0.164	20	30
5BZQJ0635-7516	60160272002	57362.11875	15173	0.072	1.46±0.18	0.105 ^{+0.418} _{-0.418}	0.51±0.03	0.99±0.08	0.84	-11.583±0.015	-11.384±0.040	20	40
PMN J0641M0320	8001003002	56776.41736	21353	0.586	1.17±0.07	-0.140 ^{+0.09} _{-0.09}	1.25±0.04	0.99±0.03	0.93	-11.177±0.007	-10.752±0.009	35	60

Table B2: continued.

Name	ObsID	Time(MJD)	Exposure(s)	N_{H}	α	β	Norm	Const	C/d.o.f.	$\log F_{\text{S}}^{\text{logpar}}$	$\log F_{\text{H}}^{\text{logpar}}$	$E_{\text{max}} (\text{keV})$	Radius (arcsec)
5BZQJ0646+4451	60201011002	57720.538888	32065	0.108	2.14±0.28	-0.750 ^{+0.724} _{-0.693}	0.12±0.01	0.99±0.14	0.82	-12.221±0.027	-12.102±0.071	20	30
5BZBJ0710+5908	60101037002	57266.24375	3931	0.043	2.24±0.12	0.008 ^{+0.292} _{-0.285}	2.94±0.14	1.02±0.06	0.89	-10.857±0.011	-11.021±0.024	25	70
5BZBJ0710+5908	60101037004	57266.50763	26440	0.043	2.16±0.04	0.247 ^{+0.085} _{-0.085}	2.96±0.06	0.99±0.02	0.90	-10.857±0.004	-11.044±0.009	65	70
5BZBJ0710+5908	60101037006	57267.24375	4641	0.043	2.20±0.11	0.135 ^{+0.266} _{-0.266}	3.07±0.14	0.98±0.06	0.92	-10.840±0.011	-11.015±0.023	25	70
5BZBJ0721+7120	90002003002	57046.11527	18564	0.029	2.15±0.07	-0.456 ^{+0.137} _{-0.139}	1.62±0.05	1.03±0.04	0.98	-11.101±0.007	-11.082±0.012	35	60
5BZQJ0733+0456	60501037002	58779.45208	60473	0.069	1.99±0.60	0.504 ^{+1.415} _{-1.347}	0.02±0.01	1.09±0.27	0.80	-12.899±0.046	-12.641±0.106	20	30
5BZQJ0809+5341	80001004002	56785.43819	28004	0.038	1.08±0.61	0.096 ^{+1.380} _{-1.382}	0.04±0.01	1.28±0.32	0.78	-12.666±0.062	-12.278±0.126	20	30
3HSPI08.1003.3-752724	60001142002	56901.119861	112366	0.078	1.54±0.23	0.304 ^{+0.126} _{-0.126}	0.06±0.01	1.10±0.12	0.94	-12.529±0.024	-12.428±0.045	25	30
5BZQJ0841+7053	60002045002	56641.65347	29678	0.028	1.65±0.04	-0.012 ^{+0.503} _{-0.503}	2.85±0.05	0.99±0.02	0.88	-10.846±0.005	-10.709±0.005	65	70
5BZQJ0841+7053	60002045004	56667.50208	36324	0.028	1.60±0.03	0.078 ^{+0.642} _{-0.642}	4.40±0.06	0.99±0.02	0.99	-10.656±0.003	-10.518±0.003	79	70
5BZUJ0847-2337	60101059002	57375.63263	32066	0.082	2.31±0.09	0.091 ^{+0.230} _{-0.230}	0.78±0.03	1.01±0.05	0.89	-11.438±0.009	-11.655±0.021	35	40
5BZBJ0854+2006	90201054002	57852.44861	52838	0.024	2.12±0.07	-0.098 ^{+0.148} _{-0.148}	0.83±0.02	1.00±0.04	0.87	-11.401±0.006	-11.473±0.014	35	40
5BZBJ0854+2006	90601616002	58973.85833	29268	0.024	2.46±0.10	-0.193 ^{+0.258} _{-0.258}	0.80±0.03	1.04±0.06	0.78	-11.424±0.010	-11.643±0.024	25	40
5BZBJ0915+2933	90101021002	57433.24722	49991	0.018	2.47±0.23	0.204 ^{+0.741} _{-0.741}	0.13±0.01	1.04±0.13	0.77	-12.210±0.024	-12.537±0.071	20	30
5BZBJ0915+2933	90201047002	57794.52500	31066	0.018	2.79±0.32	-1.158 ^{+1.647} _{-1.647}	0.09±0.01	1.12±0.20	0.88	-12.351±0.034	-12.465±0.129	20	30
5BZQJ0948+0022	60201052002	57696.17083	192097	0.047	1.48±0.06	-0.146 ^{+0.100} _{-0.100}	0.25±0.01	1.02±0.03	0.86	-11.896±0.006	-11.629±0.009	45	40
5BZUJ0955+3551	90501658002	58859.04583	25389	0.011	2.25±0.12	-0.044 ^{+0.305} _{-0.305}	0.68±0.03	0.94±0.06	0.92	-11.493±0.011	-11.644±0.030	25	40
5BZQJ0956+2515	60301019002	58105.99027	63387	0.034	1.79±0.17	0.035 ^{+0.395} _{-0.395}	0.16±0.01	1.03±0.09	0.86	-12.108±0.013	-12.055±0.039	25	30
5BZQJ1028-0844	6037301002	58089.20902	30593	0.046	1.66±0.26	0.065 ^{+0.652} _{-0.652}	0.16±0.02	1.08±0.13	0.86	-12.101±0.025	-11.991±0.057	20	30
5BZQJ1044+8054	90201018002	57490.28194	14653	0.021	1.44±0.13	0.119 ^{+0.257} _{-0.257}	0.79±0.04	1.03±0.06	0.92	-11.394±0.013	-11.193±0.022	25	50
5BZUJ1058+0133	60466004002	58230.63263	19514	0.029	1.70±0.16	-0.007 ^{+0.354} _{-0.354}	0.43±0.03	1.01±0.08	1.00	-11.665±0.020	-11.550±0.034	25	40
5BZBJ103-2329	60101033002	57399.875569	52097	0.051	2.40±0.03	0.260 ^{+0.666} _{-0.666}	4.25±0.05	0.95±0.01	0.97	-10.707±0.003	-11.015±0.006	79	70
5BZBJ1104+3812	10002015001	56115.08055	42014	0.013	2.78±0.01	0.213 ^{+0.382} _{-0.382}	24.32±0.14	1.00±0.01	0.98	-9.951±0.001	-10.434±0.003	79	70
5BZBJ1104+3812	10002016001	56116.07361	24870	0.013	2.82±0.01	0.238 ^{+0.332} _{-0.332}	27.22±0.18	1.03±0.01	0.98	-9.902±0.002	-10.412±0.005	79	70
5BZBJ1104+3812	60002023002	56294.77847	9146	0.013	3.14±0.05	-0.305 ^{+0.130} _{-0.130}	7.63±0.16	0.97±0.03	0.96	-10.440±0.005	-10.979±0.014	45	70
5BZBJ1104+3812	60002023004	56302.05277	22639	0.013	3.08±0.04	-0.143 ^{+0.126} _{-0.126}	5.35±0.09	0.98±0.02	0.89	-10.598±0.004	-11.148±0.010	79	70
5BZBJ1104+3812	60002023006	56307.038888	24183	0.013	2.94±0.02	0.213 ^{+0.352} _{-0.352}	18.46±0.15	0.99±0.01	0.92	-10.071±0.002	-10.648±0.005	79	70
5BZBJ1104+3812	60002023008	56312.09791	24947	0.013	3.02±0.03	0.101 ^{+0.259} _{-0.259}	6.36±0.09	0.97±0.02	1.01	-10.529±0.003	-11.109±0.010	79	70
5BZBJ1104+3812	60002023010	56329.01111	19317	0.013	2.83±0.02	0.382 ^{+0.094} _{-0.094}	23.94±0.20	0.97±0.01	0.99	-9.961±0.002	-10.509±0.005	79	70
5BZBJ1104+3812	60002023012	56335.01111	14797	0.013	2.66±0.02	0.206 ^{+0.048} _{-0.048}	27.22±0.23	0.97±0.01	0.92	-9.902±0.002	-10.324±0.004	79	70
5BZBJ1104+3812	60002023014	56339.98333	17374	0.013	2.98±0.03	0.125 ^{+0.053} _{-0.053}	10.59±0.14	0.99±0.02	0.96	-10.309±0.003	-10.872±0.009	79	70
5BZBJ1104+3812	60002023016	56355.96250	16859	0.013	2.95±0.02	0.177 ^{+0.084} _{-0.084}	27.34±0.22	0.98±0.01	0.93	-9.898±0.002	-10.460±0.004	79	70
5BZBJ1104+3812	60002023018	56362.95902	17461	0.013	3.03±0.02	0.201 ^{+0.051} _{-0.051}	20.94±0.19	0.97±0.01	0.95	-10.014±0.002	-10.621±0.006	79	70
5BZBJ1104+3812	60002023020	56368.00763	16559	0.013	2.68±0.02	0.231 ^{+0.047} _{-0.047}	27.98±0.23	0.98±0.01	0.94	-9.890±0.002	-10.328±0.004	79	70
5BZBJ1104+3812	60002023022	56384.71944	24786	0.013	2.64±0.01	0.278 ^{+0.023} _{-0.023}	67.32±0.28	0.98±0.01	0.97	-9.510±0.001	-9.940±0.002	79	70
5BZBJ1104+3812	60002023024	56392.89305	5768	0.013	2.77±0.02	0.352 ^{+0.042} _{-0.042}	103.86±0.73	0.95±0.01	0.93	-9.323±0.002	-9.839±0.005	79	70
5BZBJ1104+3812	60002023025	56393.04236	57645	0.013	2.51±0.01	0.338 ^{+0.066} _{-0.066}	159.24±0.28	0.98±0.01	0.98	-9.136±0.001	-9.518±0.001	79	70
5BZBJ1104+3812	60002023027	56394.88333	76667	0.013	2.45±0.01	0.420 ^{+0.098} _{-0.098}	340.99±1.14	0.97±0.01	0.93	-8.806±0.001	-9.181±0.002	79	70
5BZBJ1104+3812	60002023029	56395.90000	16533	0.013	2.65±0.01	0.387 ^{+0.022} _{-0.022}	127.69±0.48	0.98±0.01	0.91	-9.234±0.001	-9.698±0.002	79	70
5BZBJ1104+3812	60002023031	56396.90347	15701	0.013	2.14±0.01	0.382 ^{+0.072} _{-0.072}	353.19±0.79	0.98±0.01	1.02	-8.783±0.001	-8.993±0.001	79	70
5BZBJ1104+3812	60002023032	56397.91736	17306	0.013	2.46±0.01	0.295 ^{+0.018} _{-0.018}	133.59±0.47	0.97±0.01	0.96	-9.211±0.001	-9.559±0.002	79	70
5BZBJ1104+3812	60002023035	56398.93125	20317	0.013	2.25±0.01	0.320 ^{+0.018} _{-0.018}	142.20±0.44	0.97±0.01	0.95	-9.180±0.001	-9.430±0.001	79	70
5BZBJ1104+3812	60002023037	56400.01111	17782	0.013	2.73±0.02	0.323 ^{+0.052} _{-0.052}	23.39±0.20	0.97±0.01	0.96	-9.970±0.002	-10.455±0.005	79	70
5BZBJ1104+3812	60002023039	56401.02152	15939	0.013	2.88±0.02	0.173 ^{+0.058} _{-0.058}	21.90±0.21	0.97±0.01	0.96	-9.995±0.002	-10.522±0.006	79	70
5BZBJ1104+3812	60202048002	57756.99375	23692	0.013	2.36±0.01	0.202 ^{+0.020} _{-0.020}	67.02±0.28	0.95±0.01	0.94	-9.506±0.001	-9.778±0.002	79	70

Table B2: continued.

Name	ObsID	Time(MJD)	Exposure(s)	N_{H}	α	β	Norm	Const	C/d.o.f.	$\log F_{\text{S}}^{\text{logpar}}$	$\log F_{\text{H}}^{\text{logpar}}$	$E_{\text{max}} (\text{keV})$	Radius (arcsec)
5BZBJ1104+3812	60202048004	577784.99027	21586	0.013	2.32±0.01	0.288±0.021	71.37±0.30	0.97±0.01	0.90	-9.480±0.001	-9.755±0.002	79	70
5BZBJ1104+3812	60202048006	57812.92430	23908	0.013	2.37±0.01	0.282±0.020	71.06±0.29	0.96±0.01	0.95	-9.483±0.001	-9.781±0.002	79	70
5BZBJ1104+3812	60202048008	57839.91041	31158	0.013	2.60±0.02	0.180±0.038	20.95±0.14	0.97±0.01	0.90	-10.014±0.002	-10.399±0.003	79	70
5BZBJ1120+4212	60101062002	57330.23333	22465	0.018	2.82±0.12	0.173±0.383	0.79±0.04	0.97±0.06	0.87	-11.436±0.011	-11.932±0.038	25	40
5BZQJ1130-1449	90701608002	59274.45555	23063	0.035	1.52±0.07	-0.107±0.128	1.26±0.04	0.98±0.04	0.89	-11.190±0.008	-10.957±0.011	35	60
3C264	60501016002	58678.80277	55098	0.019	2.16±0.20	0.556±0.356	0.17±0.01	1.00±0.10	0.93	-12.109±0.018	-12.377±0.048	25	30
5BZQJ1159+2914	60463037002	58626.66388	16921	0.016	1.45±0.46	0.478±0.265	0.11±0.02	0.95±0.20	0.77	-12.246±0.035	-12.155±0.114	20	30
5BZQJ1159+2914	60463037004	59390.53194	17418	0.016	1.49±0.13	0.133±0.178	0.76±0.04	1.03±0.07	0.92	-11.412±0.013	-11.239±0.021	25	40
5BZQJ11220+0203	60301001002	57910.86875	50415	0.018	1.75±0.07	0.055±0.142	0.76±0.02	1.03±0.04	0.89	-11.427±0.008	-11.357±0.013	35	40
5BZQJ11221+3010	60101034002	57349.04583	49457	0.019	2.44±0.04	0.350±0.116	1.81±0.03	0.99±0.02	0.89	-11.080±0.004	-11.433±0.010	65	60
5BZQJ11222+0413	60301018002	57931.60486	32153	0.016	1.39±0.16	0.089±0.318	0.28±0.02	1.00±0.07	0.92	-11.845±0.015	-11.609±0.026	25	40
5BZQJ11229+4203	00015011001	56109.87569	2882	0.017	1.51±0.05	0.052±0.388	1.70±0.38	1.00±0.03	0.94	-10.060±0.006	-9.871±0.007	45	70
5BZQJ11229+4203	00015012001	56109.94166	2894	0.017	1.55±0.06	-0.030±0.080	1.72±0.43	0.99±0.03	0.93	-10.057±0.006	-9.864±0.009	35	70
5BZQJ11229+4203	00015013001	5610.01111	2575	0.017	1.51±0.06	0.107±0.106	1.69±0.43	0.96±0.03	0.96	-10.065±0.007	-9.895±0.008	35	70
5BZQJ11229+4203	00015014001	5610.08055	2609	0.017	1.61±0.06	-0.081±0.105	1.66±0.44	0.90±0.03	0.93	-10.073±0.005	-9.892±0.011	35	70
5BZQJ11229+4203	00015015001	5610.14652	2848	0.017	1.53±0.06	-0.036±0.108	1.578±0.42	0.89±0.03	0.97	-10.094±0.007	-9.890±0.009	35	70
5BZQJ11229+4203	00015017001	5610.28194	3005	0.017	1.54±0.07	0.039±0.118	1.592±0.44	0.91±0.03	0.88	-10.092±0.006	-9.912±0.008	35	70
5BZQJ11229+4203	10002020001	56122.00416	244059	0.017	1.64±0.01	0.057±0.048	1.447±0.04	1.00±0.01	1.04	-10.140±0.001	-10.019±0.001	79	70
5BZQJ11229+4203	10002020003	57216.58402	49370	0.017	1.70±0.01	0.025±0.023	1.087±0.07	0.98±0.01	0.92	-10.267±0.002	-10.163±0.002	79	70
5BZQJ11229+4203	10012001002	56121.07361	5160	0.017	1.64±0.04	-0.004±0.087	1.480±0.26	0.99±0.02	0.93	-10.129±0.005	-9.990±0.005	65	70
5BZQJ11229+4203	10012002001	56121.19513	6191	0.017	1.61±0.04	0.080±0.059	1.475±0.25	1.00±0.02	1.02	-10.131±0.004	-9.998±0.006	65	70
5BZQJ11229+4203	10012003001	56121.33055	6219	0.017	1.64±0.04	0.034±0.055	1.488±0.25	1.01±0.02	0.95	-10.128±0.004	-10.000±0.006	79	70
5BZQJ11229+4203	10012004001	56121.46597	6226	0.017	1.69±0.04	-0.016±0.062	1.521±0.27	0.85±0.02	0.92	-10.119±0.005	-9.998±0.005	65	70
5BZQJ11229+4203	10012005001	56121.60138	6147	0.017	1.61±0.04	0.063±0.063	1.486±0.27	1.02±0.02	0.92	-10.128±0.004	-9.993±0.006	65	70
5BZQJ11229+4203	10012006001	56121.73680	5211	0.017	1.57±0.06	0.052±0.062	1.434±0.34	0.99±0.03	0.96	-10.140±0.006	-9.982±0.009	35	70
5BZQJ11229+4203	10012007001	56121.86875	4534	0.017	1.64±0.04	0.034±0.055	1.421±0.37	1.04±0.03	0.91	-10.149±0.006	-10.031±0.009	35	70
5BZQJ11229+4203	10202020002	57565.79930	35403	0.017	1.57±0.01	0.069±0.08	2.494±0.13	0.99±0.01	0.97	-9.900±0.001	-9.748±0.002	79	70
5BZQJ11229+4203	10302020002	57930.73680	35333	0.017	1.61±0.02	0.060±0.025	1.274±0.09	0.98±0.01	0.94	-10.194±0.002	-10.059±0.002	79	70
5BZQJ11229+4203	10402020002	58271.08402	16063	0.017	1.62±0.02	0.031±0.034	1.333±0.14	0.98±0.01	0.92	-10.174±0.003	-10.035±0.003	79	70
5BZQJ11229+4203	10402020004	58284.18819	21117	0.017	1.63±0.02	0.059±0.033	1.073±0.11	0.99±0.01	0.94	-10.269±0.003	-10.140±0.003	79	70
5BZQJ11229+4203	10402020006	58303.72291	40180	0.017	1.67±0.02	0.051±0.033	1.091±0.08	0.99±0.01	0.93	-10.265±0.002	-10.154±0.002	79	70
5BZQJ11229+4203	10502620002	586666.32708	49119	0.017	1.68±0.02	0.022±0.024	9.33±0.07	0.99±0.01	0.91	-10.333±0.002	-10.222±0.002	79	70
5BZQJ11229+4203	10602606002	59036.20555	43684	0.017	1.65±0.02	0.053±0.023	1.152±0.08	1.02±0.01	0.92	-10.240±0.002	-10.121±0.002	79	70
5BZQJ11229+4203	10702608002	59374.77500	35767	0.017	1.63±0.02	0.001±0.023	8.16±0.07	0.99±0.01	0.91	-10.387±0.002	-10.241±0.003	79	70
5BZQJ11229+4203	60601004002	59318.61527	18321	0.022	1.63±0.03	0.026±0.024	8.14±0.11	0.98±0.02	0.91	-10.389±0.003	-10.254±0.005	79	70
5BZQJ11229+4203	80301602002	58257.57069	60655	0.017	1.60±0.01	0.056±0.014	11.22±0.07	0.98±0.01	0.93	-10.348±0.001	-10.248±0.001	79	70
5BZQJ11229+4203	60002020002	56642.24375	39512	0.022	1.72±0.04	0.019±0.016	1.95±0.03	1.03±0.02	0.91	-11.15±0.004	-10.923±0.006	65	70
5BZQJ1256-0547	60105047002	56657.99027	42733	0.022	1.71±0.03	0.043±0.022	4.09±0.05	0.97±0.01	0.86	-10.692±0.003	-10.602±0.004	79	70
5BZQJ1256-0547	60601005001	59317.12916	18321	0.022	1.90±0.07	-0.133±0.132	1.72±0.05	1.15±0.04	0.93	-11.074±0.007	-11.024±0.012	35	60
5BZQJ1256-0547	60370003002	58130.42777	20643	0.018	1.97±0.55	-0.571±0.555	0.08±0.02	0.86±0.24	0.88	-12.404±0.046	-12.259±0.142	20	30
5BZQJ1256-0547	60160541002	57902.34097	21281	0.020	1.42±0.38	0.098±0.613	0.11±0.02	1.06±0.18	0.96	-12.229±0.036	-12.009±0.093	20	30
5BZQJ1256-0547	60160547002	59072.57708	14040	0.054	1.83±0.13	-0.044±0.858	0.83±0.04	1.05±0.07	0.93	-11.388±0.014	-11.330±0.026	25	50
5BZQJ1256-0547	60201012002	57878.92083	53037	0.030	1.39±0.33	0.065±0.780	0.07±0.01	1.01±0.15	0.76	-12.472±0.028	-12.228±0.066	20	30
5BZQJ1335+1919	60463043002	59003.93125	21595	0.030	1.60±0.14	0.140±0.768	0.59±0.03	0.96±0.06	0.88	-11.533±0.013	-11.413±0.028	25	40
5BZGJ11407+2827	60201043002	57557.00763	50899	0.014	1.19±0.33	-0.298±0.791	0.06±0.01	1.07±0.15	0.70	-12.473±0.025	-12.011±0.059	20	30
5BZQJ1424+2256	60301020002	58117.87916	100962	0.035	2.08±0.17	0.514±0.482	0.12±0.01	1.03±0.09	0.92	-12.244±0.015	-12.463±0.039	25	30

Table B2: continued.

Name	ObsID	Time(MJD)	Exposure(s)	N_{H}	α	β	Norm	Const	C/d.o.f.	$\log F_{\text{S}}^{\text{logpar}}$	$\log F_{\text{H}}^{\text{logpar}}$	$E_{\text{max}} (\text{keV})$	Radius (arcsec)
5BZBJ1428+4240	60601024002	59042.71597	53782	0.010	2.21±0.03	0.185±0.068	2.99±0.04	0.98±0.02	0.88	-10.853±0.004	-11.048±0.006	79	70
5BZBJ1428+4240	90701613002	59311.24027	27743	0.010	2.01±0.03	0.005±0.051	6.02±0.08	0.99±0.02	0.93	-10.538±0.003	-10.583±0.006	79	70
5BZQJ1429+5406	60501036002	58680.89305	45024	0.010	1.70±0.28	-0.302±0.883	0.09±0.01	1.24±0.16	0.83	-12.348±0.025	-12.146±0.064	20	30
5BZQJ1430+4204	60001103002	56852.59444	49069	0.009	1.50±0.16	0.171±0.359	0.24±0.02	1.02±0.08	0.82	-11.917±0.014	-11.758±0.026	25	30
3C303	60463048002	59094.04583	21728	0.017	1.78±0.18	-0.096±0.439	0.38±0.03	0.98±0.08	0.99	-11.728±0.016	-11.628±0.034	20	40
5BZQJ1443+2501	90101004002	57137.11180	38177	0.031	2.31±0.22	-0.428±0.622	0.18±0.02	0.96±0.11	0.90	-12.069±0.020	-12.141±0.057	20	30
5BZUJ1459+7140	60160603002	57618.96250	23555	0.029	1.75±0.19	-0.469±0.497	0.29±0.02	1.01±0.09	0.87	-11.837±0.016	-11.604±0.045	20	40
5BZUJ1459+7140	60401024002	58491.58055	60888	0.029	1.58±0.11	0.045±0.235	0.30±0.01	1.03±0.06	0.93	-11.814±0.010	-11.658±0.021	25	40
5BZGJ1505+0326	60201044002	57796.28888	115134	0.035	1.32±0.23	-0.363±0.426	0.06±0.01	0.94±0.10	0.80	-12.525±0.020	-12.107±0.036	25	30
5BZQJ1510+5702	60201013002	57873.15000	36763	0.015	1.50±0.37	-0.536±0.830	0.07±0.01	0.96±0.16	0.87	-12.423±0.037	-12.041±0.073	20	30
5BZUJ1511+0518	60401024002	58924.19444	35117	0.042	1.68±0.16	0.006±0.360	0.26±0.02	1.06±0.08	0.92	-11.891±0.015	-11.775±0.026	25	40
3HSPl51803.6-273131	90501608002	58544.59791	33728	0.075	2.62±0.07	0.101±0.174	1.40±0.04	0.96±0.04	0.94	-11.188±0.007	-11.565±0.017	35	50
5BZQJ1556-7914	60160627002	57581.44166	17293	0.090	1.67±0.08	0.139±0.162	1.28±0.04	1.00±0.04	0.95	-11.198±0.009	-11.112±0.012	35	60
5BZQJ1559+0304	60373003002	58160.64305	53208	0.056	1.60±0.57	0.301±1.376	0.03±0.01	1.12±0.29	0.79	-12.870±0.037	-12.435±0.084	20	30
5BZUJ1626-2951	60160638002	57653.02847	20652	0.136	1.63±0.10	0.066±0.205	1.01±0.04	0.95±0.04	0.89	-11.300±0.010	-11.173±0.018	25	50
5BZQJ1642+3948	60160647002	58068.08055	24333	0.009	1.58±0.12	-0.036±0.240	0.67±0.03	0.96±0.05	0.90	-11.466±0.012	-11.285±0.022	25	40
5BZQJ1644+2619	60301017002	58136.21250	52318	0.050	1.61±0.22	0.436±0.337	0.14±0.01	1.07±0.11	0.93	-12.162±0.020	-12.132±0.042	20	30
5BZB1653+3945	60002024002	56395.10486	18269	0.017	2.19±0.03	0.164±0.538	1.057±0.12	1.03±0.02	0.93	-10.304±0.003	-10.485±0.004	79	70
5BZB1653+3945	60002024004	56420.833402	26143	0.017	2.18±0.02	0.119±0.053	1.495±0.12	0.99±0.01	0.97	-10.152±0.002	-10.314±0.004	79	70
5BZB1653+3945	60002024006	56485.89652	10848	0.017	2.02±0.02	0.170±0.036	35.73±0.29	0.99±0.01	0.92	-9.769±0.002	-9.864±0.003	79	70
5BZB1653+3945	60002024008	56486.84444	10338	0.017	2.02±0.02	0.218±0.037	32.40±0.28	0.97±0.01	0.96	-9.812±0.002	-9.920±0.004	79	70
5BZB1653+3945	60202049002	57870.93472	23127	0.017	2.14±0.03	0.132±0.036	9.49±0.10	0.96±0.01	1.01	-10.348±0.003	-10.494±0.005	79	70
5BZB1653+3945	60202049004	57897.92430	23774	0.017	2.66±0.04	0.091±0.115	3.64±0.07	0.99±0.02	0.95	-10.772±0.005	-11.166±0.010	65	70
5BZB1653+3945	60466606002	58227.62916	23040	0.017	2.69±0.06	0.184±0.173	2.08±0.05	0.99±0.03	0.93	-11.018±0.007	-11.453±0.016	35	60
5BZQJ1656-3302	60160657002	57292.35833	21127	0.235	1.56±0.10	0.106±0.169	0.90±0.04	1.00±0.05	0.97	-11.349±0.010	-11.198±0.019	25	50
5BZGJ1653+3945	60160662002	57350.19513	22348	0.020	1.74±0.13	-0.095±0.298	0.56±0.03	1.11±0.07	0.94	-11.555±0.014	-11.438±0.028	25	40
5BZQJ1723+6547	6051101002	58756.58402	74126	0.034	1.40±0.51	0.507±1.373	0.03±0.01	1.04±0.24	0.74	-12.780±0.045	-12.677±0.115	20	30
5BZQJ1723+6547	60511002002	58758.94166	77397	0.034	1.55±0.48	-0.104±1.233	0.03±0.01	1.01±0.23	0.79	-12.836±0.050	-12.619±0.109	20	30
5BZQJ1719+4858	60511003002	58760.28541	68363	0.034	1.52±0.56	1.918±0.333	0.04±0.01	0.91±0.23	0.81	-12.750±0.043	-13.051±0.176	20	30
5BZQJ1723+6547	60511005002	58852.55625	84338	0.034	1.57±0.65	0.844±2.674	0.03±0.01	1.02±0.30	0.78	-12.838±0.053	-12.904±0.221	20	40
5BZQJ1723+6547	60511008001	58910.32708	70234	0.034	2.16±0.61	-1.388±1.598	0.03±0.01	0.85±0.26	0.84	-12.888±0.061	-12.570±0.144	20	30
5BZQJ1723+6547	60511009001	58911.60138	68280	0.034	1.34±0.63	0.462±1.674	0.02±0.01	1.11±0.31	0.89	-12.895±0.049	-12.747±0.150	20	30
5BZB1723+6547	60464146002	59350.73680	19580	0.032	1.38±0.12	0.207±0.235	0.75±0.03	0.99±0.05	0.96	-11.416±0.010	-11.211±0.018	25	50
5BZQJ1809+4552	60464148002	58231.58750	24610	0.096	1.51±0.20	0.756±0.231	0.36±0.03	1.01±0.10	0.90	-11.760±0.018	-11.771±0.053	20	40
5BZQJ1829+4844	60160690002	58928.79236	19482	0.063	1.61±0.11	0.071±0.215	0.82±0.04	1.05±0.06	0.92	-11.385±0.011	-11.253±0.020	25	50
5BZQJ1833-2103	60160692002	57492.76805	21784	0.187	1.37±0.05	0.106±0.224	2.56±0.05	0.96±0.02	0.91	-10.878±0.004	-10.632±0.006	45	70
5BZQJ1833-2103	8046028002	58550.84791	41050	0.187	1.37±0.03	0.066±0.049	2.38±0.04	0.95±0.02	0.89	-10.910±0.004	-10.655±0.005	79	70
5BZQJ1849+4705	60463066002	59002.59791	25728	0.049	1.96±0.40	-0.029±0.128	0.09±0.01	0.95±0.19	0.73	-12.342±0.037	-12.354±0.134	20	30
5BZQJ1924-2914	60464163002	59314.87569	16341	0.069	1.83±0.14	0.210±0.393	0.71±0.04	1.05±0.07	0.94	-11.467±0.012	-11.481±0.033	25	40
5BZQJ1924-2914	60464163004	59317.62916	21639	0.069	1.83±0.12	0.212±0.321	0.75±0.04	1.03±0.06	0.89	-11.442±0.011	-11.458±0.023	25	40
5BZQJ1927+7358	60160712002	57760.54930	33198	0.066	1.76±0.08	0.063±0.158	0.84±0.03	0.99±0.04	0.86	-11.383±0.007	-11.319±0.012	35	50
5BZB191936-4719	60101057002	57469.73680	20833	0.052	2.37±0.08	0.187±0.153	1.31±0.05	0.98±0.05	0.92	-11.215±0.009	-11.488±0.016	35	50
5BZQJ1939-1002	60373040002	58200.58055	39106	0.097	2.09±0.21	-0.478±0.207	0.19±0.02	1.00±0.10	0.80	-12.038±0.022	-11.980±0.057	20	30
5BZGJ1958-3011	60101056002	57340.80625	52763	0.075	2.35±0.05	0.103±0.124	1.18±0.03	1.03±0.03	0.89	-11.259±0.007	-11.502±0.012	45	50

Table B2: continued.

Name	ObsID	Time(MJD)	Exposure(s)	N_{H}	α	β	Norm	Const	C/d.o.f.	$\log F_{\text{S}}^{\text{logpar}}$	$\log F_{\text{H}}^{\text{logpar}}$	E_{max} (keV)	Radius (arcsec)
5BZBJ1959+6508	60002055002	56917.10833	19589	0.101	2.28±0.03	0.0355±0.052	14.79±0.16	0.98±0.01	0.96	-10.159±0.003	-10.348±0.004	79	70
5BZBJ1959+6508	60002055004	56922.08750	20311	0.101	2.46±0.03	0.1778±0.057	11.71±0.13	0.96±0.01	0.96	-10.267±0.003	-10.585±0.005	79	70
5BZQJ2007-4434	60201045002	57684.52500	60474	0.030	1.73±0.16	-0.078±0.353	0.18±0.01	1.00±0.08	0.88	-12.047±0.017	-11.927±0.031	25	30
5BZQJ2007-4434	80201024002	57517.68125	49070	0.030	1.59±0.20	0.158±0.434	0.16±0.01	1.07±0.10	0.78	-12.109±0.016	-11.990±0.040	25	30
5BZQJ2007-4434	90501649002	58788.54930	29872	0.030	1.33±0.25	-0.004±0.357	0.17±0.02	1.16±0.13	0.76	-12.048±0.024	-11.753±0.048	20	30
5BZQJ2011-1546	60160729002	57689.09097	20879	0.058	1.48±0.10	0.095±0.211	0.82±0.03	1.03±0.05	0.85	-11.377±0.010	-11.185±0.021	25	50
5BZUJ2015+3710	30460021002	58129.10833	59299	1.080	1.60±0.09	0.076±0.167	0.54±0.02	1.02±0.04	0.83	-11.587±0.009	-11.432±0.015	35	40
5BZUJ2015+3710	60160732002	57537.61875	12636	1.080	1.54±0.12	0.044±0.163	1.07±0.05	0.99±0.06	0.89	-11.284±0.011	-11.089±0.019	25	50
5BZQJ2022+6136	60401023002	58306.83055	64139	0.136	1.16±0.41	-1.026±0.785	0.04±0.01	1.00±0.15	0.84	-12.668±0.033	-11.935±0.064	20	30
5BZQJ2056-4714	60160748002	58955.50416	32753	0.028	1.49±0.11	-0.060±0.753	0.59±0.03	1.01±0.05	0.90	-11.515±0.010	-11.283±0.016	25	40
3HSPI205642.7+494006	3016101002	57339.79583	32667	1.010	2.33±0.03	0.535±0.084	4.75±0.07	0.98±0.02	0.86	-10.685±0.004	-11.008±0.008	79	70
5BZQJ2129-1538	60401029002	58386.09791	33166	0.045	1.52±0.06	0.155±0.083	1.33±0.03	0.99±0.03	0.84	-11.172±0.006	-11.017±0.010	45	60
5BZBJ1246-1344	60401026002	58256.16041	42137	0.037	2.28±0.17	0.131±0.098	0.25±0.02	1.14±0.10	0.92	-11.927±0.018	-12.142±0.040	25	30
5BZQJ1248+0657	60160768002	58074.20902	21278	0.044	1.53±0.09	-0.074±0.433	1.03±0.04	0.98±0.04	0.83	-11.277±0.007	-11.058±0.012	35	50
5BZQJ2151-3027	6001099002	56643.20902	38429	0.016	1.31±0.03	0.065±0.046	3.97±0.05	1.06±0.01	0.92	-10.680±0.003	-10.396±0.003	79	70
5BZQJ2151-3027	6001099004	56765.62916	44015	0.016	1.40±0.03	0.056±0.038	3.40±0.04	0.99±0.01	0.89	-10.754±0.003	-10.513±0.003	79	70
5BZBJ1258-3013	10002010001	56116.60833	33807	0.013	2.94±0.04	0.246±0.137	3.92±0.06	0.98±0.02	0.91	-10.743±0.003	-11.314±0.012	79	70
5BZBJ1258-3013	60002022002	56405.82361	44949	0.013	2.80±0.05	-0.315±0.110	1.55±0.03	0.99±0.03	0.94	-11.136±0.005	-11.494±0.013	45	60
5BZBJ1258-3013	60002022004	56489.95208	13822	0.013	2.59±0.08	-0.008±0.226	2.17±0.07	1.02±0.04	0.96	-10.994±0.010	-11.328±0.018	35	60
5BZBJ1258-3013	60002022006	56506.91041	10923	0.013	3.01±0.08	0.109±0.279	2.23±0.08	0.99±0.05	0.91	-10.981±0.010	-11.557±0.025	25	60
5BZBJ1258-3013	60002022008	56512.91736	13438	0.013	2.89±0.11	-0.268±0.374	1.28±0.06	0.99±0.06	0.87	-11.218±0.012	-11.639±0.034	25	50
5BZBJ1258-3013	60002022010	56518.91041	10493	0.013	2.93±0.09	-0.013±0.285	2.08±0.08	0.98±0.05	0.88	-11.012±0.009	-11.515±0.028	25	60
5BZBJ1258-3013	60002022012	56530.82708	11341	0.013	2.53±0.06	0.286±0.162	3.80±0.10	1.01±0.03	0.93	-10.757±0.007	-11.137±0.014	35	70
5BZBJ1258-3013	60002022014	56539.91388	12259	0.013	2.76±0.08	0.160±0.159	2.23±0.08	0.95±0.04	0.98	-10.988±0.009	-11.451±0.025	25	60
5BZBJ1258-3013	60002022016	56563.95555	11499	0.013	2.74±0.12	-0.207±0.337	1.29±0.06	0.87±0.06	0.94	-11.216±0.013	-11.574±0.033	25	50
5BZBJ1258-3013	60002022016	56272.60833	21856	0.175	1.90±0.04	-0.063±0.076	3.37±0.06	0.95±0.02	0.90	-10.787±0.004	-10.756±0.006	65	70
5BZBJ1258-3013	60501024002	58740.23333	210850	0.175	1.89±0.03	-0.250±0.044	0.97±0.01	0.99±0.02	0.93	-11.321±0.003	-11.231±0.004	50	70
5BZBJ1258-3013	90601630002	59133.58750	30430	0.175	1.61±0.06	-0.063±0.093	1.49±0.04	1.01±0.03	0.99	-11.126±0.005	-10.947±0.008	45	60
5BZBJ122024+2116	90701628002	59442.08750	20005	0.175	1.65±0.05	-0.031±0.083	2.78±0.06	0.99±0.03	0.89	-10.857±0.005	-10.709±0.008	45	70
5BZQJ2221+1841	60301015002	58080.65347	101573	0.041	1.85±0.03	0.059±0.053	1.53±0.02	0.98±0.02	0.94	-11.127±0.003	-11.106±0.005	79	60
5BZQJ2202+4216	60101061002	57172.07361	21655	0.050	2.50±0.26	-0.237±0.297	0.21±0.02	1.14±0.16	0.76	-12.009±0.029	-12.233±0.085	20	30
3HSPI223248.8-202226	90202044002	57752.53800	28549	0.049	1.31±0.02	0.005±0.026	8.52±0.09	1.02±0.01	0.89	-10.311±0.002	-10.006±0.003	65	70
5BZQJ2224+2117	60160805002	58975.23600	48905	0.046	1.69±0.21	0.220±0.541	0.17±0.01	1.02±0.10	0.84	-12.079±0.022	-12.028±0.053	20	30
5BZGJ2313+4444	60101061002	57172.07361	21655	0.050	2.50±0.26	-0.237±0.297	0.21±0.02	1.14±0.16	0.76	-12.009±0.029	-12.233±0.085	20	30
5BZUJ2333-2343	60160832002	57233.00416	21085	0.017	1.87±0.06	0.036±0.164	2.09±0.05	0.99±0.03	1.00	-10.993±0.006	-10.975±0.010	35	70
5BZBJ2347+5142	60160836002	59052.80972	20744	0.141	2.33±0.07	0.106±0.159	1.94±0.05	1.00±0.04	0.91	-11.044±0.006	-11.273±0.015	35	60
5BZBJ2359-3037	60160840002	57526.68819	21829	0.012	2.11±0.05	0.191±0.100	3.17±0.06	1.00±0.03	0.90	-10.825±0.004	-10.974±0.010	45	70

This paper has been typeset from a $\text{\TeX}/\text{\LaTeX}$ file prepared by the author.